BULLETIN OF THE EARTHQUAKE RESEARCH INSTITUTE,
UNIVERSITY OF TOKYO. Vol. 38, Part 3. September, 1960.

東京大学

地震研究所彙報

第38号　第3册

昭和35年9月

目次

論文及報告

頁
22. 表面波と地球の内部摩擦（英文）……吉山良一 361
23. 構造物の剪断振動と弾性地盤の相互作用 附：ロッキングの最大倍率（英文）……佐藤泰夫・山口林造 369
24. 海洋底を伝わるレーリー波の分散（第二報）（英文）……三東哲夫 385
25. 地球熱学（第4報）マントル内熱対流その他に伴なう熱流量（英文）……力武常次・宝来帰一 403
26. 地球熱学（第6報）秋田県院内油田，および，関東地方三地点における地殻熱流量（英文）……上田誠也・宝来帰一 421
27. 非定常ダイナモ（2）（英文）……行武毅 437
28. 北海道，駒ケ岳火山の軽石流堆積物（英文）……村井勇 451

(The titles in occidental languages are given on the back cover.)

地震研究所彙報は，年4回定期に（ただし，第1号より第6号までは不定期に，第7号は3冊として刊行された），彙報別冊は不定期に刊行される．

この彙報に載せられた論文及び報告についての責任は，すべてその著者のみにある．

この彙報についての照会通信は，すべて東京大学地震研究所長にあてられたい．

The Bulletin is published quarterly. (Vols. 1–6 were published at irregular intervals and Vol. 7 consisted of three parts.)

Supplementary Volume is published at irregular interval.

The authors of the papers alone are responsible for the statements and opinions contained in their respective papers.

All communications relating to this Bulletin should be addressed to the Director of the Earthquake Research Institute, University of Tokyo, Japan.

Earthquake Research Institute, University of Tokyo
Address:
No. 1, Motofuji-cho, Bunkyo-ku,
Tokyo Metropolis, Japan.
Telephone: 921-3161-Extension 6506
Cable address: ZISINKEN, TOKYO.

東京大学地震研究所
所在地
東京都文京区本富士町一番地
電話　小石川 921—3161（代）構内 6506
電略　ブンケウ　トウダイ　ヂシン

Bulletin of the Earthquake Research Institute
Vol. 38 (1960). pp. 361-368

22. *Propagation of Surface Waves and Internal Friction.*

By Ryoichi YOSHIYAMA,

Earthquake Research Institute.

(Read June 23, 1959; April 26, 1960.—Received May 31, 1960.)

1. Introduction.

Ewing and Press[1] studied the attenuation constant of the "Mantle Rayleigh waves" from the observations of its "earlier" and "later" orders, and found out the magnitude of internal friction of the earth's interior, which seems reasonable from a laboratory experiment. Their studies were followed by Satô's[2] of the "Mantle Love waves" or "G waves." His method of mathematical treatment seems more rigorous than that adopted by Ewing and Press; in his studies, the waves are analyzed into a complete set of monochromatic waves by Fourier's transforms, and applications of a complicated theory of waves of group are avoided. The results seem to give excellent data, perhaps incomparable for the present at least, for theoretical study of the wave, and yet there is something incomprehensible to the present writer. Because, the quantity $1/Q$ which is presumed constant for some range of period of waves turned out in his studies to vary beyond measure with the period of waves, moreover, in quite a different way from that noticed by Ewing and Press. And, it seems the way to interpret such a suspected discordant point reasonably has an important effect on the theoretical study of wave propagation as well as on the estimate of the amplitude of the wave at the hypocentral or epicentral region.

Theoretically rigorous studies of the problem are clearly difficult by any means, and, in this paper, it is hoped to get an empirical formula for theoretical studies in future.

2. Discordant point revealed.

Regarding an infinite train of monochromatic surface wave over an idealized spherical earth, the theoretically expected relation between its amplitude A and its travel or epicentral distance is given, under a certain condition, by

---

[1] M. EWING and F. PRESS, "An Investigation of Mantle Rayleigh Waves." *B.S.S.A.*, **44** (1954) 127-147; "Mantle Rayleigh Waves from the Kamchatka Earthquake of November 4, 1952." *B.S.S.A.*, **44** (1954) 471-479.

[2] Y. SATÔ, "Attenuation, Dispersion, and the Wave Guide of the G Wave." *B.S.S.A.* **48** (1958) 231-251.

$$A \propto (1/\sqrt{|\sin\theta|})\exp(-k\Delta) \cdots\cdots\cdots\cdots \quad (1)$$

where θ is epicentral angular distance, $\Delta = R\theta$ travel distance over the earth's surface, R radius of the earth. Reduction of the observations of surface waves has been generally based on this formula (1). And, according to Born, Birch and other senior authors, most laboratory experiments and field experiments by small explosions indicate that k is inversely proportional to the period of the wave. Then, putting

$$k = \pi/QVT \cdots\cdots\cdots\cdots\cdots\cdots\cdots \quad (2)$$

where V is the phase velocity of the wave and T the period, $1/Q$ is a dimensionless constant of the medium, named internal friction; laboratory experiment shows, also, that $1/Q$ of the same material decreases as temperature or pressure increases. Therefore, concerning seismic surface waves, because of changes of materials or state of materials towards the interior of the earth and because of the effect of penetration of the wave energy to the depth, apparent $1/Q$ is not necessarily constant, and, for a wave of long period, may be small as already pointed out by Ewing and Press in their studies, though numerical precision of their results will not yet be free from some questions.

On the other hand, as reproduced in Table 1, the results of Satô's study of $1/Q$ of New Guinea Earthquake, on Feb. 1, 1938, and Kamchatka Earthquake, on Nov. 4, 1952, are clearly discordant with the above explained presumption; $1/Q$ from his results remarkably increases with T, the period of the wave. There are two ways to study the discordancy, one is to put aside the presumption and assume a different dependency of the friction on the period T; the other is to find out some reasonable unknown factors which disturb the generally used formula (1). In this paper, following the above-mentioned results of laboratory experiments, the latter is studied. Because, studying Satô's paper in detail, systematic differences are observed not only between the

Table. 1. $1/Q$ from Satô's paper

Period T	360	210	108	72	54	43.2	sec.
New Guinea Earthq.	13½	8½	9	8	6	4	$\times 10^{-3}$
Kamchatka Earthq.	19	12	11	8			$\times 10^{-3}$

two series of $1/Q$-values in Table 1 of the two earthquakes, but also between two series of k-values, or γ-value in his notation, computed for each earthquake from two combinations respectively of different orders, i.e. G1N–G3N, or G1K–G3K, and G2N–G4N, or G2K–G4K. k-value from the former combination, G1–G3, is always larger than that from the latter, G2–G4, regardless of the period of the wave, and a similar tendency is observed also in the figures given by Ewing and Press in their studies. Those two series of k-values for each earthquake, four series of k-values in all, are presented in his paper graphically, though not numerically, and are expected to give as many series of $1/Q$-values. But, it seems mean values of each two are used respectively in his computation of $1/Q$ for each earthquake. The present writer tries to deduce a characteristic internal friction $1/Q_0$ from the four series of apparent $1/Q$-values. The studies are naturally directed to the re-examination of the factor $1/\sqrt{|\sin\theta|}$ of the formula (1).

3. Preliminary reasoning and formula obtained.

Wave front between two wave rays which make an angle $\delta\varphi$ at the epicentre spreads as $\delta\varphi R|\sin\theta|$. And, as far as the factor $1/\sqrt{|\sin\theta|}$ is concerned, the formula (1) implies a perfect and repeated convergence of wave front to a point at the epicentre and its antipode, and implies a conservation of wave energy along the wave ray over the spherical and homogeneous surface of the idealized earth. However, it is rather unreasonable to expect such a perfect convergence of wave front and conservation of wave energy along the wave ray over the surface of the earth. Because of geographical as well as geological irregularities of its surface, phase relation between the waves that rules boundary conditions of the waves propagated along contiguous wave rays, must undergo a change every moment on the way of propagation, and, accordingly, wave energies are partly refracted out of the proper wave ray resulting in a noise.

Based on the above-mentioned idea of wave propagation, a function of epicentral distance $f(\varDelta)$ is introduced in place of $|\sin\theta|$. Since we have no theoretical basis at present to determine the mathematical expression of $f(\varDelta)$, the following is expediently assumed for its empirical formula,

$$f(\varDelta)=\alpha\{R|\sin\theta|+\beta\varDelta^m\} \cdots\cdots\cdots\cdots\cdots (3)$$

By changing α-and β-value, the formula (3) is likely adaptable to various presumable features of diffusing wave front as follows:

i) If $\beta=0$ and $\alpha=1, f(\varDelta)=R|\sin\theta|$; this is the idealized case.

ii) If $\beta\to\infty, \alpha\to 0, \alpha\beta=1$ and $m=1, f(\varDelta)=\varDelta$; this is a case that even a slight convergence of wave front does not occur.

iii) An intermediate case of i) and ii) is given by certain α- and β-value, some convergence of wave front being implied.

Then we have, instead of (1), as an amplitude-distance relation,

$$A\propto\frac{1}{\sqrt{f(\varDelta)}}\exp(-k_0\varDelta)\ \cdots\cdots\cdots\cdots\cdots\ (4)$$

or, by a simple mathematical transformation,

$$A\propto\exp\left\{-k_0\varDelta-\frac{1}{2}\log f(\varDelta)\right\}.\ \cdots\cdots\cdots\cdots\ (5)$$

If A_1 and A_2 are respectively the amplitudes of the wave at two stations where travel distances of the wave are $\varDelta_1$ and $\varDelta_2$, while epicentral angular distances are θ_1 and θ_2, we get from (5),

$$\log\frac{A_1}{A_2}=(\varDelta_2-\varDelta_1)\left\{k_0+\frac{1}{2}\frac{1}{\varDelta_2-\varDelta_1}\log\frac{f(\varDelta_2)}{f(\varDelta_1)}\right\}\ \cdots\cdots\ (6)$$

So that k-value, if calculated by the generally used formula (1), must be related to k_0, $\varDelta_1$, $\varDelta_2$, θ_1 and θ_2 by the following formula,

$$k=k_0+\frac{1}{2}\frac{1}{\varDelta_2-\varDelta_1}\log\frac{f(\varDelta_2)\,|\sin\theta_1|}{f(\varDelta_1)\,|\sin\theta_2|}$$

and $1/Q$ by,

$$\frac{1}{Q}=\frac{1}{Q_0}+\frac{TV}{2\pi}\frac{1}{\varDelta_2-\varDelta_1}\log\frac{f(\varDelta_2)\,|\sin\theta_1|}{f(\varDelta_1)\,|\sin\theta_2|}\ \cdots\cdots\ (7)$$

where $k_0=\pi/Q_0TV$, and $1/Q_0$ is the expected characteristic internal friction. It is evident from (7) that, even when $1/Q_0$ is a constant, apparent $1/Q$ is a function of T; and, roughly speaking, as the phase velocity V changes but slightly for some range of T, it is nearly a linear function of T, and its gradient with respect to T depends on the epicentral distances of the stations concerned; and also, in the idealized case, since $f(\varDelta)=R\,|\sin\theta|$, the gradient term vanishes.

If we take for A_1 and A_2 the amplitudes of the wave of every other order at a station, $\sin\theta_1=\sin\theta_2$, $\varDelta_2-\varDelta_1=40{,}000$km and $f(\varDelta_2)>f(\varDelta_1)$ except the idealized case. And, the formula (7) will be accepted to give $1/Q$ of a tendency consistent with that in question of Table 1.

4. Further numerical computation based on Satô's results.

According to Satô, the epicentral angular distances of the station are $\theta=109.°6$ for the New Guinea earthquake, and $\theta=58.°6$ for the Kamchatka earthquake. So that the travel distances for respective G-waves are given by Table 2.

Table 2.

	G1	G2	O3	G4	
New Guinea Earthq.	120	280	520	680	10^2 km
Kamchatka Earthq.	64	336	464	736	10^2 km

Satô also gives a formula of the phase velocity as follows;

$$V=V_0/(1-\kappa T),\qquad V_0=4.4\ \text{km/sec},\qquad \kappa=5.3\times10^{-4}\ \text{sec}^{-1}.$$

Substituting those together with $\varDelta_2-\varDelta_1=40{,}000$ km into (7), we get

$$\frac{1}{Q}=\frac{1}{Q_0}+0.175\cdot10^{-4}\frac{T}{1-\kappa T}\log\frac{f(\varDelta_2)}{f(\varDelta_1)}\cdots\cdots\cdots\cdots(8)$$

From the observations of sufficient accuracy, it will be possible in future

Table 3. $0.175\cdot10^{-4}\log\dfrac{f(\varDelta_2)}{f(\varDelta_1)}$ in 10^{-5} sec^{-1}

m	β (km)$^{1-m}$	New Guinea Earthq.			Kamchatka Earthq.		
		G1−G3	G2−G4	mean	G1−G3	G2−G4	mean
	∞	7.70	4.66	6.18	10.40	4.11	7.25
3	$3\cdot10^{-10}$	3.55	4.38	3.96	3.21	3.52	3.36
	$1\cdot10^{-10}$	2.12	4.23	3.17	1.77	2.80	2.28
	∞	5.12	3.10	4.11	6.93	2.75	4.84
2	$10\cdot10^{-5}$	4.55	2.99	3.77	5.51	2.68	4.09
	6.10^{-5}	4.27	2.94	3.60	4.98	2.64	3.81
	$2\cdot10^{-5}$	3.33	2.65	2.99	3.60	2.45	3.02
	∞	3.85	2.33	3.09	5.20	2.06	3.63
3/2	$5\cdot10^{-2}$	3.71	2.29	3.00	4.88	2.04	3.46
	$1\cdot10^{-2}$	3.18	2.17	2.67	4.04	1.95	2.99
	∞	2.57	1.55	2.06	3.46	1.37	2.41
1	10	2.50	1.53	2.01	3.34	1.32	2.35
	1	2.11	1.36	1.73	2.67	1.24	1.95

to obtain the expression of the function $f(\Delta)$ empirically. In this paper, assuming (3), β and m are determined from the data given by Satô. Since κ is small, i.e. phase velocity V of the wave changes but slightly for some range of the period T, $(\partial/\partial T)(1/Q)\doteqdot 0.175\cdot 10^{-4}\log f(\Delta_2)/f(\Delta_1)$, which is given in Table 3 with several numerical examples of β and m for the two earthquakes.

Remarkable points that we learn from Satô's results, though he himself does not point them out, are as follows; i) apparent $1/Q$ from the Kamchatka earthquake seems a little greater than that from the New Guinea earthquake, ii) apparent $1/Q$ from G1–G3 seems a little greater than that from G2–G4, and the difference between the two seems more remarkable in case of Kamchatka earthquake than in case of New Guinea earthquake, iii) if we assume, from Table 1, $1/Q=4\times 10^{-3}$ for $T=43.2$ sec and $1/Q=19\times 10^{-3}$ for $T=360$ sec, mean gradient of $1/Q$ is not greater than $5\times 10^{-5}\text{sec}^{-1}$ at most, but, on the other hand, its lower limit seems about $2\times 10^{-5}\text{sec}^{-1}$. Therefore, perhaps we can find the most appropriate values of m and β when $1\leqq m\leqq 2$; if we take $m=2$, $\beta=2\sim 10\times 10^{-5}\,\text{km}^{-1}$, or, if we take $m=1$, $\beta>1\,\text{km}^0$ seems plausible.

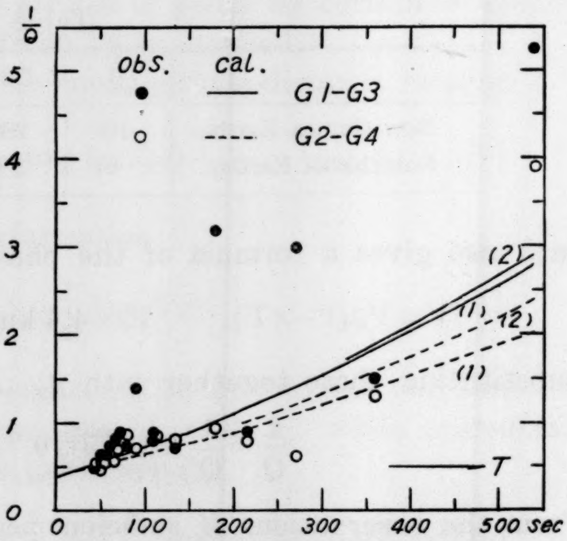

Fig. 1. Obs. and Cal. relations between $1/Q$ and period of wave of the New Guinea Earthq.
(1): $m=3/2$ $\beta=10^{-2}\text{km}^{-1/2}$
(2): $m=2$ $\beta=2\times 10^{-5}\text{km}^{-1}$
Obs.: Computed from Satô's paper.
$1/Q$ in 10^{-2}.

The four series of $1/Q$ value are calculated by the writer, though considerable errors from misreading might have been introduced, from Satô's figures of spectrum of the wave and γ-values, Figs. 3, 6, 9 and 11 in his paper, and are given in the Figs. 1 and 2 together with the calculated $1/Q$ when 1) $m=3/2$, $\beta=1\times 10^{-2}\,\text{km}^{-1/2}$, $1/Q_0=4\times 10^{-3}$, and 2) $m=2$, $\beta=2\times 10^{-5}\,\text{km}^{-1}$, $1/Q_0=4\times 10^{-3}$ respectively. These two examples of m and β are adopted from various considerations of Satô's results; to pick up from Table 3 a pair of m and β which satisfies the four series of $1/Q$-values at the same time is not so easy. This fact indicates namely that m and β will be obtained uniquely, or, at least, in a limited range of magnitudes. So far as these two earthquakes are concerned,

$m=3/2$ and $\beta=10^{-2}$ km$^{-1/2}$ seem more suitable than $m=2$ and $\beta=2\times10^{-5}$ km^{-1}, and, from these figures, characteristic internal friction $1/Q_0$ is estimated about 4×10^{-3}. Of course, it is absolutely difficult to arrive at a conclusion from these figures alone, but certainly we can expect in future study on the observations of high accuracy. In future study, our interest is also in a re-examination of observations concerning remarkably large $1/Q$, apparent in the figures for the wave of period of 60–100 sec: it may be attributed to selective absorption of wave energy by some mechanism of propagation of wave through the earth's crust, or, to a branch for $T<100$ sec expressed by large m and β. It is evident from the figures that observations and study of $1/Q$-value for the wave whose period $T<50$ sec have an important effect on the interpretation.

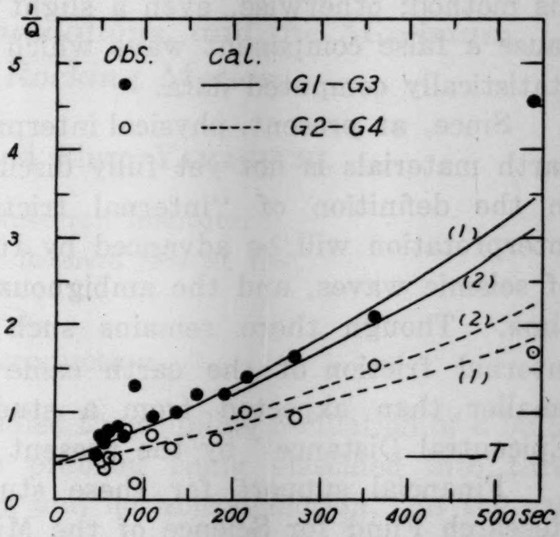

Fig. 2. Obs. and Cal. relation between $1/Q$ and period of wave of the Kamchatka Earthq.

(1): $m=3/2$ $\beta=10^{-2}$km$^{-1/2}$

(2): $m=2$ $\beta=2\times10^{-5}$km^{-1}

Obs.: Computed from Satô's paper. $1/Q$ in 10^{-2}.

5. Concluding remarks and acknowledgement

Before anything, the author expresses his respect to Dr. Y. Satô for his works that present such excellent data. His results of $1/Q$ alone, ingeniously and carefully obtained for so wide a range of period of wave from each earthquake, enable us to study the characteristic constant of friction. Although the systematic slip out of the observations from the expected linearity apparent in Fig. 10 and Fig. 3 of the two papers respectively by Ewing and Press will be well explained by the method in this paper, their method of analysis will give $1/Q$ of but a limited range of period from each earthquake, and, therefore, statistical studies of observations of many earthquakes are necessary to get sufficient numbers of data of $1/Q$ for the study of the "characteristic constant." In that respect, Satô's method, not to mention its theoretical lucidness, is extremely convenient giving sufficient number of data even from single earthquake. However, careful arrangement of observations and equally careful operation of the computor are strictly demanded in his method; otherwise, even a slight misreading of the seismogram will cause a false component wave which may be conveniently reduced in a statistically computed data.

Since, at present, physical interpretation of anelastic property of the earth materials is not yet fully discussed, there is something ambiguous in the definition of "internal friction of the earth." The physical interpretation will be advanced by future study of attenuation constant of seismic waves, and the ambiguous points will be cleared at the same time. Though there remains such ambiguous point in its definition, internal friction of the earth came out, in this paper, $4\cdot 10^{-3}$, a little smaller than expected from a study of "Maximum Amplitude and Epicentral Distance" by the present writer.

Financial support for these studies was partly granted from the Research Fund for Science of the Ministry of Education.

---

22. 表面波と地球の内部摩擦

地震研究所 吉山良一

地震波の走距離による減衰を調査して地球の内部摩擦係数 $1/Q$ を計算することは Gutenberg 等により取上げられてきた研究課題であるが，その最も困難な点は各観測所の観測状況が同一でないことと，それら観測所に達する地震波の energy が震源をでる時すでに必しも同一でないことであつた．Ewing と Press は同一地点に於ける Mantle Rayleigh wave の観測を使うことによつてこの困難を除去して成果をあげた．それにつづいて Satô は G-wave の観測を使つて更に精度の高い数値をだした．しかしこれら三氏が $1/Q$ としている値は純粋な内部摩擦 $1/Q_0$ の上に波面の拡散ともいうべき現象による影響があるらしく思われる．現在の資料ではそれを定量的にはもちろんのこと定性的にすら断言するには早すぎるかも知れないが，地震波の理論的な見通しが観測の整理方針延いては資料の精度に与える影響も無視し得ないと思われるので一応の計算結果を示した次第である．

Bulletin of the Earthquake Research Institute
Vol. 38 (1960), pp. 369-383

23. *Coupling Effect of Shear Vibrations of the Structure with Elastic Foundations, and the Maximum Response of Rocking Motion.*

By Yasuo SATÔ and Rinzo YAMAGUCHI,

Earthquake Research Institute.

(Read Oct. 22, 1957.—Received June 30, 1960.)

1. Introduction

In our previous paper[1] we studied the coupling oscillation of a building and an elastic foundation, the problem being classified into three kinds, namely the vertical, rocking and horizontal motion. In the case of the third kind of problem, we assumed a one mass system for simplicity in calculation. In the present paper, however, we assumed a uniform circular cylinder and studied the mechanical characteristics of the shear vibration of this system, the basic part of the calculation being adopted from the study of I. Toriumi[2] as before. Consequently, the following assumptions of his also hold in our study.

1) The stress is uniform within the circular base of the structure and vanishes outside this circle.

2) Purely horizontal seismic waves are incident from vertical downward.

Parameters are assumed to vary more extensively than before so that the obtained result may also be applicable to the structures such as piers. As an appendix formulas are given in the last chapter connecting the maximum amplitude and other physical quantities.

2. Notations

$A \quad =2\mu\pi r_0/(f_{1H}+if_{2H})$.

A_H Amplitudes of the incident waves. (Horizontal)

---

[1] Y. SATÔ and R. YAMAGUCHI, "Vibration of Buildings on the Ground," *Zisin* [ii], **9** (1957), 156. (in Japanese) Y. SATÔ and R. YAMAGUCHI, "Vibration of a Building upon the Elastic Foundation," *Bull. Earthq. Res. Inst.*, **35** (1957), 545.

[2] I. TORIUMI, "Vibrations in Foundations of Machines," *Technology Reports of the Osaka Univ.*, **5** (1955), 103. I. TORIUMI "Vibrations in Foundation of Machine on the Ground," *Zisin* [ii], **7** (1955), 216.

a_0	$=pr_0\sqrt{\rho/\mu}=pr_0/V_s=2\pi r_0/$(Wave length of S-waves).
a_{0MAX}	Values of a_0 that gives the maximum magnification.
E_0	$=\pi r_0^2$.
f_{1H}, f_{2H}	f_1 and f_2 in Toriumi's paper. (Horizontal motion)
l_0	Height of a structure from its base to the center of gravity.
p	Circular frequency of incident waves.
Q_H	Horizontal force transmitted from a structure to the ground.
r_0	Radius of a structure.
U_1	Displacement at the free surface. (Horizontal motion)
U_D	Additional displacement of the center of the base caused by the existence of a structure. (Horizontal motion)
U_R	Horizontal displacement of the center of gravity. (Rocking motion)
V_s, V_{s0}	Velocity of S-waves of the foundation and structure respectively.
$\|X\|$	$=\|U_R/U_1\|$.
$\|Y'\|$	$=\|l_0\Gamma_R/U_1\|$.
y_x	Absolute displcement of the structure at the height x.
Γ_R	Angle of inclination of a structure. (Rocking motion)
μ, μ_0	Rigidity of the foundation and structure respectively.
ρ, ρ_0	Density of the foundation and structure respectively.
ϑ_H	Phase difference between the incident waves and the oscillation of the structure. (Horizontal motion)
$\mathfrak{V}_{HB}$	Magnification of the displacement of the base.
$\mathfrak{V}_{HT}$	Magnification of the displacement of the top.

3. Shear vibration of a continuous body

We assume a uniform circular cylinder and solve the problem of its forced oscillation excited by purely horizontal waves incident from the vertical downward with the amplitude A_H and the circular frequency p. In Fig. 1 the oscillation at the free surface is, if there is no structure upon the surface

$$U_1=2A_H\exp(ipt)\ . \tag{3.1}$$

Put additional displacement caused by the existence of a structure as

$$U_D=U\exp(ipt)\ , \tag{3.2}$$

and the displacement of the structure at the height x relative to the base as

$$y = Y \exp(ipt) , \tag{3.3}$$

then the absolute displacement of the structure at x is

$$y_x = U_1 + U_D + y . \tag{3.4}$$

The equation of motion for the structure is

$$\rho_0 \frac{\partial^2 y_x}{\partial t^2} = \mu_0 \frac{\partial^2 y}{\partial x^2} . \tag{3.5}$$

Introducing the above relation we have

$$\frac{d^2 Y}{dx^2} + k^2 (2A_H + U + Y) = 0 , \tag{3.6}$$

where

$$k^2 = p^2 \rho_0 / \mu_0 = p^2 / V_{s0}^2 .$$

The solution of this equation is given in the form

$$2A_H + U + Y = \alpha \cos kx + \beta \sin kx , \tag{3.7}$$

where the constants α and β are determined by the boundary conditions.

At the base of the structure $x=0$, we have

$$Y = 0 \text{ and } E_0 \mu_0 \cdot dY/dx = Q_H , \tag{3.8}$$

where Q_H is the force related to the additional displacement U_D caused by the existence of a structure. From the theory of I. Toriumi we have

$$U_D = \frac{1}{A} Q_H \exp(ipt) , \tag{3.9}$$

or

$$AU = Q_H .$$

Using the equations in (3.8) the relations

$$2A_H + U = \alpha , \quad AU = E_0 \mu_0 k \beta , \tag{3.10}$$

are obtained.

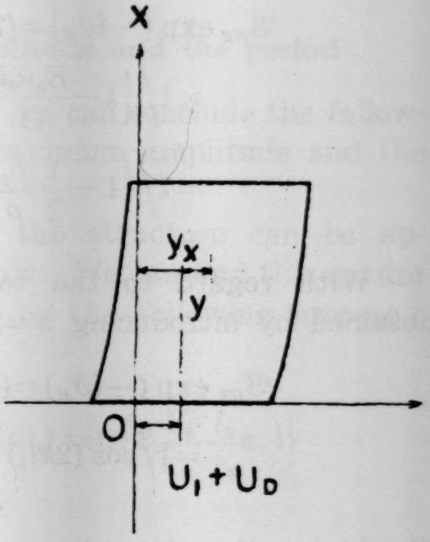

Fig. 1.

At the top of the structure $x=2l_0$ we have

$$E_0\mu_0 \cdot dY/dx=0 \ . \tag{3.11}$$

Consequently

$$-\alpha \sin(2kl_0)+\beta \cos(2kl_0)=0 \ . \tag{3.12}$$

From (3.10) and (3.12) α, β and U are obtained as follows:

$$\begin{aligned} \alpha &=2A_H \cdot A \cos(2kl_0)/\Delta \ , \\ \beta &=2A_H \cdot A \sin(2kl_0)/\Delta \ , \\ U &=2A_H \cdot E_0\mu_0 k \sin(2kl_0)/\Delta \ , \\ \Delta &=A \cos(2kl_0)-E_0\mu_0 k \sin(2kl_0) \ . \end{aligned} \tag{3.13}$$

Introducing the above expressions into (3.7), we have

$$2A_H+U+Y=2A_H \cdot A \cos\{k(2l_0-x)\}/\Delta \ , \tag{3.14}$$

or

$$Y=2A_H \cdot A[-\cos(2kl_0)+\cos\{k(2l_0-x)\}]/\Delta \ . \tag{3.15}$$

From the last expression the displacement of a structure at any height can be obtained.

The first expression of (3.10) is the absolute displacement of the base of the structure, therefore the magnification of the displacement is given in the following form:

$$\begin{aligned} \mathfrak{V}_{HB} \exp(-i\vartheta_H) &=(2A_H+U)/(2A_H) \\ &=1\Big/\left\{1-\frac{E_0\mu_0 k}{A}\tan(2kl_0)\right\} \\ &=1\Big/\left\{1-\frac{1}{2}\frac{\rho_0 V_{s0}}{\rho V_s}a_0(f_{1H}+if_{2H})\tan\left(2\frac{V_s}{V_{s0}}\frac{l_0}{r_0}a_0\right)\right\} \ . \end{aligned} \tag{3.16}$$

With regard to the top of the structure a similar expression is obtained by introducing $x=2l_0$ into equation (3.14). Namely

$$\begin{aligned} \mathfrak{V}_{HT} \exp(-i\vartheta_H) &=(2A_H+U+Y)_{x=2l_0}/(2A_H) \\ &=1\Big/\cos(2kl_0)\left\{1-\frac{E_0\mu_0 k}{A}\tan(2kl_0)\right\} \ . \end{aligned} \tag{3.17}$$

Combining the above two expressions, we have

$$\mathfrak{V}_{HT}=\mathfrak{V}_{HB}\Big/\cos\left(2\frac{V_s}{V_{s0}}\frac{l_0}{r_0}a_0\right). \tag{3.18}$$

3.1 Numerical computation of $\mathfrak{V}_{HB}$ and $\mathfrak{V}_{HT}$.

In this section the result of numerical computation is given assuming various values for the quantities in (3.16) (3.17) and (3.18).

At first we assume that $\rho_0/\rho=1/4$.

Fig. 2 gives the relation $\mathfrak{V}_{HB}$ versus $a_0=pr_0/V_s$, the parameter being the (l_0/r_0), and V_s and V_{s0} are assumed to be equal. A similar relation with regard to $\mathfrak{V}_{HT}$ is given in Fig. 3.

In Fig. 2 the zero points of curves correspond to the resonance of the structure. General tendencies of these curves are similar to those of our previous paper, but we can find second resonances in the present case.

Fig. 4 gives $\mathfrak{V}_{HB}$. In this figure, the parameter is the ratio (V_s/V_{s0}), and $(l_0/r_0)=1.0$ is assumed. Fig. 5 is a similar relation with regard to $\mathfrak{V}_{HT}$. Figs. 6-9 are the similar graphs, in which $(l_0/r_0)=1.5$ and 2.0.

In Figs. 10-13 the angle of phase difference (ϑ_H) is given corresponding to the above cases. As is seen in the equations (3.16) and (3.17) there is no difference in the phase angles for the base and the top of the structure.

If the vibrating structure is a building we may safely assume that $\rho_0/\rho=1/4$. However, for the case such as piers we must adopt a larger value of (ρ_0/ρ). The cases of that ρ_0/ρ being assumed to be 1.0 and 2.0 are shown in § 4.

4. Relation between the maximum amplitude and the period

Summalizing the results obtained above we can conclude the following characteristics which hold between the maximum amplitude and the period.

1) Maximum amplitude of the base of the structure can be approximately expressed as a function of a_0 only. We can find this nature in Fig. 14, but it is also proved analytically by the following process.

From (3,16)

$$\begin{aligned}\mathfrak{V}_{HB}(-i\vartheta_H)&=1\Big/\left\{1-\frac{1}{2}\frac{\rho_0}{\rho}\frac{V_{s0}}{V_s}a_0(f_{1H}+if_{2H})\tan\left(2\frac{V_0}{V_{s0}}\frac{l_0}{r_0}a_0\right)\right\}\\&\equiv 1/\{1-c_0(f_{1H}+if_{2H})\}\\&=\exp(-i\vartheta_H)/\sqrt{(1-c_0f_{1H})^2+c_0^2f_{2H}^2}\end{aligned} \tag{4.1}$$

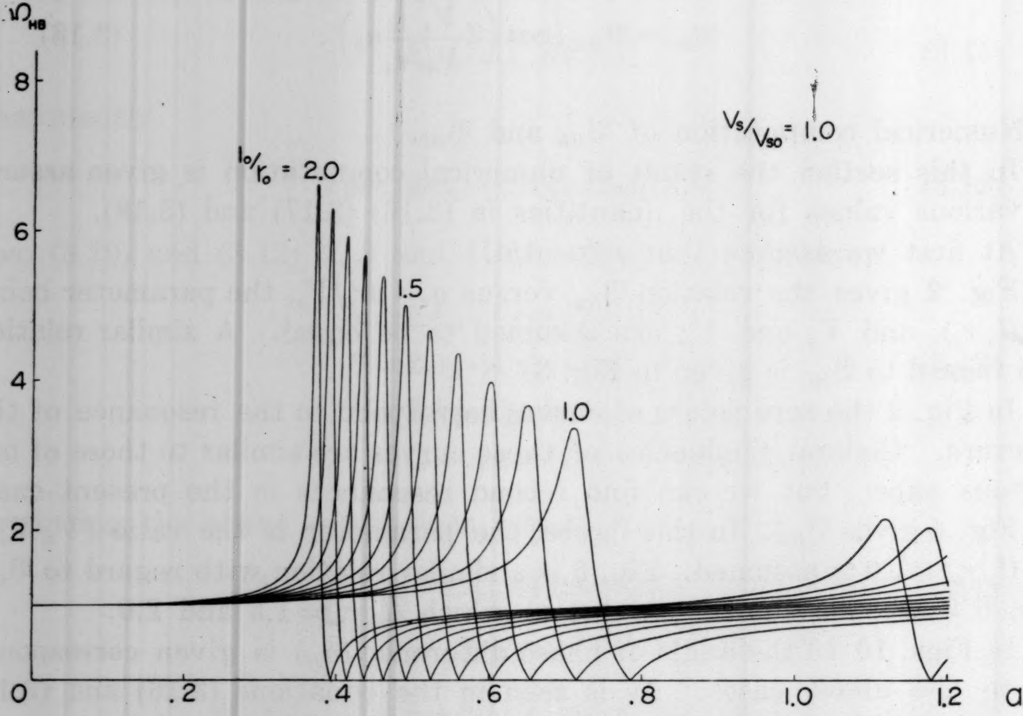

Fig. 2. Amplitude of the base of structure for the case $V_s = V_{s0}$.

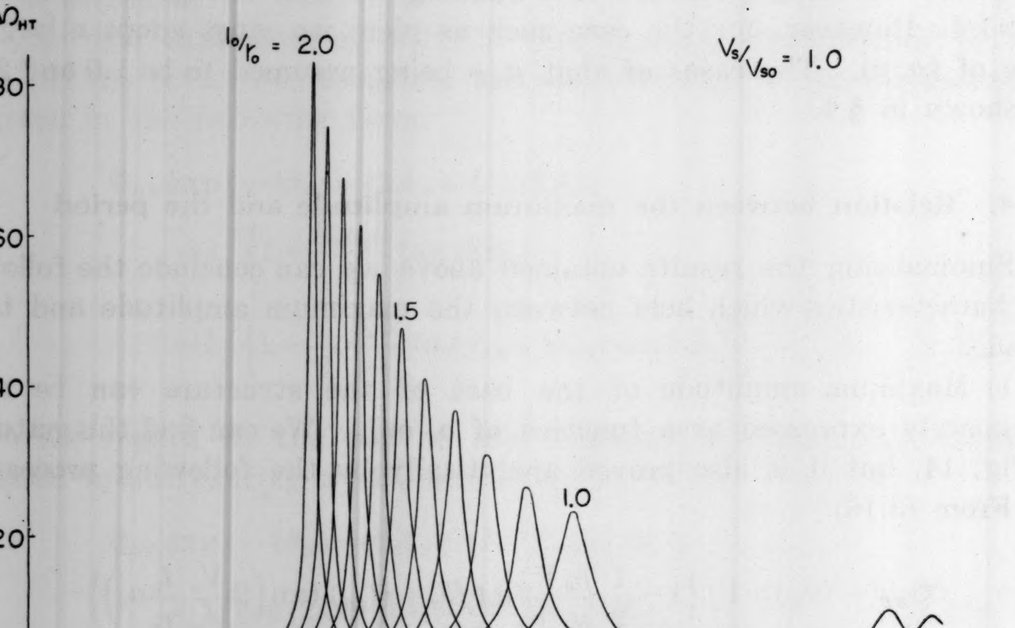

Fig. 3. Amplitude of the top of structure for the case $V_s = V_{s0}$.

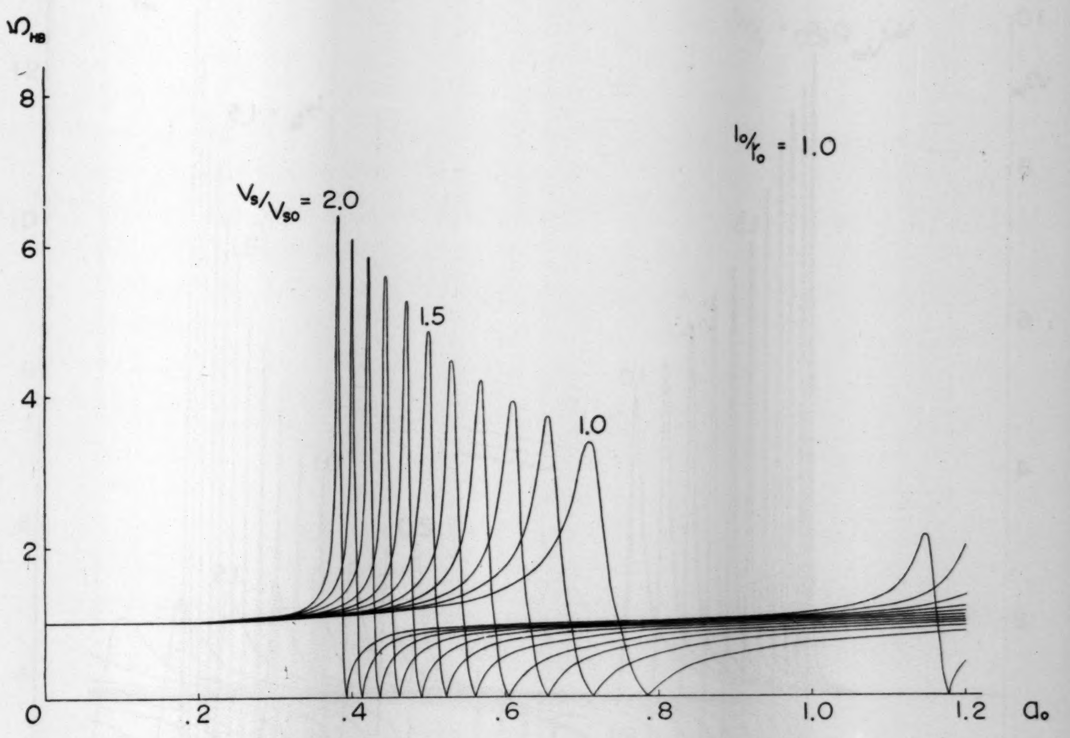

Fig. 4. Amplitude of the base of structure for the case $l_0/r_0=1.0$.

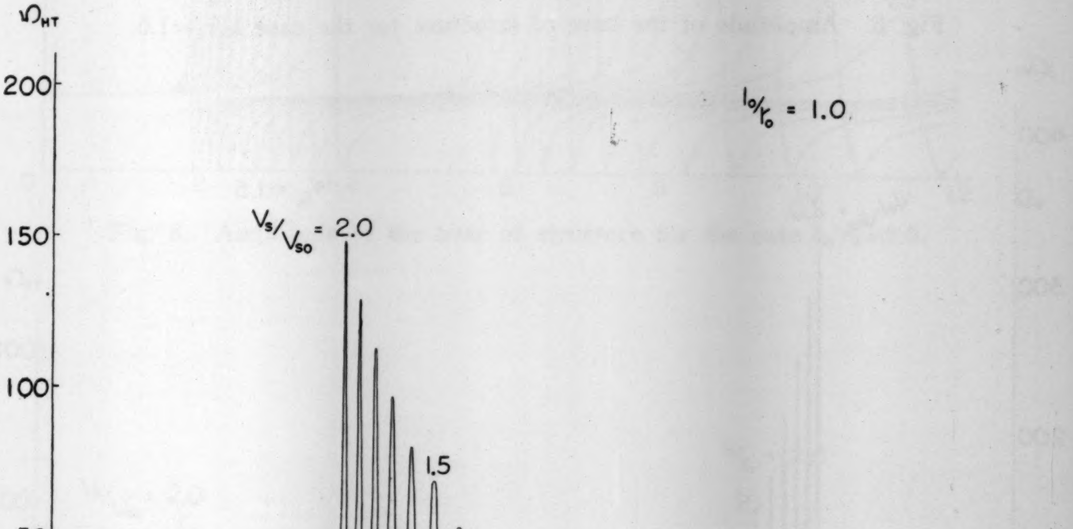

Fig. 5. Amplitude of the top of structure for the case $l_0/r_0=1.0$.

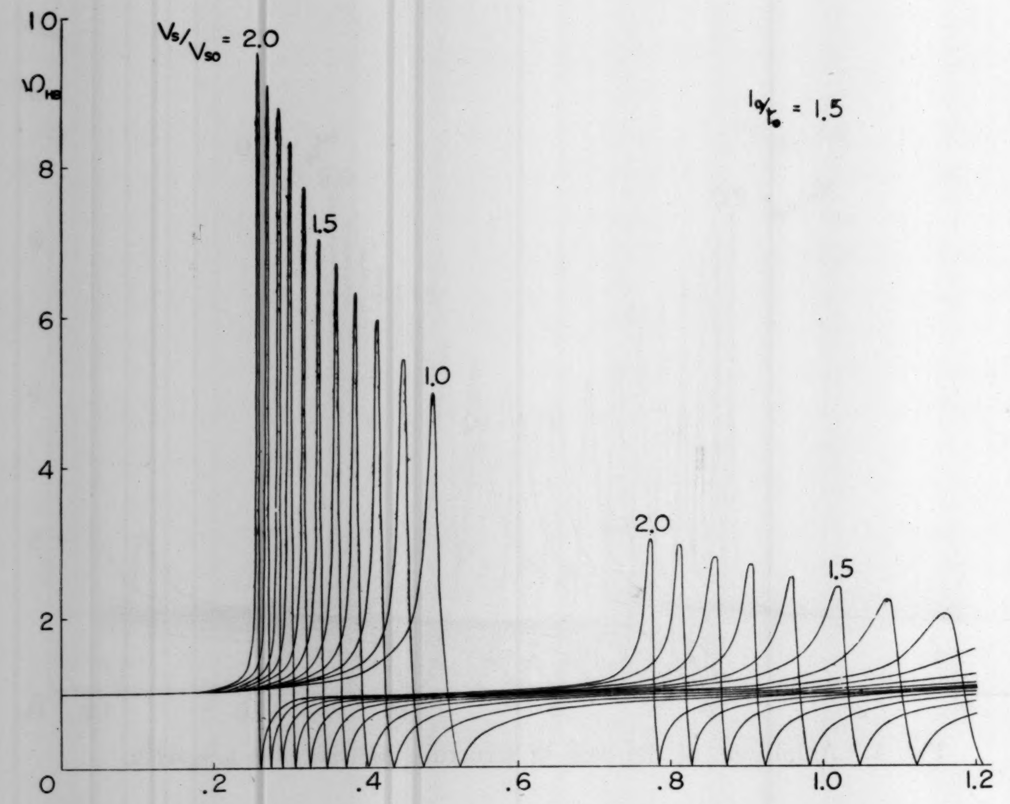

Fig. 6. Amplitude of the base of structure for the case $l_0/r_0=1.5$.

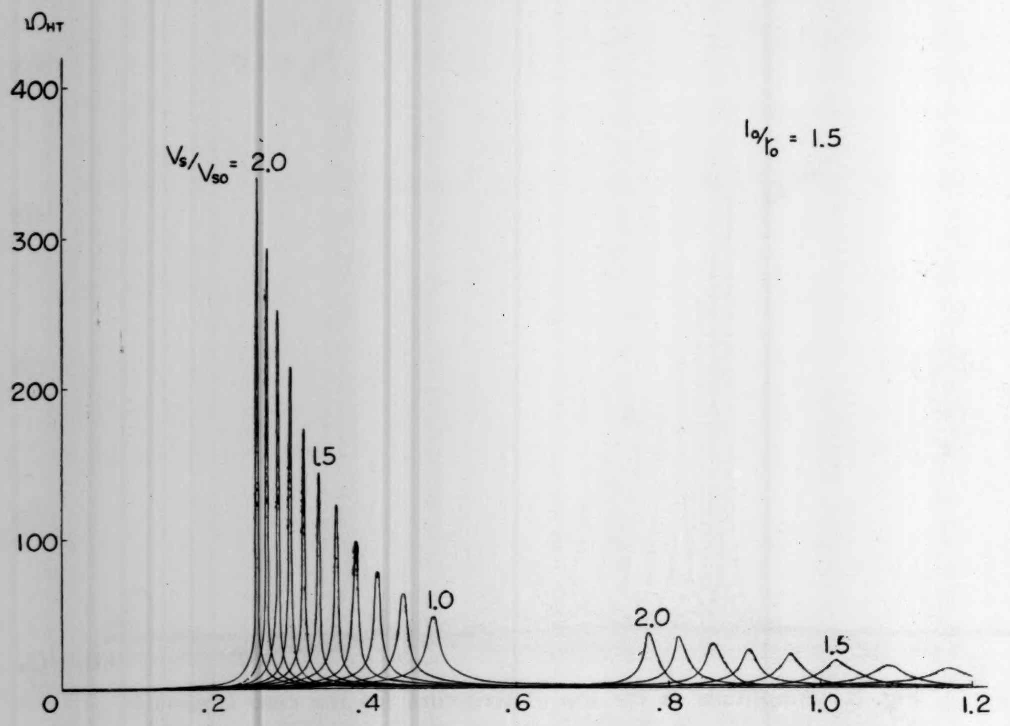

Fig. 7. Amplitude of the top of structure for the case $l_0/r_0=1.5$.

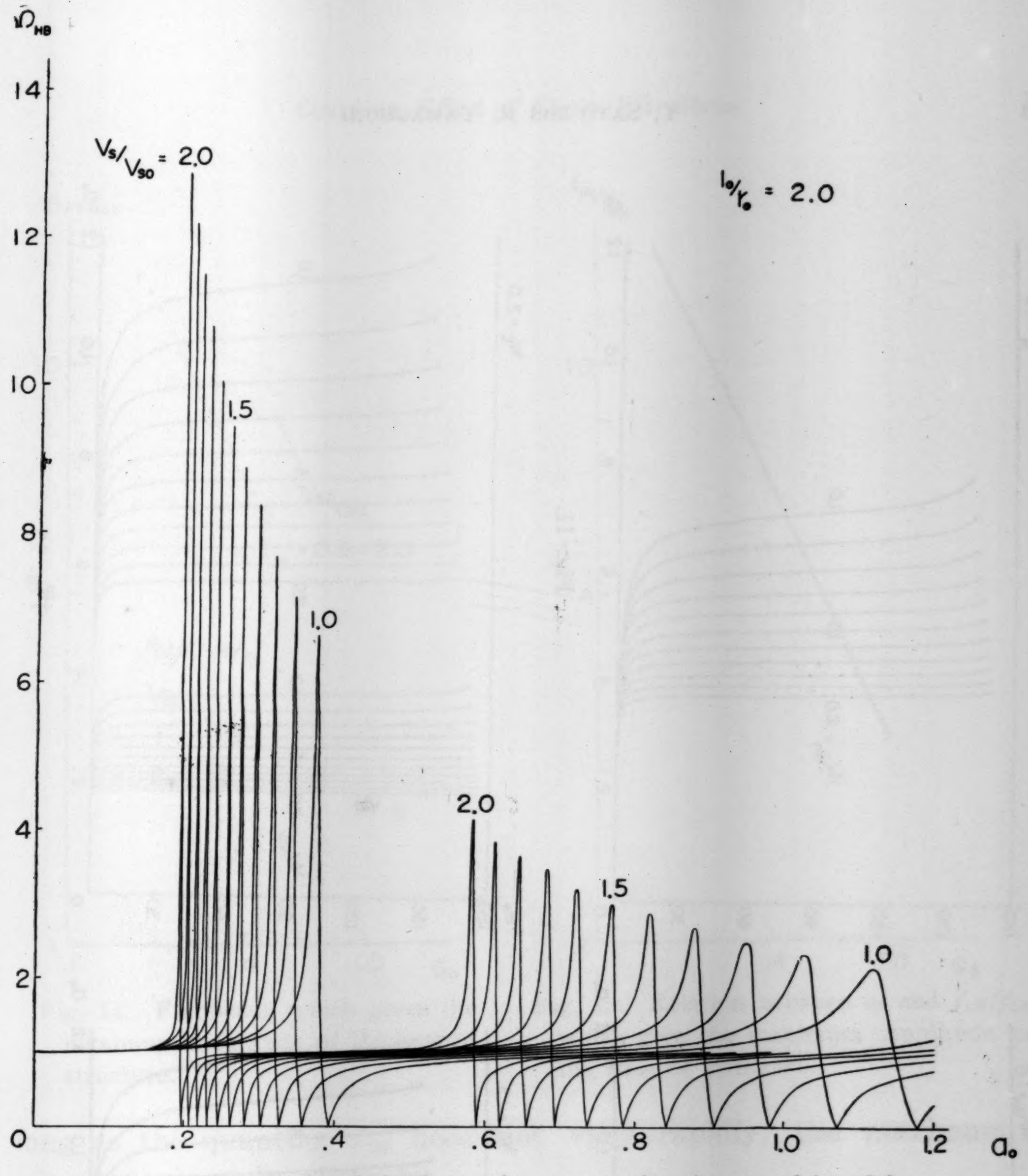

Fig. 8. Amplitude of the base of structure for the case $l_0/r_0=2.0$.

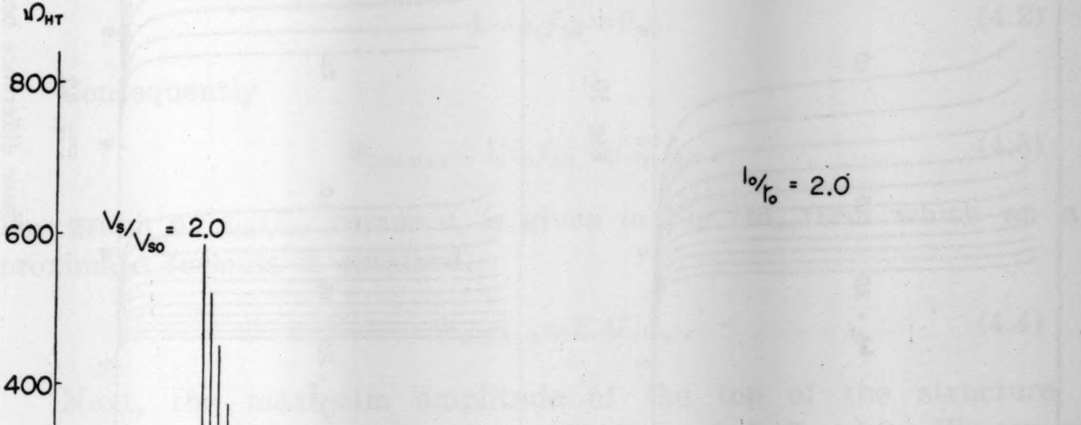

Fig. 9. Amplitude of the top of structure for the case $l_0/r_0=2.0$.

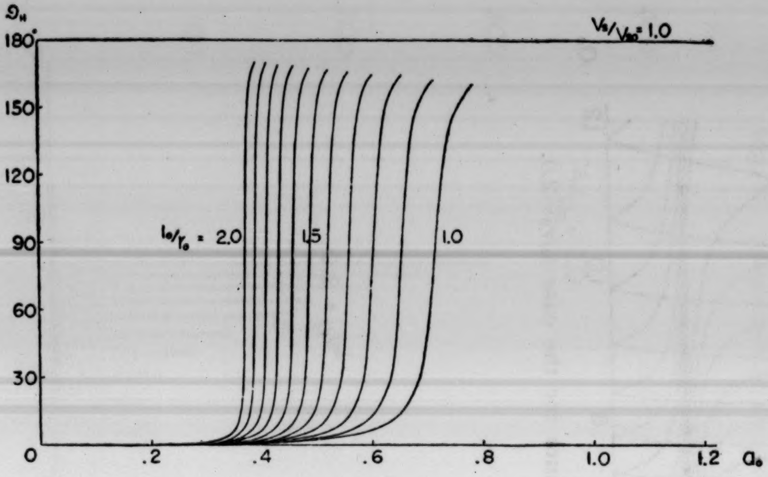

Fig. 10.

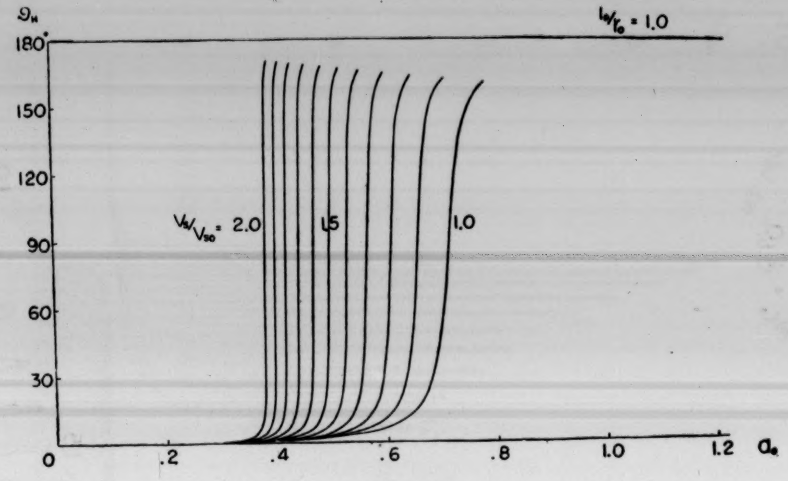

Fig. 11.

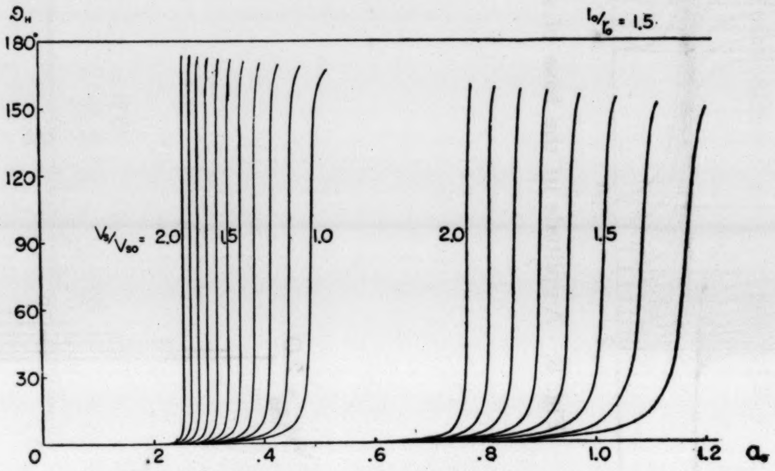

Fig. 12.

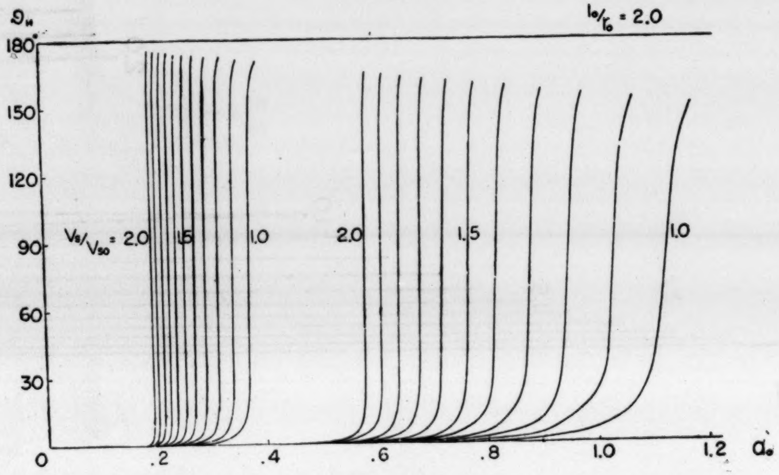

Fig. 13.

Phase difference between the incident waves and the oscillation of structure.

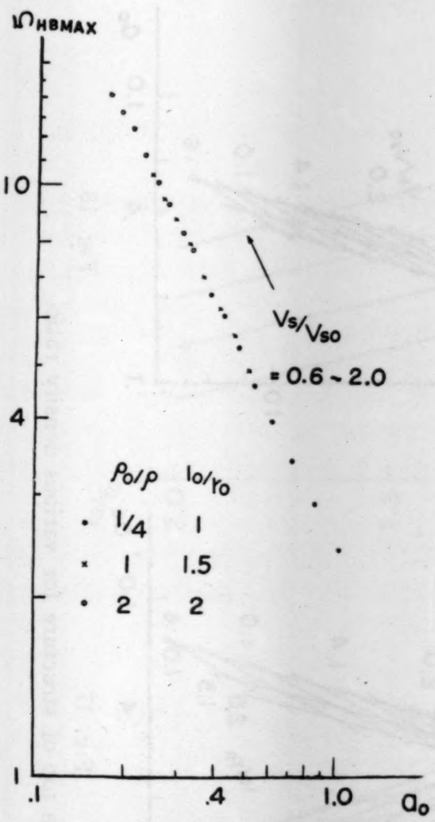

Fig. 14. Frequency which gives the maximum amplitude of the base of structure.

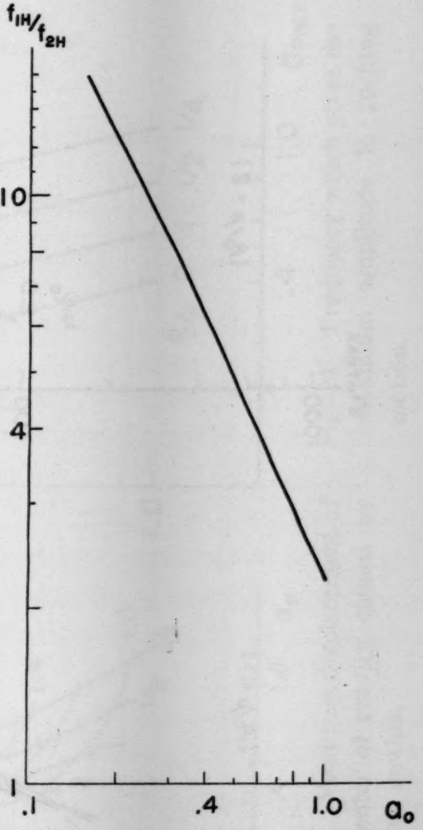

Fig. 15. Relation between a_0 and f_{1H}/f_{2H} which give the maximum amplitude of the base of structure.

So long as the quantity f_{2H} does not vary rapidly, the maximum of $\mathfrak{V}_{HB}$ is approximately given by

$$1 - c_0 f_{1H} = 0\ . \tag{4.2}$$

Consequently

$$\mathfrak{V}_{HB,\mathrm{MAX}} \doteqdot 1/c_0 f_{2H} = f_{1H}/f_{2H}\ . \tag{4.3}$$

The graph of f_{1H}/f_{2H} versus a_0 is given in Fig. 15, from which an approximate formula is obtained.

$$\mathfrak{V}_{HB,\mathrm{MAX}} \doteqdot 2.45/a_0\ . \tag{4.4}$$

Next, the maximum amplitude of the top of the structure is given in Fig. 16 when $\rho_0/\rho = 1/4$. (Cf. Figs. 3, 5, 7 and 9.) We can get the following approximation formulas.

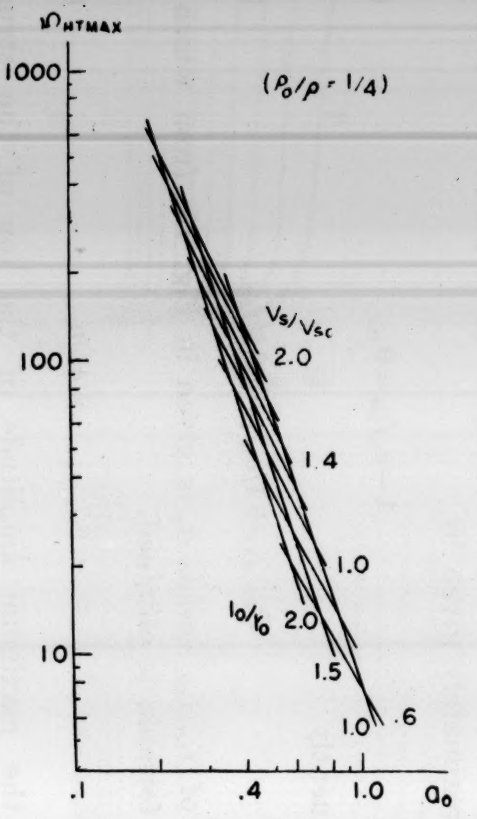

Fig. 16.

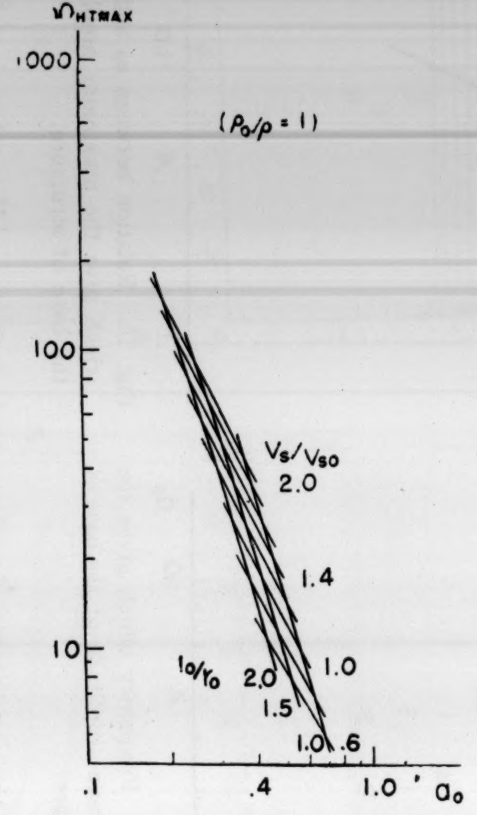

Fig. 17.

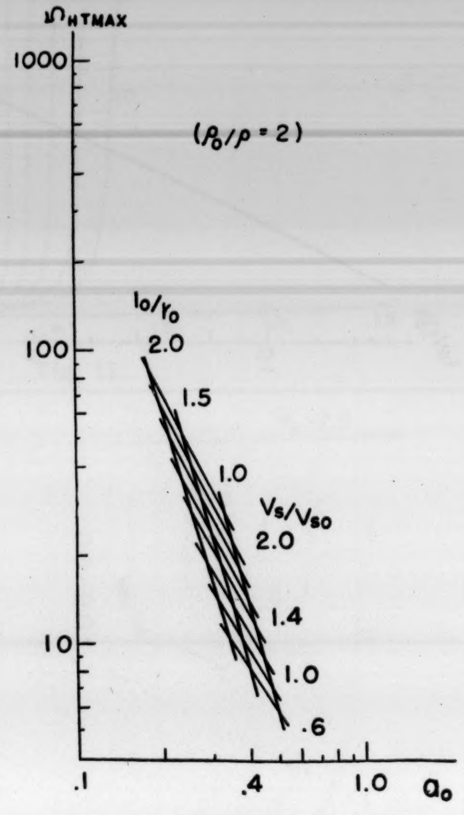

Fig. 18.

Maximum amplitudes of the top of structure for various density ratio.

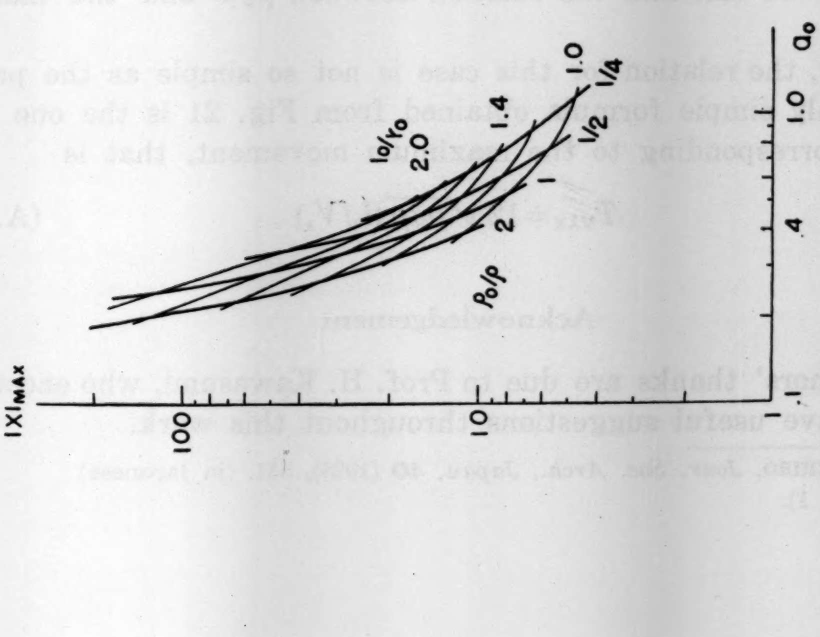

Fig. 19. Maximum amplitude of the center of gravity in horizontal motion.

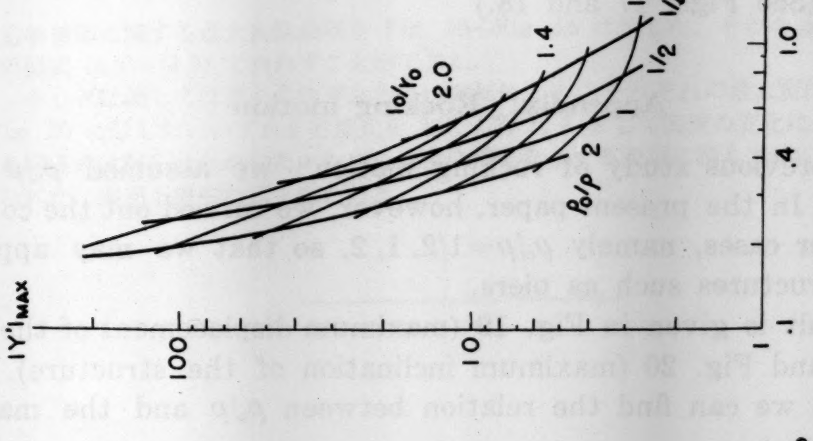

Fig. 20. Maximum displacement of the center of gravity caused by angular motion.

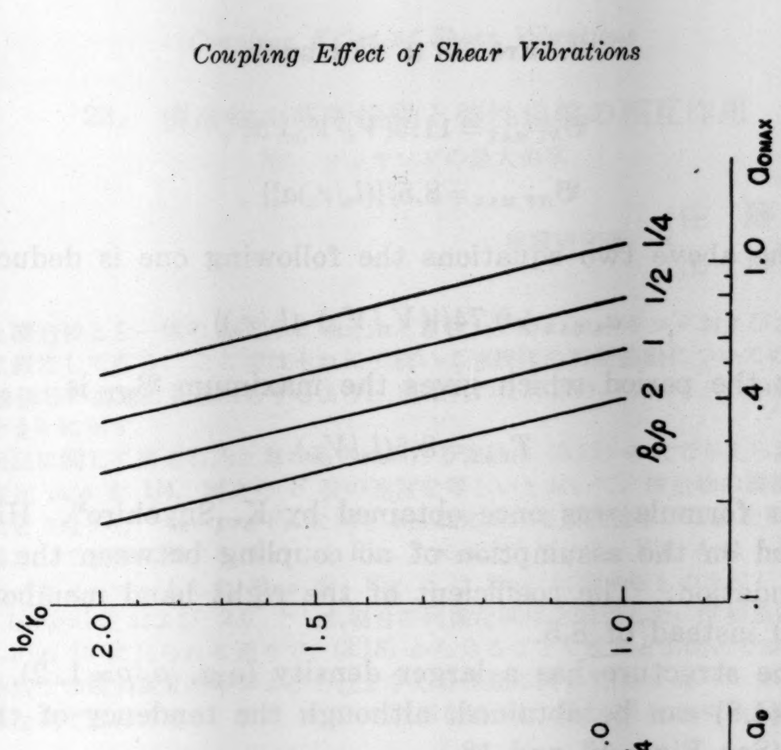

Fig. 21. Frequency which gives the maximum amplitude in rocking motion.

$$\mathfrak{V}_{HT,\mathrm{MAX}} \doteqdot 11.5(V_s/V_{s0})/a_0^2 \, , \tag{4.5}$$

$$\mathfrak{V}_{HT,\mathrm{MAX}} \doteqdot 8.5/\{(l_0/r_0)a_0^3\} \, . \tag{4.6}$$

Combining the above two equations the following one is deduced.

$$a_{0,\mathrm{MAX}} \doteqdot 0.74/\{(V_s/V_{s0})\cdot(l_0/r_0)\} \, . \tag{4.7}$$

Consequently the period which gives the maximum $\mathfrak{V}_{HT}$ is

$$T_{\mathrm{MAX}} \doteqdot 8.5(l_0/V_{s0}) \, . \tag{4.8}$$

A similar formula was once obtained by K. Suyehiro[3]. His calculation was based on the assumption of no coupling between the structure and the foundation. The coefficient of the right hand member of (4.8) was then 8.0 instead of 8.5.

When the structure has a larger density (e.g. $\rho_0/\rho=1, 2$), no simple formula like (4.8) can be obtained, although the tendency of the curves are similar. (See Figs. 17 and 18.)

Appendix. Rocking motion

In our previous study of rocking motion[4] we assumed ρ_0/ρ to be always 1/4. In the present paper, however, we carried out the computation for other cases, namely $\rho_0/\rho=1/2, 1, 2$, so that we may apply the theory to structures such as piers.

The result is given in Fig. 19 (maximum displacement of the center of gravity) and Fig. 20 (maximum inclination of the structure). From these figures we can find the relation between ρ_0/ρ and the maximum movement.

However, the relation for this case is not so simple as the previous one. The only simple formula obtained from Fig. 21 is the one giving the period corresponding to the maximum movement, that is

$$T_{\mathrm{MAX}} \doteqdot 12\sqrt{\rho_0/\rho}\,(l_0/V_s) \, . \tag{A.1}$$

Acknowledgement

The authors' thanks are due to Prof. H. Kawasumi, who encouraged them and gave useful suggestions throughout this work.

---

[3] K. SUYEHIRO, *Jour. Soc. Arch., Japan*, **40** (1926), 531. (in Japanese)

[4] *loc. cit.*, 1).

23. 構造物の剪断振動と弾性地盤の相互作用

附: ロッキングの最大倍率

地震研究所 {佐藤泰夫
山口林造

1. 地盤と構造物とを一体の振動系と考えたときの上下動，ロッキングおよび水平動についての計算はすでに報告してある．ここではそれに引続いて連続体の剪断振動についての振動性能を求めた．そして橋脚等の振動にも適用しうるよう，前に行つた計算のパラメーターの範囲を拡張した．

2. 記号を§2 に示す．

3. 剪断振動に関して構造物内任意の高さにおける変位は (3.15) の式で与えられる．先づ構造物と地盤の密度比 ρ_0/ρ を 1/4，両方の S 波の速度を等しいとおいて，構造物の縦横の比 l_0/r_0 をパラメーターにとりながら，$a_0=pr_0/V_s$ に対する底面における変位倍率 $\mathfrak{V}_{HB}$ を示したのが Fig. 2 である．同様にして頂部に関する $\mathfrak{V}_{HT}$ は Fig. 3 に示されている．Fig. 4 は $l_0/r_0=1$ とおき，S 波の速度比をパラメーターとした $\mathfrak{V}_{HB}$ を，Fig. 5 は $\mathfrak{V}_{HT}$ に関するものを示している．Fig. 6〜Fig. 9 には $l_0/r_0=1.5$ および 2.0 とした場合の同様な関係を図示した．位相差に関してはそれぞれ Fig. 10〜Fig. 13 に見られる通りで，(3.18) から分るごとく底面と頂部とでは相違がない．

4. 構造物底面の最大変位倍率およびそれを与える周期に関しては Fig. 14 から近似的に (4.4) のような簡単な式で表わされる．また (4.3) の関係を使つた Fig. 15 にも明らかにそのことが見られる．

次に構造物頂部に関する最大変位倍率を Fig. 16〜Fig. 18 に示した．その中 $\rho_0/\rho=1/4$ の場合には簡単な近似式 (4.5)〜(4.8) で表わすことができた．

附．ロッキングに関しては重心の水平あるいは回転による，それぞれの最大変位倍率を Fig. 19 および Fig. 20 に示した．いずれも密度比を 1/4, 1/2, 1, 2 として密度の変化に伴う様子を調べたが，簡単な関係式は得られなかつた．ただ最大変位倍率を与える周期に関しては，(A.1) のような関係が求められた．実用上便利な式と思われる．

BULLETIN OF THE EARTHQUAKE
RESEARCH INSTITUTE
Vol. 38 (1960), pp. 385-401

24. Rayleigh Wave Dispersions across the Oceanic Basin around Japan (Part II).

By Tetsuo A. SANTÔ,

Earthquake Research Institute.

(Read May 24, 1960.—Received June 28, 1960.)

1. Introduction

In the previous paper,[1] the writer investigated the dispersion of Rayleigh waves which passed through the various oceanic paths around Japan.

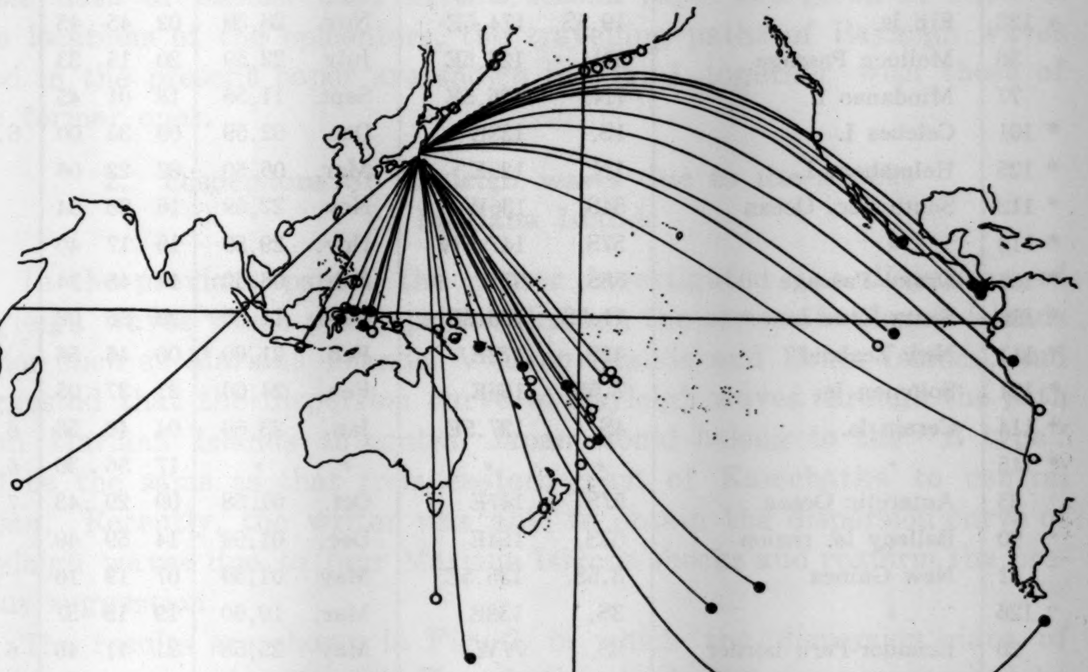

Fig. 1. Epicenters and travelling paths of Rayleigh waves across the oceanic basin. The epicenters newly added and of the previous ones are represented by black and white circles respectively.

---

[1] T. A. SANTÔ, "Observation of Surface Waves by Columbia-type Seismograph Installed at Tsukuba Station, Japan (Part I).—Rayleigh Wave Dispersions across the Oceanic Basin—," *Bull. Earthq. Res. Inst.*, **38** (1960), 237.

Table 1.

No.	District	Epicenter (λ, φ)		Date		Origin Time (G.M.T.)			Mag.
						h	m	s	
78	Kamchatka	63N,	160E	Oct.	10,58	08	30	19	
* 120	Mariana Is.	19.5N,	145.5E	Aug.	14,58	02	28	25	
* 117	〃	21.5N,	143.5E	Jan.	31,60	03	34	42	
* 118	〃	22N,	144E	Jan.	30,60	18	38	10	
* 119	〃	21.5N,	142.5E	〃	〃	17	56	05	
* 104	Galapagos Is.	4.5S,	104.5W	Aug.	27,58	02	25	32	
* 124	Peru	15S,	75W	Jan.	15,60	09	30	24	6.5
27	Northern Chile	21S,	69W	July	11,58	19	10	20	6.5
18	Pacific Ocean	5S,	106.5W	July	12,58	00	48	30	
30	Chile-Argentin	33.5S,	69.5W	Sept.	4,58	21	51	08	7
10	Kermadec Is.	29S,	176.5W	Sept.	29,59	15	41	57	6.5
* 127	Loyality Is.	22.5S,	174E	Mar.	30,60	15	19	30	
* 128	Fiji Is.	19.5S,	174.5E	Nov.	28,59	02	45	45	
56	Molluca Passage	2N,	126.5E	July	22,59	20	15	33	
77	Mindanao I.	7N,	126.5E	Sept.	11,58	18	01	45	
* 101	Celebes I.	1S,	123E	Dec.	02,59	09	34	00	6.55
* 125	Helmahera I.	1N,	129E	Mar.	06,60	02	22	06	
* 112	South Pac. Ocean	54S,	136W	Nov.	22,59	16	26	34	
* 113	〃	57S,	147.5W	Nov.	29,59	19	17	40	
* 105	Drake Passage	58S,	67W	Feb.	08,60	12	45	34	
* 116	Santa Cruz Is.	11.5S,	166.5E	Feb.	11,60	20	56	08	
* 111	New Zealand	42S,	173E	Feb.	21,60	00	46	56	
* 121	Solomon Is.	7.5S,	156E	Feb.	24,60	21	37	05	
* 114	Ceram Is.	4S,	127.5E	Jan.	23,60	04	40	56	6.5
* 115	〃	〃	〃	〃	〃	17	56	30	6.5
33	Antarctic Ocean	57S,	147E	Oct.	01,58	09	29	43	7
* 90	Balleny Is. region	63S,	154E	Dec.	01,59	14	59	40	
21	New Guinea	3.5S,	135.5E	May	01,59	07	19	16	
* 126	〃	3S,	138E	Mar.	19,60	19	15	37	
20	Ecuador-Peru border	3S,	77W	May	25,58	21	11	45	6.5
* 92	Costa Rica	8N,	85W	June	06,58	09	11	18	6.75
* 105	〃	5.5N,	82.5W	〃	〃	19	15	28	6
* 122	Panama	7.5N,	82W	Mar.	28,60	00	13	38	
* 123	Jalisco	20N,	105.5W	May	28,60	20	15	46	

* Newly added shocks.

Through the previous investigations, two important facts were observed. The first one was that the dispersions of Rayleigh waves with the paths across northern and eastern Pacific Ocean were quite the same as each other, while they gradually became continental when the path shifts from southern to western part. The second fact was that the dispersion of Rayleigh waves which passed near or over the series of volcanic islands beside trenches showed remarkable difference from the dispersion with the other ordinary oceanic paths. We called the former dispersive feature "B type" and the latter "A type."

After the first paper was written, the writer was able to study the dispersion of Rayleigh waves due to twenty-four shocks which also passed across the various regions of oceanic basin and reaffirm these conclusions. As before, the vertical component records of Columbia type seismographs at Tsukuba Station were used. The epicenters, dates and other data of shocks used in this second paper are given in Table 1. The locations of the epicenters, the travelling paths of Rayleigh waves used in the present paper are shown in Fig. 1 together with those of the former ones.

2. Dispersions of Rayleigh waves due to the shocks of Mariana Islands

In the previous paper, the writer investigated the dispersion of Rayleigh waves which partly passed through the series of volcanic islands region such as Mariana Islands, Volcano Islands and Bonin Islands, and suggested that the dispersion curve of Rayleigh waves through the path from Mariana Islands to central Japan would belong to the "B type" and be the same as that from eastern coast of Kamchatka to central Japan. Recently, the writer was able to obtain the dispersion curve of Rayleigh waves due to four Mariana Islands shocks and reaffirm the previous suggestion.

The results are shown in Fig. 2, in which the dispersion data of Rayleigh waves due to the Kamchatka shock (78) are represented by white circles. This figure shows that the Rayleigh wave dispersion due to the Mariana Islands shock (120) resembles well that due to the Kamchatka shocks. Further, it is interesting that the dispersive character of these four Mariana Islands shocks shows the same nature as those due to the Kurile Islands shocks. That is, just as was the case of the Kurile Islands shocks,[2] the dispersive character due to each shock

---

[2] *loc. cit.* 1). p. 232.

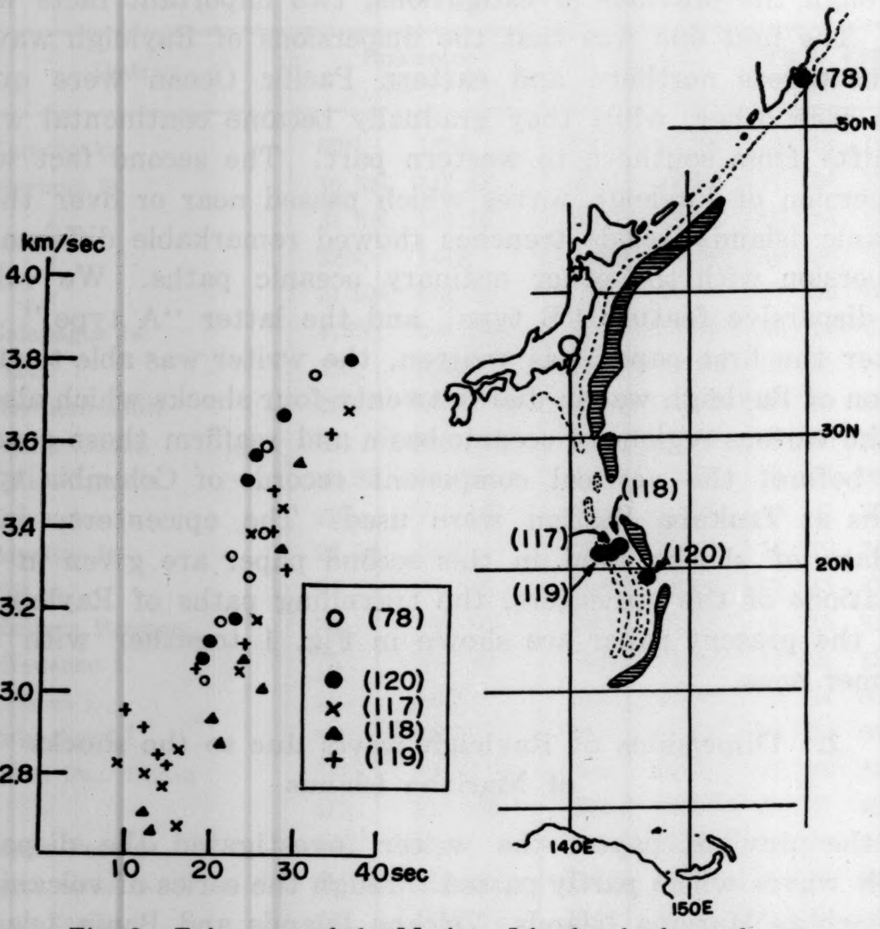

Fig. 2. Epicenters of the Mariana Islands shocks and group velocities of Rayleigh waves due to them. The dispersion data due to the Kamchatka shock (78) are also represented for comparison.

differs very much in spite of rather compact distribution of their epicenters. Though research into the cause of these facts has to be postponed to the future, it must be remarked here that this fact was obtained for the same condition when the epicenters and the travelling paths of Rayleigh waves are both located closely beside the trenches.

3. Additional dispersion data for the paths across the northern, central and eastern Pacific Ocean

Adding the new dispersion data due to the shocks of Galapagos Islands (104) and Peru (124), the dispersion of Rayleigh waves through the northern, central and eastern Pacific Ocean can be summarized in Fig. 3. As is well recognized in this figure, they lie on one smooth

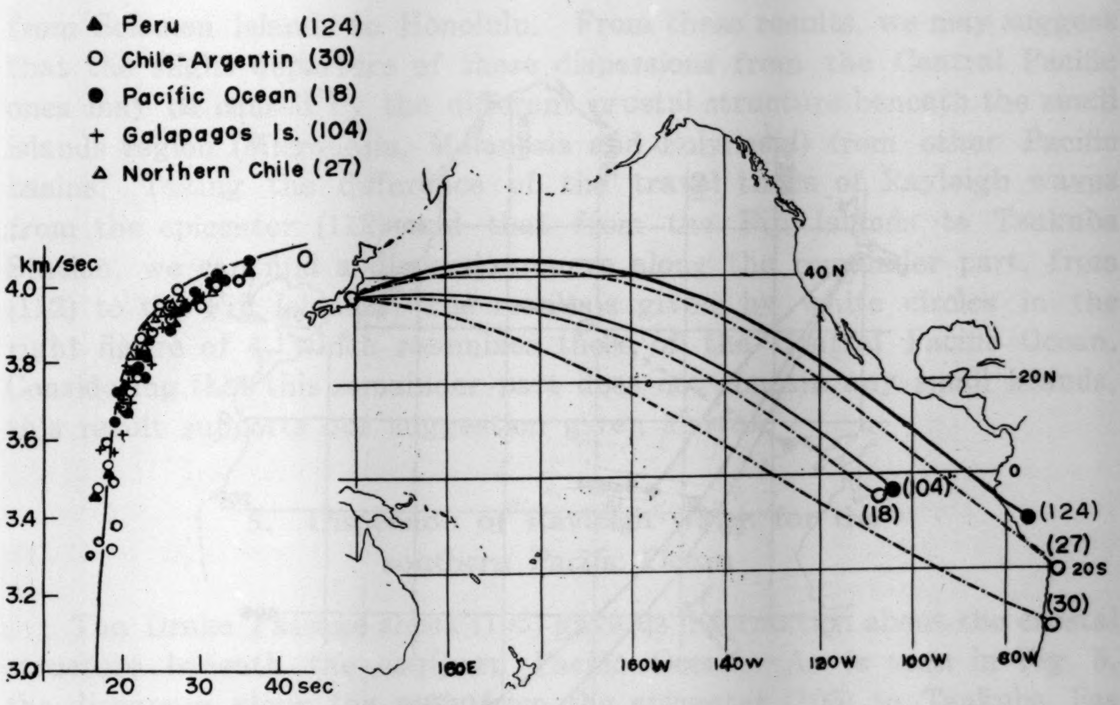

Fig. 3. Left: Dispersive characters of Rayleigh waves for the paths in the northern Pacific Ocean.

Right: Epicenters (black circles) and travelling paths (solid curves) newly studied and those for the previous ones (white circles and broken curves respectively).

curve which lies quite near the theoretical curve (O) of oceanic ones,[3] which fact tells us that the average crustal structures of these regions are all the same and typically oceanic.

4. Dispersion of Rayleigh waves due to the South Pacific Ocean shocks

Dispersion of Rayleigh waves due to two shocks in South Pacific Ocean (112, 113) shows, as is seen in Fig. 4, a slight difference from those due to the Central Pacific Ocean shocks. These are similar to the dispersion curve due to the shocks of Samoa Islands, which was given in the previous paper. It must be noticed that they are also similar to the dispersion obtained by M. Ewing and F. Press[4] for the path

---

[3] W. S. JARDETZKY, F. PRESS, "Crustal Structure and Surface Wave Dispersion, Part III; Theoretical Dispersion Curves for Suboceanic Rayleigh Waves," *Bull. Seis. Soc. Amer.*, **43** (1953), 137.

[4] M. EWING, F. PRESS, "Crustal Structure and Surface-Wave Dispersion, Part II: Solomon Islands Earthquake of July 29 1950," *Bull. Seis. Soc. Amer.*, **24** (1952), 315.

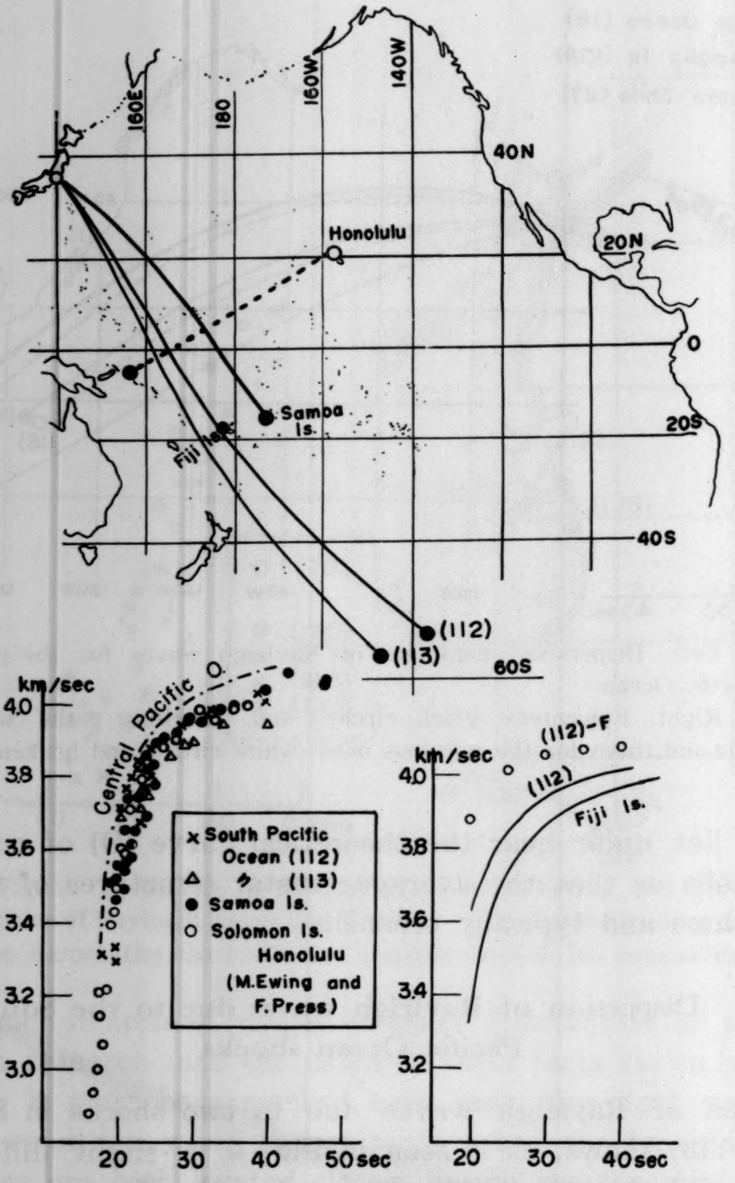

Fig. 4. Dispersive characters of Rayleigh waves due to two South Pacific Ocean shocks (112) and (113). Dispersion data and travelling paths for the Solomon Islands shock and for the Samoa Islands shock are also shown for comparison. White circles in the right figure mean the group velocities obtained by subtracting the travel times for the Fiji Islands shock from those for the shock (112).

from Solomon Islands to Honolulu. From these results, we may suggest that the slight departure of these dispersions from the Central Pacific ones may be caused by the different crustal structure beneath the small islands region (Micronesia, Melanesia and Polynesia) from other Pacific basins. Taking the difference of the travel times of Rayleigh waves from the epicenter (112) and that from the Fiji Islands to Tsukuba Station, we can find a dispersion curve along the remainder part, from (112) to the Fiji Islands. The result is given by white circles in the right figure of 4, which resembles those of the Central Pacific Ocean. Considering that this remainder part does not contain any small islands, this result supports our suggestion given above.

5. Dispersion of Rayleigh waves for the southern Pacific Ocean

The Drake Passage shock (105) gave us information about the crustal structure beneath the southern Pacific Ocean. As is seen in Fig. 5, the dispersion along the path from the epicenter (105) to Tsukuba lies

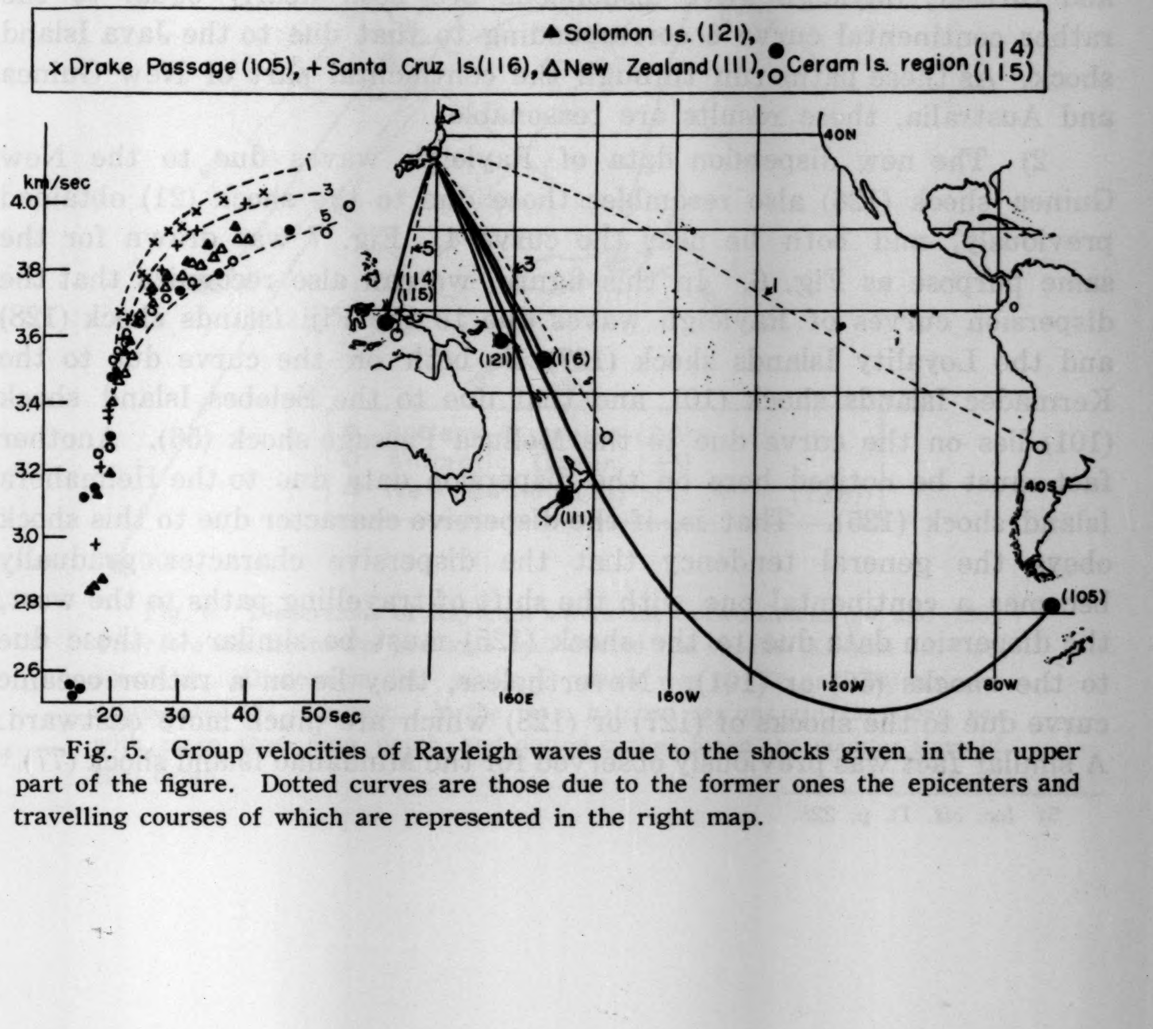

Fig. 5. Group velocities of Rayleigh waves due to the shocks given in the upper part of the figure. Dotted curves are those due to the former ones the epicenters and travelling courses of which are represented in the right map.

quite near the curve 1 (for central or northern Pacific Ocean). On the other hand, the dispersive character due to the Santa Cruz Islands shock (116) resembles the dispersion curve 3 which was obtained previously by the Kermadec Islands shocks. (The path is represented by a broken line in the map.) From these facts, we can suggest that the dispersion curve along the path from the epicenter (105) to (116) must be as oceanic as the curve 1. It means that the crust of the earth along the path from the epicenter (105) to (116) is as thin as northern or central Pacific Ocean.

The Ceram Island shocks (114) and (115) show the same dispersive character of Rayleigh waves as the Banda Sea shocks, the path of which is represented by a broken line 5. The New Zealand shock (111) and the Solomon Islands shock (121), however, show the dispersive characters between the curves 3 and 5, which well obey the tendency previously reported.

Fig. 6 shows the following two facts. That is:

1) The dispersive character of Rayleigh waves as well as Love waves due to the Balleny Islands region shock (90) resembles very well those due to the Antarctic shock (33) which was previously obtained, and further, Rayleigh wave dispersions are both nearly equal to the rather continental curve 6 corresponding to that due to the Java Island shock. As these paths run through the continental part of New Guinea and Australia, these results are reasonable.

2) The new dispersion data of Rayleigh waves due to the New Guinea shock (126) also resembles those due to the shock (21) obtained previously, and both lie near the curve 4. Fig. 7 was drawn for the same purpose as Fig. 6. In this figure, we can also recognize that the dispersion curves of Rayleigh waves due to the Fiji Islands shock (128) and the Loyality Islands shock (127) lie both on the curve due to the Kermadec Islands shock (10), and that due to the Selebes Island shock (101) lies on the curve due to the Molluca Passage shock (56). Another fact must be noticed here on the dispersion data due to the Helmahera Island shock (125). That is, if the dispersive character due to this shock obeys the general tendency that the dispersive character gradually becomes a continental one with the shift of travelling paths to the west, the dispersion data due to the shock (125) must be similar to those due to the shocks (56) or (101). Nevertheless, they lie on a rather oceanic curve due to the shocks of (127) or (128) which are much more eastward. A similar fact was previously observed for the Mindanao Island shock (77).[5]

---

[5] *loc. cit.* 1). p. 228.

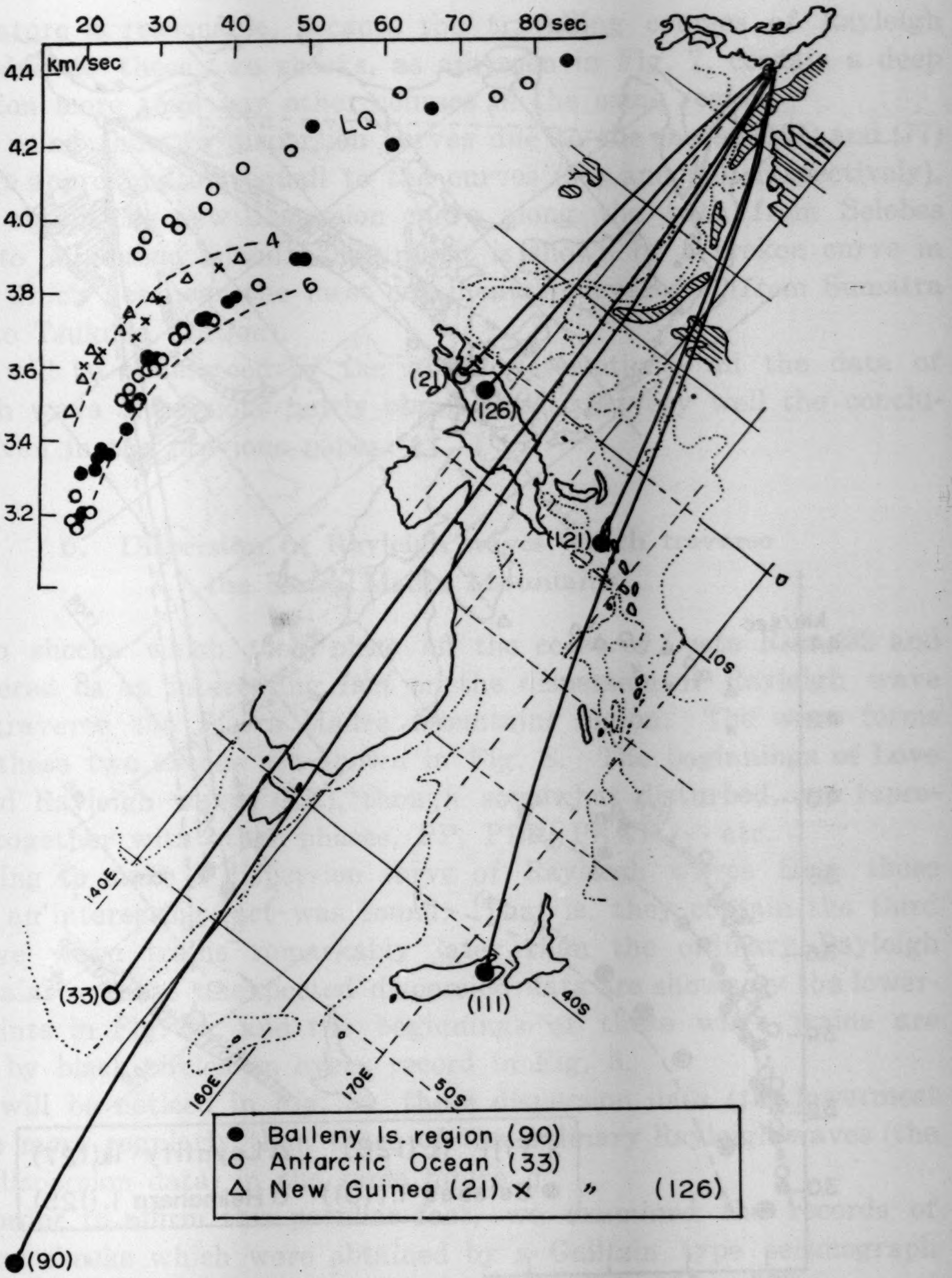

Fig. 6. Dispersions of Rayleigh waves due to two shocks (90) and (126). They are similar to the previous ones due to the shocks (33) and (21) respectively. Dispersion data of Love waves due to (33) and (90) are also represented for reference. In the map, hatched regions are the deep sea with more than 6km depth, and dotted curves mean the counter lines of 2km depth.

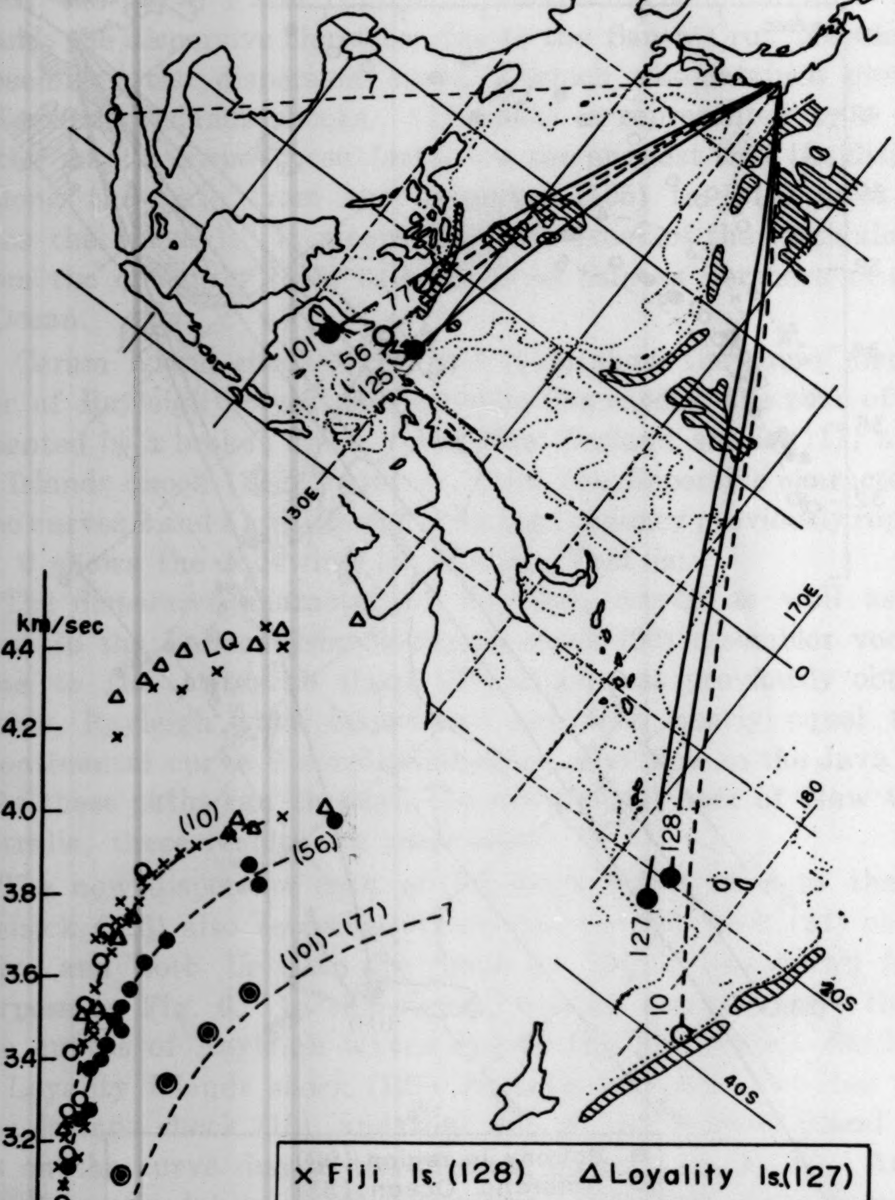

Fig. 7. Dispersions of Rayleigh waves due to two shocks (127) and (128), and those due to the shock (101). The former two resemble that due to the Kermadec Islands shock (10) and the last one resembles that due to the Molluca Passage shock (56).

The dispersion due to the shock (125) resembles those due to the shock 10 (uppermost broken curve) though the path lies western.

This feature is reasonable, because the travelling courses of Rayleigh waves due to these two shocks, as are seen in Fig. 7, contain a deep sea region more than any other courses in the same region.

By using the two dispersion curves due to the shocks (101) and (77) (they are approximately equall to the curves (56) and (10) respectively), we can obtain the new dispersion curve along the path from Selebes Island to Mindanao Island. The result is shown by a broken curve in Fig. 7, which lies near the most continental curve of 7 (from Sumatra Island to Tsukuba Station).

As will be understood by the above descriptions, all the data of Rayleigh wave dispersions newly obtained satisfy very well the conclusions given in the previous paper.

6. Dispersion of Rayleigh waves which traverse the Sierra Madre Mountains

Two shocks which took place off the coast of Costa Rica (92 and 100) offered us an interesting fact on the dispersion of Rayleigh wave which traverse the Sierra Madre Mountains region. The wave forms due to these two shocks are shown in Fig. 8. The beginnings of Love (LQ) and Rayleigh waves (LR), though somewhat disturbed, are represented together with other phases, PP, PPP, PKKP ··· etc.

Trying to make a dispersion curve of Rayleigh waves from these records, an interesting fact was found. That is, they contain the third dispersive wave trains remarkably later than the ordinary Rayleigh wave trains. These unexpected dispersion data are shown by the lowermost points in Fig. 9a, and the beginnings of these wave trains are marked by black circles on every record in Fig. 8.

As will be noticed in Fig. 9a, these dispersion data (the lowermost ones) lie more regularly than those of the ordinary Rayleigh waves (the middle dispersion data) in the same figure.

In order to affirm this peculiar fact, we examined the records of the same shocks which were obtained by a Galitzin type seismograph at Matsushiro Observatory, Meteorological Agency, Japan. The record of EW component for the shock (92) was also shown in Fig. 8. (Regrettable to say, the records of the other two components for this shock are missing on account of some defects on the instruments, and the traces for the shock (100) were too small). From this record, the same results were observed. The dispersion data by this record are also added

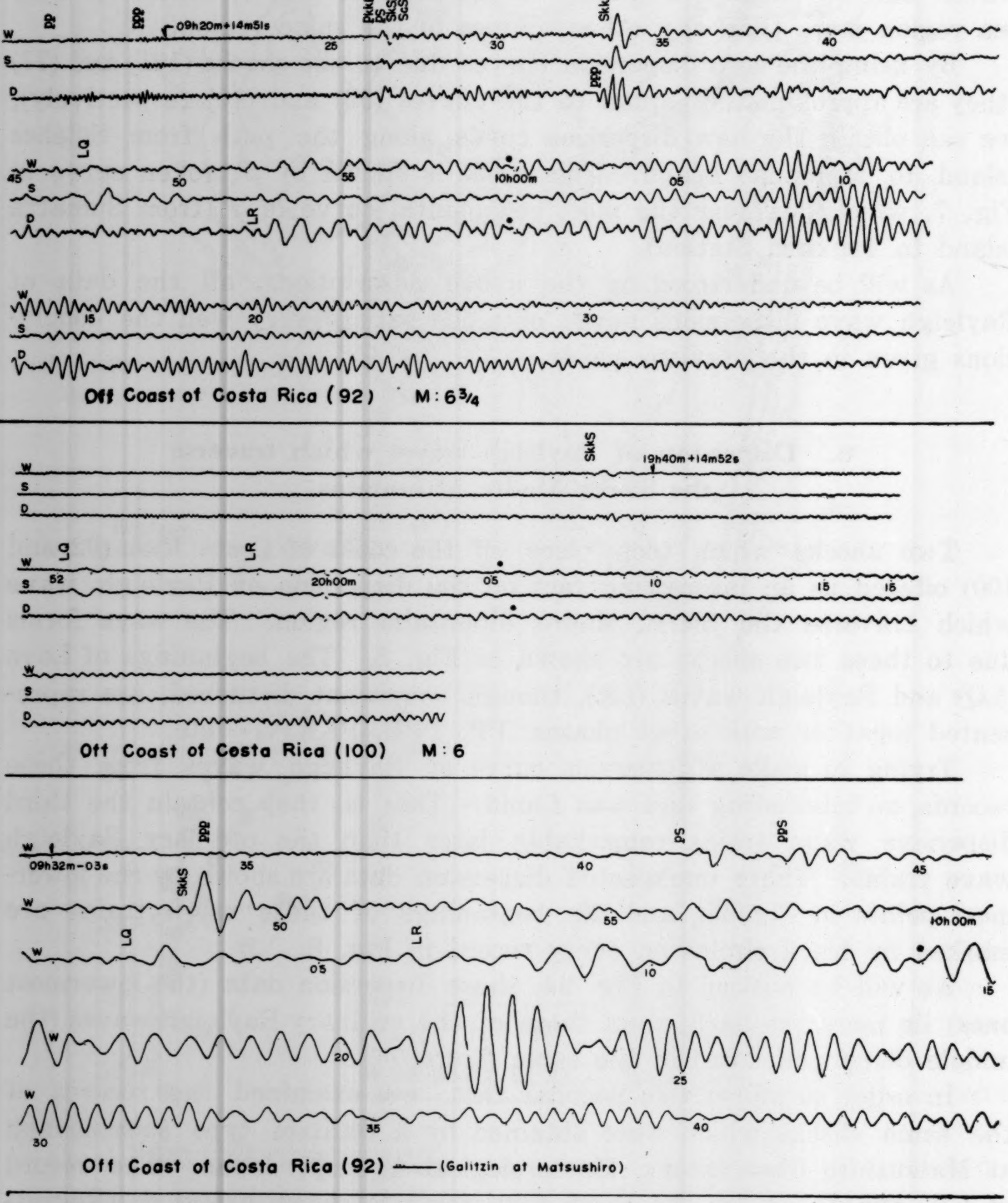

Off Coast of Costa Rica (92) M: 6 3/4

Off Coast of Costa Rica (100) M: 6

Off Coast of Costa Rica (92) —— (Galitzin at Matsushiro)

Fig. 8. Seismograms of two Costa Rica shocks (92) and (100). Unexpected slow Rayleigh waves begin around the times given by black circles.

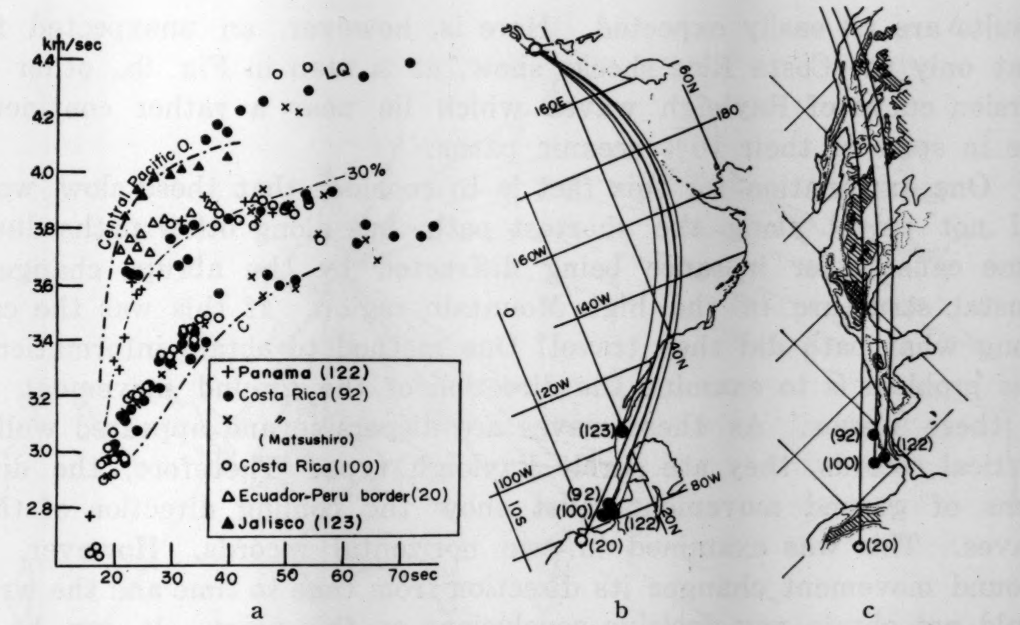

Fig. 9a. Dispersions of Rayleigh waves which passed the mountain region in Mexico. Dispersion of Love waves and two kinds of Rayleigh waves due to two Costa Rica shocks are respectively shown as the uppermost, middle and lowermost dispersion data marked by circles. Ordinary Rayleigh wave dispersions for these shocks together with those for other shocks, are reasonably distributed around a 30% continental curve.

Fig. 9b. Travelling paths of Rayleigh waves which passed around the mountain region in Mexico.

Fig. 9c. Detail map of Sierra Madre Mountains region and three travelling paths. Hatched and double hatched regions respectively mean those of more than 2km and 4km in height.

in Fig. 9a by X marks.

In Fig. 9b, three other travelling paths of Rayleigh waves due to three shocks of Jalisco (123), Ecuador-Peru border (20) and Panama (122) are shown. As is seen, these paths lie near the ones for the Costa Rica shocks.

Along the first path for (123) which mostly passes through northern Pacific Ocean, dispersion data of Rayleigh waves (black triangles) lie just on the purely oceanic one. Along the latter two paths for (20) and (122) which run on both sides of the path for the Costa Rica shocks, the dispersion data of Rayleigh waves (white triangles and crosses) are distributed around the curve for 30% continental and 70% oceanic crustal structure. (This curve was calculated in the previous paper.[6]). The Costa Rica shocks also give the dispersion data on the same curve. These results are all easily expected. Here is, however, an unexpected fact that only the Costa Rica shocks show, as is seen in Fig. 9a, other dispersion curve of Rayleigh waves which lie near a rather continental one in spite of their 70% oceanic paths.

---

[6] *loc. cit.* 1). p. 238.

One explanation for this fact is to consider that these slow waves did not travel along the shortest path, but along other paths due to some causes, for instance being diffracted by the abrupt change of crustal structure in the high Mountain region. If this was the case, along what path did they travel? One method to obtain information on this problem is to examine the direction of the ground movement due to these waves. As these waves are dispersive and appeared well on vertical records, they are surely Rayleigh type. Therefore, the directions of ground movement must show the coming direction of these waves. This was examined in two horizontal records. However, the ground movement changes its direction from time to time and the writer could not obtain any decisive conclusions on this point. It can be recognized for instance, by the phase relations of two horizontal records due to the shock (92) in Fig. 8, that their directions are approximately EN–WS around 10h 04m, 10m to 11m, while ES–WN around from 10h 07m to 09m.

Fig. 9c was drawn to find some special conditions, if any, along the paths for the Costa Rica shocks. From this map, however, it is hard to find any special condition about the travelling paths. Two neighboring paths for the shocks (20) and (122) were also added, and the path for the shock (20) showed a special feature in traversing the steep inclined region beside the Sierra Madre Mountains. The dispersive character of Rayleigh waves due to this shock (20) is shown in Fig. 9a by white triangles, from which we can see some departure from others in short period range. At present, it is also difficult, to explain this special character.

In any case, we may say that Rayleigh waves take some peculiar travelling path when they traverse high mountain regions.

7. Conclusions

Dispersion of Rayleigh waves due to twenty-four shocks across the oceanic basin were added to the previous study.

We found two important conclusions in the previous paper, that is:

1) The dispersions of Rayleigh waves across the northern, central

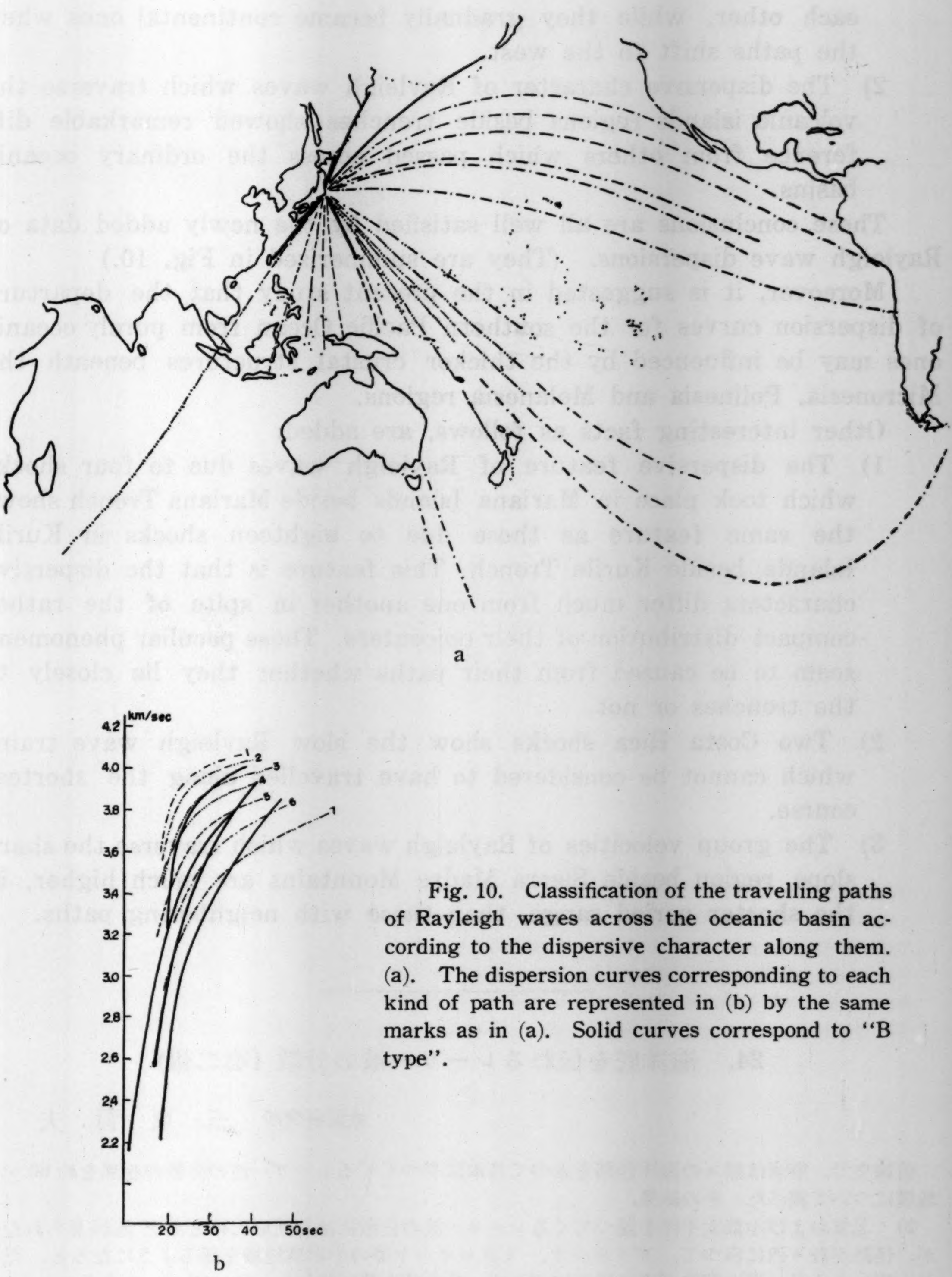

Fig. 10. Classification of the travelling paths of Rayleigh waves across the oceanic basin according to the dispersive character along them. (a). The dispersion curves corresponding to each kind of path are represented in (b) by the same marks as in (a). Solid curves correspond to "B type".

and eastern part of the Pacific Ocean were all quite the same as each other, while they gradually became continental ones when the paths shift to the west.

2) The dispersive character of Rayleigh waves which traverse the volcanic islands regions beside trenches showed remarkable difference from others which passed across the ordinary oceanic basins.

These conclusions are all well satisfied by the newly added data of Rayleigh wave dispersions. (They are summerized in Fig. 10.)

Moreover, it is suggested in the present study that the departure of dispersion curves for the southern Pacific Ocean from purely oceanic ones may be influenced by the thicker crustal structures beneath the Micronesia, Polinesia and Melanesia regions.

Other interesting facts as follows, are added:

1) The dispersive feature of Rayleigh waves due to four shocks which took place in Mariana Islands beside Mariana Trench shows the same feature as those due to eighteen shocks in Kurile Islands beside Kurile Trench. This feature is that the dispersive characters differ much from one another in spite of the rather compact distribution of their epicenters. These peculiar phenomena seem to be caused from their paths whether they lie closely to the trenches or not.

2) Two Costa Rica shocks show the slow Rayleigh wave trains which cannot be considered to have travelled along the shortest course.

3) The group velocities of Rayleigh waves which traverse the sharp slope region beside Sierra Madre Mountains are much higher, in the shorter period range, than those with neighboring paths.

---

24. 海洋底を伝わるレーリー波の分散 (第二報)

地震研究所　三　東　哲　夫

前論文で，筆者は種々の海洋径路をとつて日本にやつてくるレーリー波の分散の相異を約 60 ヶの地震について調べた．その結果，

1) 北部および中部太平洋を通つてくるレーリー波の分散にはお互いにほとんど差が見られないが，径路が段々西に移つて，ポリネシヤ，ミクロネシヤ等の小群島地域を通るようになると，だんだん変化が生じ，更に径路が西に移るにつれて，分散は次第に陸的なものに近づいてゆくこと．

2) 海溝にそつた火山列島の附近を縦走するレーリー波は，それ以外の普通の海洋底を通るそれ

らとは著しく様子のちがつた分散を示すこと．

等を発見した．

今回，更にその後の 24 ヶの地震についてのレーリー波の分散を調べたが．やはり，上に述べた観測事実に間違いのないことが分つた．

更に，今度新しく得られた注目すべき結果は，メキシコのシエラマドレ山脈の近くを縦走してくるレーリー波の分散のうち，コスタ・リカ地方で起つた二つの地震の場合（第 8 図）に，通常の大圏コースを通つて来たとして話が合うレーリー波とは別に，これよりもかなりおくれて，むしろより以上きれいな分散性を示すレーリー波が記録された（第 9a 図）ということである．これらのレーリー波は，その走時から考えると，大圏コース以外の径路を通つてやつて来たものと考えざるをえないが，どんな路を，そして何故に，という点は今の段階では分らない．

BULLETIN OF THE EARTHQUAKE RESEARCH INSTITUTE
Vol. 38 (1960), pp. 403-419

25. *Studies of the Thermal State of the Earth. The Fourth Paper: Terrestrial Heat Flows related to Possible Geophysical Events.*

By Tsuneji RIKITAKE,

Earthquake Research Institute

and

Ki-iti HÔRAI,

Graduate School, University of Tokyo.

(Read Feb. 23, 1960.—Received Feb. 23, 1960.)

Summary

A subcrustal convection current having a linear dimension of a few thousand kilometers accounts for the high heat flows found on the East Pacific Rise provided a velocity of several *cm/year* and 1°*C/km* temperature gradient are assumed in the earth's mantle. A long-lived magma of high temperature and a phase transformation layer can give rise to only a fraction of the world average of heat flow for conceivable cases. In general, it is therefore difficult to presume what sort of geophysical events are prevailing in the earth only from the heat flow anomalies observed.

1. Introduction

Important bearing of terrestrial heat flow on geophysics has been recently emphasized. Heat flow values as measured at various localities all over the earth scatter in a wide range as are summarized in a brief form in Table 1.

One of the most surprising results is certainly the fact that a wide variety of heat flow values has been found on ocean floors. According to Herzen[20], the ratio of the maximum to the minimum exceeds 50. Systematic distributions of high and low values of heat flow in the south-eastern Pacific seem to be even more outstanding. A number of geophysicists are now inclined to suppose that such anomalies may be caused by some convection currents in the earth's mantle. The fact

Table 1. Heat flow values from various localities.

Locality	Heat flow (10^{-6} *cal* /*cm*^{2} *sec*)	Temp. gradient ($^\circ C/100\ m$)	Authority
CANADA			
Ontario Quebec	0.69–1.32	0.9–1.6	Misener et al.1) (1951)
Resolute Bay	0.4–2.9	3.95	Misener2) (1955)
U.S.A.			
Texas New Mexico	1.1–2.0	0.77–3.4	Herrin & Clark3) (1956) Birch & Clark4) (1945) Richardson & Wells5) (1931)
California	0.66–1.3	0.86	Benfield6) (1947) Clark7) (1957)
Michigan	0.9	1.8	Birch8) (1954)
Colorado	1.6–1.9	2.0–2.4	〃 9) (1950)
Georgia	1.4	1.7–2.2	〃 10) (1947)
Kansas	1.4–1.7	2.8	〃 〃
GREAT BRITAIN	0.68–2.87	1.7–6.5	Benfield11) (1939) Bullard & Niblett12) (1951) Anderson13) (1939) Chadwick14) (1956)
HUNGARY	2.0–3.04	4.0–7.0	Boldizsar15) (1956), 16) (1959)
IRAN	0.53–1.22	0.9–2.0	Coster17) (1947)
SOUTH AFRICA	0.75–1.52	0.95–2.23	Bullard18) (1939)
PACIFIC	0.14–8.09	4.0–7.0	Revelle & Maxwell19) (1952) Herzen20) (1959)

(to be continued)

---

1) A.D. MISENER, L.G.D. THOMPSON and R.J. UFFEN, *Trans. Amer. Geophys. Uni.*, **32** (1951), 729.

2) A. D. MISENER, *Trans. Amer. Geophys. Uni.*, **36** (1955), 1055.

3) E. HERRIN and S. P. CLARK JR., *Geophysics*, **21** (1956), 1087.

4) F. BIRCH and H. CLARK, *Amer. Jour. Sci.*, **243** -A (1945) 69.

5) L. T. RICHARDSON and R. C. WELLS, *Jour. Wash. Acad. Sci.*, **21** (1931), 243.

6) A. E. BENFIELD, *Amer. Jour. Sci.*, **245** (1947), 1.

7) S. P. CLARK JR., *Trans. Amer. Geophys. Uni.*, **38** (1957), 239.

8) F. BIRCH, *Amer. Jour. Sci.*, **252** (1954), 1.

9) F. BIRCH, *Bull. Geol. Soc. Amer.*, **61** (1950), 567.

10) F. BIRCH, *Amer. Jour. Sci.*,**245** (1947), 733,

11) A. E. BENFIELD, *Proc. Roy. Soc. A*, **173** (1939), 428.

12) E. C. BULLARD and E. R. NIBLETT, *Mon. Not. Roy. Astr. Soc., Geophys. Suppl.*, **6** (1951), 222.

13) E. M. ANDERSON, *Roy, Soc. Edinb. Pr.*, **60** (1939), 192.

14) P. CHADWICK, *Nature*, **178** (1956), 105.

15) T. BOLDIZSAR, *Geofis. Pura e Applic.*, **34** (1956), 66.

16) T. BOLDIZSAR, *Publ. Faculties Min. Geotechn., Technical Univ. Sopron*, (XX) (1959), 1.

17) H. P. COSTER, *Mon. Not. Roy. Astr. Soc. Geophys. Suppl.*, **5** (1947) 131.

18) E. C. BULLARD, *Proc. Roy. Soc. A*, **173** (1939), 473.

19) R. REVELLE and A. E. MAXWELL, *Nature*, **170** (1952), 199.

20) R. HERZEN, *Nature*, **183** (1959), 882.

(continued)

Locality	Heat flow (10^{-6} *cal/cm² sec*)	Temp. gradient (°*C*/100 *m*)	Authority
ATLANTIC			
N. Atlantic	0.58–1.42	0.95–2.23	Bullard[21] (1954)
Mid-Atlantic Ridge	6.0		Bullard[22] (1957)
JAPAN			
Sasago Tunnel	2.06	2.7	Tanakadate[23] (1903) Uyeda, Yukutake & Tanaoka[24] (1958)
Tokyo Univ.	0.43	2.2	
Mt. Sirane	10.4	24.2	
Hitachi (Copper mine)	0.63–0.67(N)	0.94	Hôrai[25] (1959)
	0.78–0.90(S)	1.21	〃
Oil-field			
Yabase	2.01	4.8	Teikoku-Sekiyu Co.[26] & Hôrai[25]
Innai		4.8	〃
Kotaki		7.3	〃
Mogami		7.1	〃
Nishiyama		4.8	〃
Matsunoyama		8.5	〃
Gas-field			
Utino		2.0	〃
Nagatoro		5.0	〃

that rises and deeps on the ocean bottom accompany respectively high and low heat flow values seems also favourable to the convection theory.

Turning to heat flows on land, however, the values observed cover a range from 0.4 to 3.0×10^{-6} *cal/cm² sec*, no large differences such as found on ocean bottoms being reported except in volcanic or geothermal areas. The average value of heat flow on land has been believed to be 1.2×10^{-6} *cal/cm² sec* though, according to recent accumulation of data, a slightly higher value, 1.4×10^{-6} *cal/cm² sec* say, seems to be more likely.

Heat flow value observed at the earth's surface are affected by a number of conditions, physical and chemical, in the earth's crust. Influences of contents of radioactive matter in rocks, chemical action taking place in the crust, circulation of underground water, irregularity

---

21) E. C. BULLARD, *Proc. Roy. Soc.*, **222** (1954), 408.

22) E. C. BULLARD, *Geophysics*, **22** (1957), 432.

23) A. TANAKADATE, *Rep. Imp. Earthq. Invest. Committ.*, **45** (1903), 17.

24) S. UYEDA, T. YUKUTAKE and I. TANAOKA, *Bull. Earthq. Res. Inst.*, **36** (1958), 251.

25) K. HÔRAI, *Bull. Earthq. Res. Inst.*, **37** (1959), 571.

26) TEIKOKU-SEKIYU CO., *Unpublished data.*

of topography and such like on terrestrial heat flows have often been discussed though it seems difficult to estimate them in a general way. It is true that some of these conditions may account for high or low values of heat flow actually observed to some extent. However, it does not seem likely that all the anomalies found in heat flow values could be explained in this way.

In Japan, one of the countries where seismic and volcanic activities are most remarkable, it had been simply supposed that we should observe fairly large heat flows there prior to the actual observations. It turns out, however, that, as far as a few measurements that have been carried out so far are concerned, the heat flow values in Japan do not differ much from the world's average as can be seen in Table 1. Although the influences of the conditions discussed in the last paragraph on these Japanese values are not clear, some geophysicists are of the opinion that the terrestrial heat flows are unexpectedly small in Japan in spite of the geophysical and geological activities.

Under these circumstances, it would be of some use to estimate to what extent heat flows are affected by possible geophysical events such as thermal convection in the upper part of the mantle, existence of a magma reservoir of high temperature over a long period, occurrence of phase transformation in the earth's crust and so forth. It might be possible to explain some of the geothermal anomalies on the basis of these theoretical estimations.

The first study in this line has been already made by one of the writers[27] in relation to heat flow associated with magma intrusion though no account was taken of latent heat of solidification. It becomes clear that any intrusion of magma mass having a radius of a few kilometers does not produce a large anomaly of heat flow unless the intrusion occurs in a shallow depth, 1 *km* or so. It should be difficult to detect a high temperature mass of that size by measuring heat flow at the earth's surface provided the depth exceeds several kilometers. Since this sort of study seems to be useful for interpretations of heat flow anomalies as well as for presuming conditions of thermal processes taking place in the earth, it is intended in this paper to conduct a few studies of the sort which may be applied to possible geophysical events mentioned in the last paragraph.

---

[27] T. RIKITAKE, *Bull. Earthq. Res. Inst.*, **37** (1959), 233.

2. Heat flow accompanied by subcrustal convection currents

Subcrustal convection currents have long been supposed by a number of geologists[28)-32)] to be causes of orogenesis and associated phenomena. It is beyond the scope of this paper to deal with the details of the convection theory. We may refer to the modern reviews[33),34)] in order to see the outline of the theory.

Although the theory of convection currents in the earth's mantle has many advantages for the interpretation of geological and geophysical phenomena, no direct proofs of the existence of such currents have ever been put forward until recently. According to the measurements[18),19),20)] on ocean floors, however, high or low heat flow values which seem likely to be associated with some convection currents have been found as mentioned in the introduction. Although it is not quite certain whether or not these anomalies of heat flow are the direct evidence of subcrustal convection currents, it is surely worth-while to estimate theoretically what convection will accompany what heat flow at the earth's surface. Such a study may serve as some check of the convection theory together with the heat flow values observed. Let us suppose a steady convection current under the solid crust as schematically shown in Fig. 1 where everything is assumed to be independent of y. By assuming that the fluid is incompressible, the x, y and z components of the velocity of such a convectional motion may be expressed as

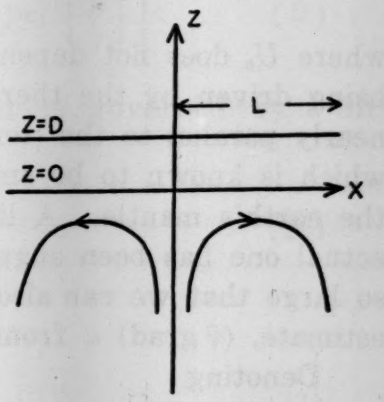

Fig. 1. Model of subcrustal convection currents.

$$\vec{v} = \begin{cases} \dfrac{AL}{l\pi}\Big(1+\dfrac{z}{l}\Big)\Big(1+\dfrac{3z}{l}\Big)\sin\dfrac{\pi x}{L} \\ 0 \\ -A\,\dfrac{z}{l}\Big(1+\dfrac{z}{l}\Big)^2\cos\dfrac{\pi x}{L}\,, \end{cases} \qquad (1)$$

---

28) A. HOLMES, *Mining Mag.*, **40** (1929), 40.

29) D. GRIGGS, *Amer. Journ. Sci.*, **237** (1939), 611.

30) H. H. HESS, *Trans. Amer. Geophys. Un.*, **32** (1951), 528.

31) H. BROOKS, *Trans. Amer. Geophys. Un.*, **27** (1941), 548.

32) F. A. VENING MEINESZ, *Quart. Journ. Geol. Soc. Lond.*, **103** (1948), 191.

33) A. E. SCHEIDEGGER, *Principles of Geodynamics*, Springer (1958).

34) W. A. HEISKANEN & F. A. VENING MEINESZ, *The Earth and Its Gravity Field*, McGraw-Hill (1958).

which satisfies div $\vec{v}=0$. It is seen from (1) that the velocity in the direction parallel to the z-axis vanishes at $z=0$ and $z=l$. Since this type of convection current is often found in experiments, it may be allowed to take (1) as a possible type of subcrustal convection currents if they existed.

The equation of heat transfer in fluid is

$$\frac{\partial U}{\partial t}+(\vec{v}\ \mathrm{grad})U=\kappa\nabla^2 U\ , \tag{2}$$

where U and κ denote the temperature and thermal diffusivity respectively. U may be put

$$U=U_0+u\ , \tag{3}$$

where U_0 does not depend on time. If we think of a portion of fluid being driven by the thermal convection, its temperature varies in a way nearly parallel to the temperature-depth curve for adiabatic gradient which is known to be smaller than the actual temperature gradient in the earth's mantle. A likely ratio[35] of the adiabatic gradient to the actual one has been suggested to be 1/8 or thereabout. In case L is so large that we can also ignore $\partial u/\partial x$, we may drop, for an approximate estimate, $(\vec{v}\ \mathrm{grad})\ u$ from equation (2) so long as $\vec{v}$ is not very large.

Denoting

$$\frac{\partial U_0}{\partial x}=0\ ,\quad -\frac{\partial U_0}{\partial z}=\beta\ , \tag{4}$$

(2) can be written as

$$\frac{\partial u}{\partial t}+A\beta\frac{z}{l}\left(1+\frac{z}{l}\right)^2\cos\frac{\pi x}{L}=\kappa\nabla^2 u\ . \tag{5}$$

Solutions of (5) may be written as

$$u=u_2(z,\ t)\cos\frac{\pi x}{L}\ , \tag{6}$$

where u_2 is a function of z and t only. Putting (6) into (5), we have

$$\frac{\partial u_2}{\partial t}+A\beta\frac{z}{l}\left(1+\frac{z}{l}\right)^2=\kappa\left\{\frac{\partial^2 u_2}{\partial z^2}-\left(\frac{\pi}{L}\right)^2 u_2\right\}\ . \tag{7}$$

---

35) J. VERHOOGEN, *Physics & Chemistry of the Earth.* I, Pergamon (1956), 17.

Subscript 2 is hereafter used for the quantities below the crust. If we write p in place of time-operator $\partial/\partial t$, (7) can be written as

$$\frac{d^2u_2}{dz^2}-\left[\left(\frac{\pi}{L}\right)^2+p\kappa_2^{-1}\right]u_2=A\beta\kappa_2^{-1}\frac{z}{l}\left(1+\frac{z}{l}\right)^2 . \qquad (8)$$

The solution of (8), that does not become infinitely large at $z\rightarrow-\infty$, becomes

$$\begin{aligned}u_2=&C_2e^{\sqrt{(\pi/L)^2+p\kappa_2^{-1}}\,z}\\&-A\beta\kappa_2^{-1}\left[\left\{\left(\frac{z}{l}\right)^3+2\left(\frac{z}{l}\right)^2+\frac{z}{l}\right\}\Big/\left\{\left(\frac{\pi}{L}\right)^2+p\kappa_2^{-1}\right\}\right.\\&\left.+\left\{6\left(\frac{z}{l}\right)+4\right\}\Big/\left\{\left\{\left(\frac{\pi}{L}\right)^2+p\kappa_2^{-1}\right\}^2l^2\right\}\right] . \qquad (9)\end{aligned}$$

In the solid crust, the conduction of heat is governed by a differential equation of the type

$$\frac{\partial u}{\partial t}=\kappa_1\nabla^2u , \qquad (10)$$

the appropriate solution of which is given by

$$u=u_1(z)\cos\frac{\pi x}{L} , \qquad (11)$$

where

$$u_1=C_1e^{\sqrt{(\pi/L)^2+p\kappa_1^{-1}}\,z}+\overline{C}_1\,e^{-\sqrt{(\pi/L)^2+p\kappa_1^{-1}}\,z}, \qquad (12)$$

in which κ_1 is the thermal diffusivity and p stands for $\partial/\partial t$ as before.

The boundary conditions by which free constants C_1, $\overline{C_1}$ and C_2 are determined are given as

$$\left.\begin{aligned}&u_1=u_2 ,\quad K_1\frac{\partial u_1}{\partial z}=K_2\frac{\partial u_2}{\partial z} , &&\text{at } z=0\\&u_1=0 , &&\text{at } z=D\end{aligned}\right\} \qquad (13)$$

where K_1 and K_2 are the thermal conductivities in the respective regions. The continuity of temperature at the mantle-crust boundary would not always hold for a sudden occurrence of convection current. In such a case, another boundary condition should be considered.

From (13), we have

$$\left.\begin{aligned} & C_1 e^{\sqrt{(\pi/L)^2+p\kappa_1{}^{-1}}\,D}+\overline{C}_1 e^{-\sqrt{(\pi/L)^2+p\kappa_1{}^{-1}}\,D}=0\ , \\ & C_1+\overline{C}_1=C_2-\frac{4A\beta\kappa_2^{-1}}{\{(\pi/L)^2+p\kappa_2^{-1}\}^2 l^2}\ , \\ & K_1(C_1-\overline{C}_1)\sqrt{(\pi/L)^2+p\kappa_1^{-1}} \\ & \quad =K_2\left[C_2\sqrt{(\pi/L)^2+p\kappa_2^{-1}}-\frac{A\beta\kappa_2^{-1}}{l\{(\pi/L)^2+p\kappa_2^{-1}\}}\right. \\ & \qquad\qquad\qquad \left.\times\left(1+\frac{6}{\{(\pi/L)^2+p\kappa_2^{-1}\}l^2}\right)\right]. \end{aligned}\right\} \tag{14}$$

Solving (14), C_1, $\overline{C}_1$ and C_2 are easily obtained. Hence we can obtain u_1 and u_2 from (12) and (9).

In order to get some idea concerning heat flow values associated with the convection currents, however, no general solutions would be needed at the moment. For an order-of-magnitude estimate, we are specially interested in the steady state which is given by putting $p \rightarrow 0$. For the sake of simplicity, we also assume

$$\kappa_1=\kappa_2=\kappa\ , \qquad K_1=K_2=K\ .$$

In that case, (14) is simplified as

$$\left.\begin{aligned} & C_1 e^{\pi D/L}+\overline{C}_1 e^{-\pi D/L}=0\ , \\ & C_1+\overline{C}_1=C_2-\frac{4A\beta\kappa^{-1}}{(\pi/L)^4 l^2}\ , \\ & C_1-\overline{C}_1=C_2-\frac{A\beta\kappa^{-1}}{(\pi/L)^3 l}\left(1+\frac{6}{(\pi/L)^2 l^2}\right), \end{aligned}\right\} \tag{15}$$

from which we obtain

$$\left.\begin{aligned} & C_1=\frac{A\beta\kappa^{-1}}{2(\pi/L)^4 l^2}e^{-2\pi D/L}\left(4-\frac{\pi l}{L}-\frac{6L}{l\pi}\right), \\ & \overline{C}_1=-\frac{A\beta\kappa^{-1}}{2(\pi/L)^4 l^2}\left(4-\frac{\pi l}{L}-\frac{6L}{\pi l}\right). \end{aligned}\right\} \tag{16}$$

With (16), the steady value of temperature gradient at the earth's surface is readily estimated. We have

$$\left(\frac{\partial u_1}{\partial z}\right)_{z=D}=\frac{\pi}{L}\left(C_1 e^{(\pi/L)D}-\overline{C}_1 e^{-(\pi/D)L}\right), \tag{17}$$

which becomes

$$\left(\frac{\partial u_1}{\partial z}\right)_{z=D}=e^{-\pi D/L}\frac{A\beta\kappa^{-1}}{(\pi/L)^3 l^2}\left(4-\frac{\pi l}{L}-\frac{6L}{\pi l}\right). \tag{18}$$

If we simply assume $L=l$, (18) can be written as

$$\left(\frac{\partial u_1}{\partial z}\right)_{z=D}=-0.0339\,e^{-\pi D/L}A\beta\kappa^{-1}L\ , \tag{19}$$

so that the temperature gradient right above the ascending current can be estimated from (19).

The temperature gradient in the earth's mantle has been supposed by one of the writers[36] to be 1.4°*C/km*. For an order-of-magnitude estimate, we may therefore assume $\beta=1°C/km$. $\kappa=0.01$ *c.g.s.* is also assumed. The temperature gradient at the earth's surface is then calculated with A and L as parameters. By multiplying by K, which is assumed to take a usual value for rocks, 5×10^{-3} *cal/cm sec °C* say, the heat flow values for various thickness of the crust are obtained as are shown in Fig. 2.

At a glance of Fig. 2, it is seen that the heat flow values are largely affected by the linear dimension of the convection current. If we suppose a convection in the earth's mantle, of which the linear scale exceeds 1000 *km* as has been supposed from the heat flow measurements in the south-eastern Pacific, we may well expect a heat flow amounting to 5×10^{-6} *cal/cm² sec* for $\beta=1°C/km$ and $A=10$ *cm/year*.

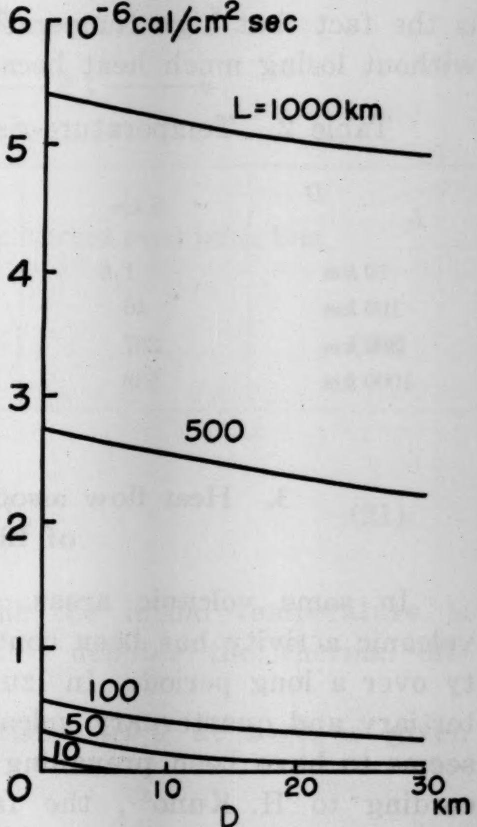

Fig. 2. Heat flows associated with the subcrustal convection currents for various thicknesses of the crust (D) and linear dimensions of the convection currents (L).

---

[36] T. Rikitake, *Bull. Earthq. Res. Inst.*, **30** (1952), 13.

Since β may be able to take slightly larger values than those cited above, the heat flow anomalies found on the ocean floor are possibly interpreted as those caused by some subcrustal convection currents having a velocity of several *cm/year*.

Meanwhile, the thickness of the crust does not much affect the heat flow values except for convections of small scale. Hence an appreciable anomaly in heat flow must be observed even on the continent, where the crust is fairly thick, if there were subcrustal convection currents on an extensive scale.

The temperature-rise at the bottom of the crust is easily calculated for each case as given in Table 2. These values harmonize well with the heat flow values at the earth's surface. The reason why such high temperatures are associated with convections of large dimension is the fact that high temperature material at great depths comes up without losing much heat because we assume $l=L$.

Table 2. Temperature-rise at the bottom of the crust (°*C*).

L \ *D*	5 *km*	10 *km*	20 *km*	30 *km*
10 *km*	1.6	1.3	1.7	1.7
100 *km*	46	80	123	145
500 *km*	257	505	950	1460
1000 *km*	538	1030	2020	2940

3. Heat flow associated with long-lived magma of high temperature

In some volcanic areas, we have evidence to believe that the volcanic activity has been continually lasting in almost the same locality over a long period. In Izu District of Japan, where we find many tertiary and quarternary volcanoes, for instance, the volcanic activity seems to have been prevailing during the past few million years. According to H. Kuno(37), the fact may suggest that the source of the volcanic activity or a magma reservoir of high temperature has survived somehow in or under the earth's crust during the period. Such a long-lived magma of high temperature would possibly cause some anomaly in heat flow observed at the earth's surface. The purpose of this section is to estimate what anomaly will be found in heat flow when a certain area at some depth in the earth has been kept at a high temperature over a long period.

---

(37) *Personal communication.*

Let us consider an infinitely wide plate that is regarded as a model of the crust. The temperature at the upper surface is always kept at zero, while the part of the bottom surface defined by $-L/2<x<L/2$ is always kept at a constant temperature Θ. For the sake of mathematical simplicity, these conditions are assumed to repeat periodically with an interval $2l$ in the x direction as can be seen in Fig. 3. If things do not depend on y, the temperature in the plate satisfies

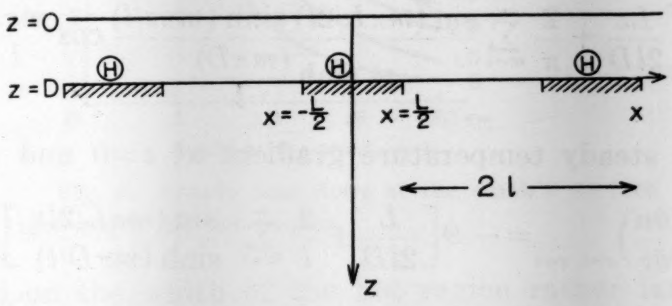

Fig. 3. The model of the crust, the hatched parts being kept at a constant temperature Θ.

$$\frac{\partial u}{\partial t}=\kappa\left(\frac{\partial^2 u}{\partial x^2}+\frac{\partial^2 u}{\partial z^2}\right), \tag{20}$$

which can be written as

$$pu=\kappa\left(\frac{\partial^2 u}{\partial x^2}+\frac{\partial^2 u}{\partial z^2}\right), \tag{21}$$

by replacing $\partial/\partial t$ by time-operator p, while the initial temperature is assumed to be zero throughout the plate. κ denotes the thermal diffusivity as usual.

The typical solution of (21), that satisfies $u=0$ at $z=0$, is given by

$$u=C_m \cos\frac{m\pi x}{l}\sinh\sqrt{(m\pi/l)^2+\kappa^{-1}p}\; z\,. \tag{22}$$

Since the temperature at $z=D$ should be

$$u_{z=D}=\Theta\left[\frac{L}{2l}+\frac{2}{\pi}\sum_{m=1}^{\infty}\frac{1}{m}\sin\frac{m\pi L}{2l}\cos\frac{m\pi x}{l}\right], \tag{23}$$

C_m is chosen so as to satisfy (23). In that case, the solution, that satisfies all the boundary conditions becomes

$$u=\Theta\left[\frac{L}{2l}\frac{\sinh \kappa^{-1/2}p^{1/2}z}{\sinh \kappa^{-1/2}p^{1/2}D}\right.$$

$$\left.+\frac{2}{\pi}\sum_{m=1}^{\infty}\frac{\sin(m\pi L/2l)\sinh\{(m\pi/l)^2+\kappa^{-1}p\}^{1/2}z}{m\sinh\{(m\pi/l)^2+\kappa^{-1}p\}^{1/2}D}\cos\frac{m\pi x}{l}\right]. \quad (24)$$

Putting $p\rightarrow 0$, let us hereafter consider the steady state which is given as

$$u=\Theta\left[\frac{Lz}{2lD}+\frac{2}{\pi}\sum_{m=1}^{\infty}\frac{\sin(m\pi L/2l)\sinh(m\pi z/l)}{m\sinh\dfrac{(m\pi D)}{l}}\cos\frac{m\pi x}{l}\right]. \quad (25)$$

From (25), the steady temperature gradient at $z=0$ and $x=0$ becomes

$$-\left(\frac{\partial u}{\partial z}\right)_{x=0,\,z=0}=-\,\Theta\left[\frac{L}{2lD}+\frac{2}{l}\sum_{m=1}^{\infty}\frac{\sin(m\pi L/2l)}{\sinh(m\pi D/l)}\right].$$

Assuming $\Theta=1000°C$ and $l=100\,km$, the temperature gradient is calculated for various combinations of L and D as given in Table 3.

Table 3. Temperature gradient at $z=0$ and $x=0$ in units of $°C/km$.

L \ D	5 *km*	10 *km*	15 *km*	20 *km*
5 *km*	131.2	37.4	17.1	9.7
10 *km*	181.3	65.1	31.9	18.7
20 *km*	194.2	89.6	51.0	32.3
30 *km*	196.1	96.7	60.4	41.0

If the thermal conductivity is assumed to take a usual value for rocks, $5\times10^{-3}\,cal/cm\,sec\,°C$ say, the gradient values in Table 3 give heat flows as shown in Fig. 4. It is seen in the figure that appreciable heat flows can be only found in the cases of shallow magma. If we take a set of likely values, $L=10\,km$ and $D=20\,km$ say, the heat flow amounts to only $0.5\times10^{-6}\,cal/sec\,cm^2$ which is about half as large as the mean value of general heat flow. It is of difficulty, therefore, to detect a magma reservoir of $1000°C$ in temperature by observing heat flow anomaly unless the magma is situated at an extremely shallow depth, 10 *km* or less. It should be also noted that the heat flow

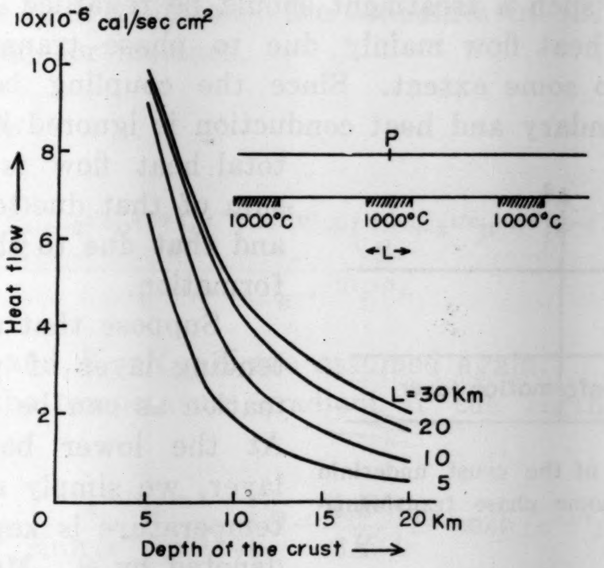

Fig. 4. Steady heat flows at the earth's surface right above the hot magma.

values depend on the width of the hot region rather largely.

4. Phase transformation and heat flow

Liberation or absorption of latent heat takes place in the earth at times of crystallization or fusion. Strictly speaking, therefore, problems related to cooling of intrusive magma must be studied with proper considerations of latent heat. It is extremely difficult, however, to take into account the movement of the solid-liquid boundary in solving the differential equation of heat conduction. Only a few studies in this line have been made by Jaeger[38] by introducing the temperature of "contact". According to Jaeger, the initial contact temperature immediately after the intrusion of magma, of which the latent heat is assumed as 100 *cal*/*gm* would be larger than that for a hypothetical liquid of zero latent heat by a factor of 1.2 or so. For an order-of-magnitude estimate of heat flow associated with magma intrusion, therefore, the effect of phase change does not seem to play a very important role.

In this section, let us consider a subterranean sheet in which some phase transformation is occurring. Ignoring the displacement of the liquid-solid boundary, the rate of heat generation is assumed in the sheet. Although such a treatment should be regarded as a crude approximation, the heat flow mainly due to phase transformation could be investigated to some extent. Since the coupling between the displacement of boundary and heat conduction is ignored in this case, the total heat flow is given by the sum of that due to the conduction and that due to the phase transformation.

---

[38] J. C. JAEGER, *Amer. Journ. Sci.*, **255** (1957), 306, **257** (1959), 44.

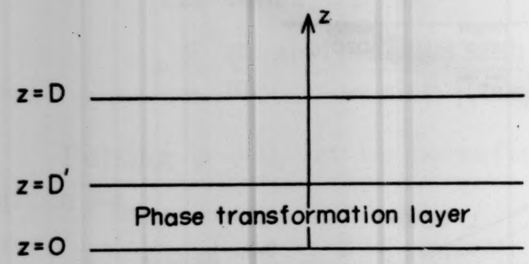

Fig. 5. The model of the crust underlain by a layer in which some phase transformation is taking place.

Suppose that an infinitely extending layer of phase transformation as can be seen in Fig. 5. At the lower boundary of the layer, we simply assume that the temperature is kept at a constant denoted by Θ. Meanwhile at the earth's surface, the temperature is always zero.

In the region between $z=D$ and $z=D'$, where we have no phase change, the temperature is governed by the usual differential equation of heat conduction and given as

$$u_1=C_1 e^{\kappa_1^{-1/2}p^{1/2}z}+\overline{C}_1 e^{-\kappa_1^{-1/2}p^{1/2}z}\,, \tag{27}$$

where the notations have the usual meanings. The equation in the phase transformation layer becomes

$$\frac{1}{\kappa_2}\frac{\partial u_2}{\partial t}=\frac{\partial^2 u_2}{\partial z^2}+\frac{A_0}{K_2}\,, \tag{28}$$

where A_0 is the heat produced in a unit volume per unit time. The solution of (28) is given as

$$u_2=C_2 e^{\kappa_2^{-1/2}p^{1/2}z}+\overline{C}_2 e^{-\kappa_2^{-1/2}p^{1/2}z}-\frac{A_0}{2K_2}z^2\,. \tag{29}$$

The boundary conditions which are to be satisfied by u_1 and u_2 are

$$\left.\begin{aligned} &z=0: u_2=\Theta\,,\\ &z=D': u_1=u_2\,,\quad K_1\frac{\partial u_1}{\partial z}=K_2\frac{\partial u_2}{\partial z}\,,\\ &z=D: u_1=0\,. \end{aligned}\right\} \tag{30}$$

From these four conditions, the constants in (27) and (29) are determined getting, for instance,

$$\left.\begin{matrix} C_1 \\ \bar{C}_1 \end{matrix}\right\} = \mp e^{-\kappa^{-1/2}p^{1/2}D}$$

$$\times \frac{\Theta - \dfrac{A_0 D'}{2K}\left[\left(\dfrac{D'}{2} - \kappa^{1/2}p^{-1/2}\right)e^{\kappa^{-1/2}p^{1/2}D'} + \left(\dfrac{D'}{2} + \kappa^{1/2}p^{-1/2}\right)e^{-\kappa^{-1/2}p^{1/2}D'}\right]}{e^{\kappa^{1/2}p^{1/2}D} - e^{-\kappa^{-1/2}p^{1/2}D}}, \quad (31)$$

while $\kappa_1 = \kappa_2 = \kappa$ and $K_1 = K_2 = K$ are assumed again.

With (31) the temperature gradient at the earth's surface is calculated as

$$\left(\frac{\partial u_1}{\partial z}\right)_{z=D} = -\frac{\kappa^{-1/2}p^{1/2}}{\sinh(\kappa^{-1/2}p^{1/2}D)}\left[\Theta - \frac{A_0 D'}{2K}\left\{D' \cosh(\kappa^{-1/2}p^{1/2}D') - \frac{2\sinh(\kappa^{-1/2}p^{1/2}D'}{\kappa^{-1/2}p^{1/2}}\right\}\right]. \quad (32)$$

Putting $p \rightarrow 0$, the steady gradient is given as

$$\left(\frac{\partial u_1}{\partial z}\right)_{z=D} = -\frac{\Theta}{D} - \frac{A_0 D'^2}{2KD}. \quad (33)$$

Since the first term of (33) is led from the condition that the temperature is kept at Θ at the bottom of the layer, only the second term is important in order to see the influence of the phase transformation.

Suppose that the latent heat amounts to 100 *cal/gm*, a likely value for magma, and that *f years* are required to solidify unit volume of magma, A_0 amounts to $f^{-1} \times 0.86 \times 10^{-6}$ *cal/cm*^{3} *sec* provided the density is taken at 2.7 *gm/cm*^{3}. The surface heat flow is then given by $0.43 \times 10^{-6} \times (D'/D) \times f^{-1}D'$ *cal/cm*^{2} *sec* from which we may estimate heat flow values for some combinations of D, D' and f as are given in Table 4.

Table 4. Heat flow values associated with solidification of magma in units of *cal/cm*^{2} *sec*.

$f^{-1}D'$ (*km/year*) / D'/D	10^{-5}	10^{-4}	10^{-3}	10^{-2}
1	4.3×10^{-7}	4.3×10^{-6}	4.3×10^{-5}	4.3×10^{-4}
0.1	4.3×10^{-8}	4.3×10^{-7}	4.3×10^{-6}	4.3×10^{-5}
0.01	4.3×10^{-9}	4.3×10^{-8}	4.3×10^{-7}	4.3×10^{-6}

We can see in the table that an appreciable heat flow, larger than 10^{-6} *cal/cm² sec* say, takes place for $f^{-1}D'>10^{-4}$ *km/year* even in the case of $D'/D=1$. For smaller values of D'/D, much larger $f^{-1}D'$ is required. It has been known, however, that the isothermals are displaced with a speed of the order of 1 *cm/year* or 10^{-5} *km/year* in the cases of cooling of magma mass having a linear scale of a few kilometers. The figure would become smaller if a bigger mass of magma were supposed. We therefore see that the heat flow considered here hardly reaches 10^{-6} *cal/cm² sec*. Even in a favourable case, heat flows of this origin would only be a fraction of the general one.

5. Concluding remarks

Terrestrial heat flows related to three possible events, namely subcrustal convection, long-living magma reservoir and phase transformation layer are estimated.

It turns out that a steady subcrustal convection current having a linear dimension of a few thousand kilometers can give rise to a heat flow several times as large as the world's average provided the velocity of several *cm/year* and temperature gradient of some 1°C/*km* are assumed in the earth's mantle. It is then conceivable that the high heat flow values observed on the East Pacific Rise may be caused by some convection currents in the earth's mantle. The high temperature suggested in this study at the bottom of the crust seems to harmonize well with the low velocity of seismic waves[39].

The possible heat flows associated with a high-temperature magma reservoir supposed in the earth's crust are not very large. It might not be possible to detect the magma by an observation of anomaly in terrestrial heat flow unless its depth does not exceed 10 *km* or so.

It seems also likely that no conceivable phase transformation layers give a considerable heat flow anomaly. But some fractions of heat flow values may be caused by subcrustal convection of a small scale, underground magma mass being kept at a high temperature over a long period or presence of a layer in which some crystallization is taking place. It is not practicable to correlate these geophysical events with the small anomalies observed in heat flow. The only thing that seems quite certain is the fact that the high heat flows such as found on the East Pacific Rise cannot be explained unless we suppose

---

[39] G. C. SHOR, *Information Bulletin, Pacific Sci. Ass.*, **11** No. 6 (1959), 12.

a large-scale convection current under the earth's crust.

There are many other geophysical events which may be associated with anomalies in heat flow. One of the most important problems is the possible coupling between mechanical strain and heat flow. Although it is no easy matter to tackle such an irresversible thermodynamical process, extensive investigations in this line are strongly recommened to perform on the basis of well-observed data of heat flow, crustal deformation and seismic activity.

---

25. 地球熱学 (第4報) マントル内熱対流その他に伴なう熱流量

地震研究所　力武常次
東京大学大学院地球物理学専門課程　宝来帰一

地球マントル内の定常熱対流に伴なう地表面熱流量を計算し，通常想像されているように温度勾配を 1°*C/km*，流速を数 *cm/year* 程度と仮定すれば，波長 1000 *km* 程度以上の対流においては，East Pacific Rise 海底で観測されるような大きな熱流量の値が期待されることを示した.

つぎに地殻内に高温マグマや相転移層が長期間存在する場合の定常熱伝導を調べたが，熱源がきわめて地表に近い場合を除けば，10^{-6} *cal/cm²* *sec* 以上の熱流量を期待することはほとんど不可能であり，このような場合には熱流量の異常を調べて，地下の状態を推定することは困難である.

BULLETIN OF THE EARTHQUAKE
RESEARCH INSTITUTE
Vol. 38 (1960), pp. 421-436

26. *Studies of the Thermal State of the Earth. The Sixth Paper: Terrestrial Heat Flow at Innai Oil Field, Akita Prefecture and at Three Localities in Kanto-District, Japan.*

By Seiya UYEDA

Earthquake Research Institute,

and

Ki-iti HÔRAI,

Graduate School, University of Tokyo.

(Read March 22, and June 28, 1960.—Received June 30, 1960).

Summary

Values of terrestrial heat flow have been determined at four localities in Honshu, the Main Island of Japan, for deep wells penetrating sedimentary layers. The sedimentary strata being saturated with water in situ, thermal conductivity of the cores was measured in the saturated state. The heat flow values are, each in the unit of 10^{-6} *cal/cm²sec*, 1.49 at Innai Oil Field, Akita Prefecture, 0.74 at Tokyo University, Tokyo, 0.76 at Kashima, Ibaraki Pref. and 0.91 at Katsuta, Ibaraki Pref. As far as the eastern part of Japan is concerned, the data so far obtained seem to suggest that the heat flow is smaller on the Pacific coast side than inland and on the Japan Sea side. Repeated temperature measurements in the wells at Kashima and Katsuta showed that the temperature data obtained immediately after the end of boring are not correct except near the bottom.

1. Introduction

The present report forms a part of the authors' attempt to determine the distribution of the terrestrial heat flow in and around the Japanese Islands. The results, reported already in this Bulletin[1),2)], are summarized in Table 1 and Fig. 1. Though the data are very insufficient, it may be suspected that the terrestrial heat flow values in

---

1) S. UYEDA, T. YUKUTAKE and I. TANAOKA, *Bull. Earthq. Res. Inst.*, **36** (1958), 251.

2) K. HÔRAI, *Bull. Earthq. Res. Inst.*, **37** (1959), 571.

Honshu, the main Island of Japan, are somewhat greater than the world's average ($1.2-1.4\times10^{-6}$ *cal/cm²sec*). On the Pacific coast side, however, rather small values were obtained at Hitachi Mine ($0.63-0.90\times10^{-6}$ *cal/cm²sec*).

In the present work, it is intended to obtain the heat flow values

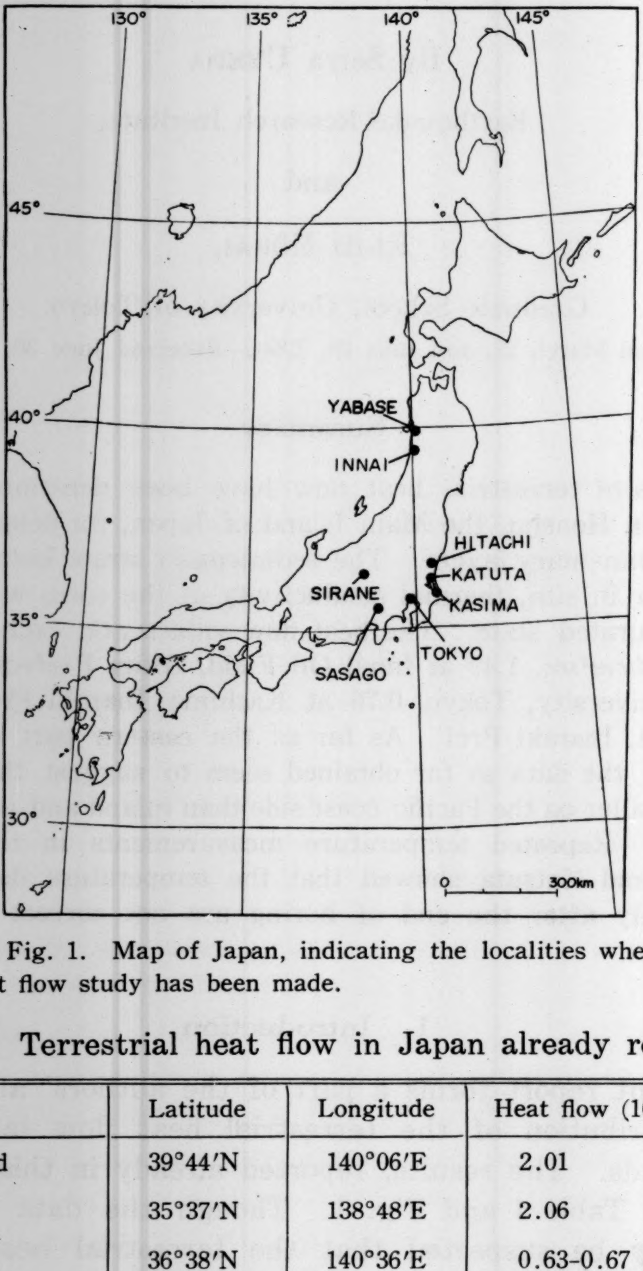
130°
135°
140°
145°
45°
40°
35°
30°
YABASE
INNAI
HITACHI
KATUTA
KASIMA
SIRANE
TOKYO
SASAGO
0
300km

Fig. 1. Map of Japan, indicating the localities where heat flow study has been made.

Table 1. Terrestrial heat flow in Japan already reported.

Locality	Latitude	Longitude	Heat flow (10^{-6} *cal/cm² sec*)
Yabase Oil Field	39°44′N	140°06′E	2.01
Sasago Tunnel	35°37′N	138°48′E	2.06
Hitachi Mine	36°38′N	140°36′E	0.63–0.67 (northern part) 0.78–0.90 (southern part)
Sirane Thermal Area	36°37′N	138°34′E	10.8

for some deep wells: one in Innai Oil Field, Akita Prefecture, two in Ibaraki Prefecture and one in Tokyo University, Tokyo (Fig. 1). The geothermal gradient in these wells were obtained from the already existing data of temperature measurements. The common features of these wells are that the strata penetrated by them are all rather soft sedimentary layers with varied grain size and that the layers are considered to be saturated with water in situ. It was, therefore, not possible to utilize the temperature data of these wells for estimating the heat flow values until the effect of water content on thermal conductivity of sediments was quantitatively elucidated as reported in our preceding communication[3], of which the outline summary is as follows: the thermal conductivity of sediments increases with water content when one adds water to a dry specimen and this increase continues until water saturates the pore of the specimen. With more addition of water, i.e., in the oversaturated state, the thermal conductivity decreases with increase of water content and finally approaches the conductivity of pure water, which is a good deal smaller than that of ordinary rock-forming minerals. An example of the experiments showing the variation of thermal conductivity with water content is reproduced in Fig. 2, in which it is observed that the conductivity takes a maximum value at

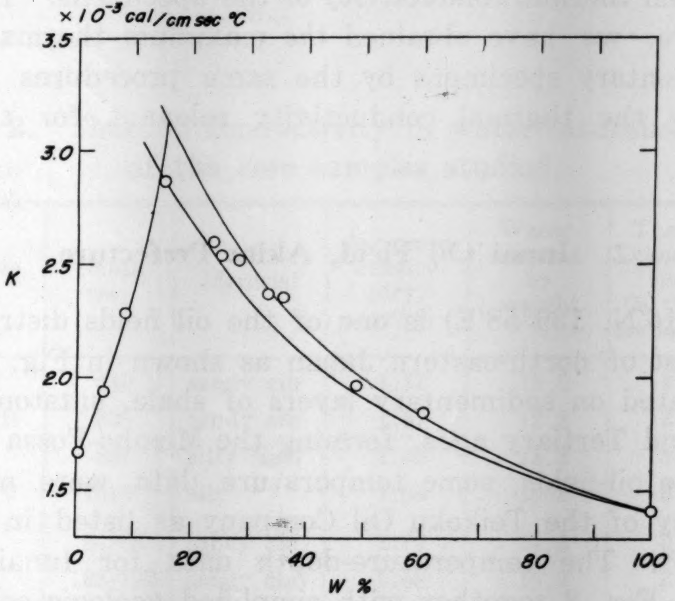

Fig. 2. Relation between thermal conductivity and water content (weight percentage): Lower Sasaoka Bed (IN VIII).

---

3) K. Hôrai and S. Uyeda, *Bull. Earthq. Res. Inst.*, **38** (1960), 217.

the water content by weight of some 18 per cent. It was shown also that, on an experimental as well as a theoretical basis, this water content should be the saturation water content of the specimen. Following the method by Bullard et al.,[4] a simple theoretical explanation was also given to the above mentioned effect of water content on thermal conductivity and *the* maximum thermal conductivity, i.e., the conductivity at the saturation point was expressed as

$$K_{\max}=k_w\frac{3-2v_p(1-k/_w k_s)}{3k_w/k_s+v_p(1-k_w/k_s)}\,, \qquad (1)$$

where k_w, k_s and v_p stand for the thermal conductivity of water and of the mineral grains and the porosity of the specimen. It seems, therefore, legitimate that in estimating the terrestrial heat flow in the cases where the strata concerned are saturated with water in situ to use *the* maximum thermal conductivity of the specimens. In the present work, therefore, we have obtained *the* maximum thermal conductivity for each sedimentary specimens by the same procedures as in 3) and regarded it as the thermal conductivity relevant for the heat flow estimation.

2. Innai Oil Field, Akita Prefecture

Innai (30°16′N, 139°58′E) is one of the oil fields distributed on the Japan Sea coast of north-eastern Japan as shown in Fig. 1. These oil-fields are situated on sedimentary layers of shale, siltstone and tuff of Quarternary and Tertiary ages, forming the Mizuho-Fossa Magna Folded Belt. Of these oil-fields, some temperature data were made available by the courtesy of the Teikoku Oil Company as listed in our previous communication[5]. The temperature-depth data for Innai Oil Field is reproduced in Fig. 3 together with simplified geologic column. Circles in the figure are the results of bottom temperature measurements for the wells with various depths in the oil-field. The measurements were usually made on finishing the drilling, after leaving the wells for at least 20 hours. As will be stated later, there are reasons for regarding the bottom temperature thus measured as the true temperatures. The mean geothermal gradient is estimated as $4.3°C/100\,m$. Some cores of the strata were given to the authors by the Teikoku Oil Company; they

---

4) E. C. BULLARD, A. E. MAXWELL and R. REVELLE, *Adv. Geophys.*, *III* (1956), 153.

5) S. UYEDA, T. YUKUTAKE and I. TANAOKA, *loc. cit.*

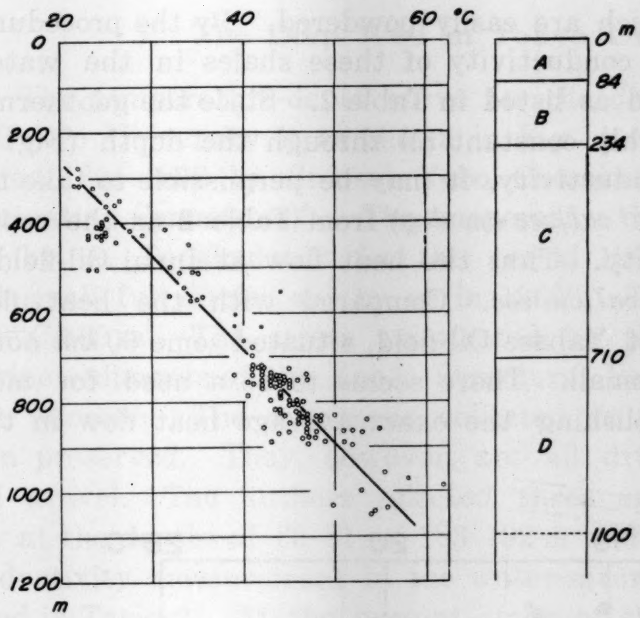

Fig. 3. Underground temperature in Innai Oil Field, Akita Prefecture, and the geologic column:
A....Magurogawa bed,
B....Upper Sasaoka bed,
C....Lower Sasaoka bed,
D....Tentokuzi bed.

Table 2. Thermal conductivity in water-saturated state of the core samples studied.

Locality	Sample No.	Depth (*m*)	Material	Apparent density (dry) (*gr/cc*)	Water-content by weight (*%*)	Thermal conductivity (10^{-3} *cal/cm sec deg*)	Temperature during measurement (*deg °C*)
Innai	IN VI	449	sandy silt	1.72	15.5	3.18	36.1
	IN VIII	635	sandy silt	1.67	15.2	2.87	22.2
	IN X	827	silty sand	1.48	14.3	3.14	31.5
	IN XIV	1019	silt	1.53	15.3	3.13	34.8
Tokyo Univ.	TU I	64-68	sandy clay	1.73	14.2	3.49	33.1
	TU II	183-192	sandy clay	1.68	15.3	2.95	32.4
	TU III	251-261	clay	1.75	12.6	3.65	30.1
Kashima	KS II	203-205	sandy silt	1.56	14.1	2.90	32.5
	KS III	322-324	sandy silt	1.61	15.7	3.65	32.2
	KS VII	555-558	sand	1.71	12.4	4.49	32.5
	KS VIII	655-658	silt	1.61	19.8	3.22	32.9
Katsuta	KT I	345	silt	1.58	19.7	2.75	34.8
	KT II	503	silt	1.65	17.2	2.67	33.1
	KT III	755	sandy silt	1.90	12.4	3.29	33.9
	KT IV	905	sandy silt	1.97	12.2	3.38	34.5

are all rather soft shale which are easily powdered. By the procedures stated already, the thermal conductivity of these shales in the water-saturated state was obtained as listed in Table 2. Since the geothermal gradient appears to be roughly constant all through the depth (Fig. 3) and so does the thermal conductivity, it may be permissible to take the simple mean value (3.11×10^{-3} *cal/sec cm deg*) from Table 2 as the representative thermal conductivity. Thus the heat flow at Innai Oil-field is estimated to be 1.49×10^{-6} *cal/cm²sec*. Compared with the heat flow value 2.01×10^{-6} *cal/cm²sec* at Yabase Oil-field, situated some 60 *km* north of Innai, it is considerably small. There seems to be a need for more determinations before establishing the exact average heat flow in this part of Japan.

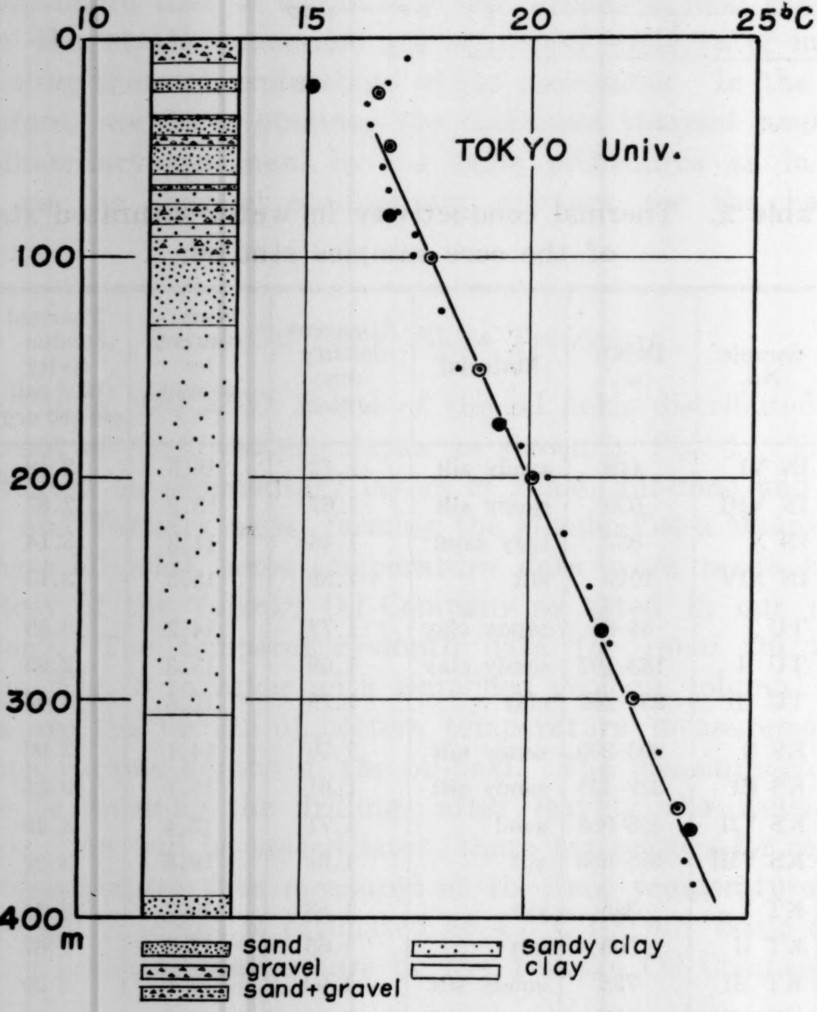

Fig. 4. Temperature-depth curve in the well at Tokyo University.

3. The Deep Well in Tokyo University, Tokyo

The temperature-depth curve for the deep well (35°42′N, 139°46′E) in Tokyo University is as shown in Fig. 4. The well was drilled in the period 1894–1898 by Shinsai Yobo Chosakai (Imperial Earthquake Investigation Committee)[6]. The temperature data shown by double circles are by A. Tanakadate[6] for the period 1901–1903, and those by large and small full circles are by us in 1957[7]. The geothermal gradient is $2.20°C/100\,m$. The strata penetrated by the well are the Quaternary marine sediments of the Kanto Structural Basin that has subsided since late Miocene. The specimens collected in the course of drilling have been preserved. They, however, are all dried clay, sandy clay, sand and gravel. The authors selected three specimens of clay and sandy clay at the depths of 65–81 *m*, 183–192 *m* and 251–261 *m* for the thermal conductivity measurement in the water-saturated state. The results are listed in Table 2. At the present stage of the accuracy of information, it was decided to take the simple mean value (3.36×10^{-3} *cal/cm sec deg*) of the individual thermal conductivity values for the representative thermal conductivity. As for the heat flow value, thus, $0.74\times10^{-6}\,cal/cm^2sec$ was obtained.

4. Two Deep Wells in Ibaraki Prefecture

For natural underground gas development, test boring at several localities in Kanto District has been conducted. Temperature-depth relations and core specimens were supplied to the authors by the Geological Survey for two survey holes in Ibaraki Prefecture owned by Nitto Chemical Industry, Tokyo: one is an 888.8 *m* deep hole at Kashima (KT-1) and the other is a 906.9 *m* deep hole at Katsuta (TR-1). The locality maps for these wells are in Fig. 5, a, b and Fig. 6, a, b. Their positions are 35°57′N, 140°41′E and 36°24′N, 140°30′E respectively.

Kashima well is located on the eastern marginal area of the Kanto Structural Basin and the core specimens belong to Quaternary (upper 50 *m*) and Tertiary (below 50 *m*) sediments. The thermal conductivity of the sediments in the water-saturated state is listed in Table 2, giving the mean value of 3.57×10^{-3} *cal/cm sec deg*. Katsuta is situated on the southern end of the thick Tertiary beds occupying the southern marginal area of Abukuma Plateau along Tanakura Sheared Zone. The

---

[6] A. TANAKADATE, *Rep. Imp. Earthq. Invest. Committ.*, **45** (1903), 17.

[7] S. UYEDA, T. YUKUTAKE, and I. TANAOKA, *loc. cit.*

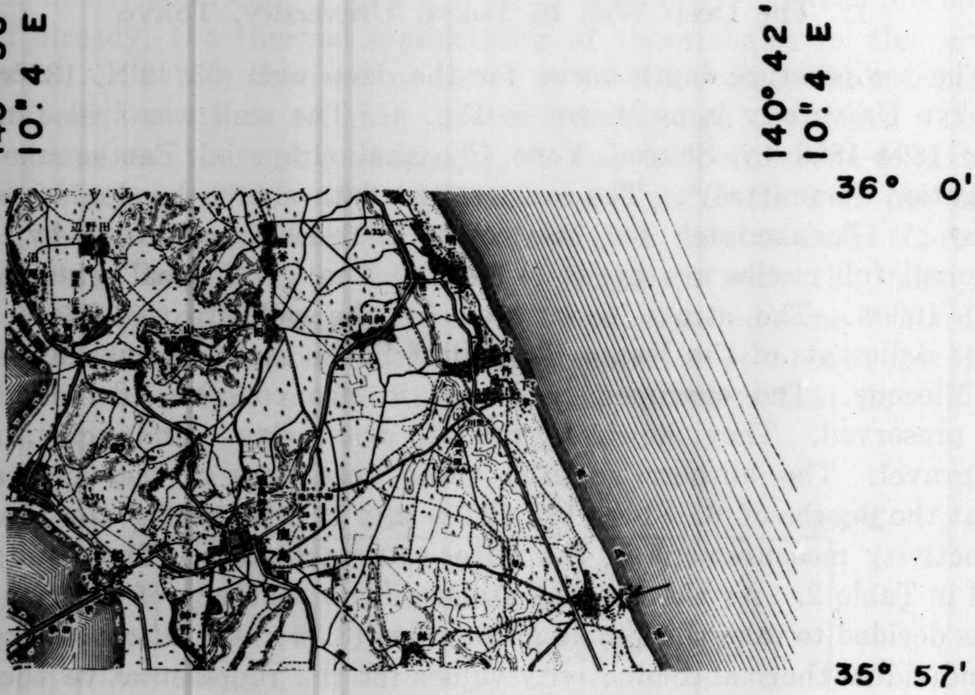
140° 36'
10".4 E
140° 42'
10".4 E
36° 0' N
35° 57' N

Fig. 5, a. Locality map of Kashima well.

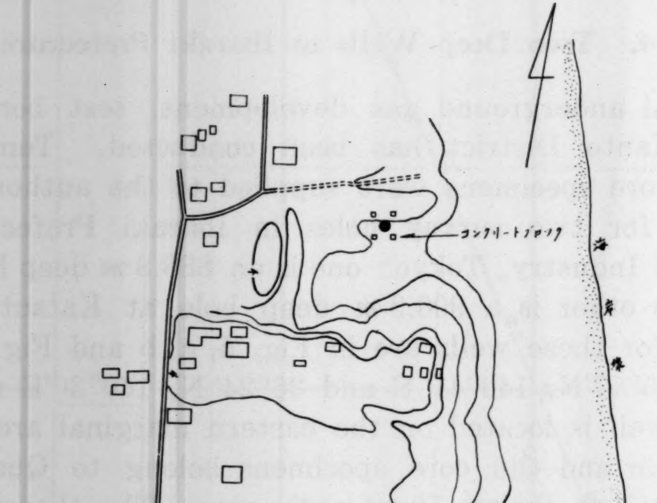
コンクリートブロック
海
岸
至鹿島麻薬所
灯台
0
50
100m

Fig. 5, b. Sketch map of Kashima well.

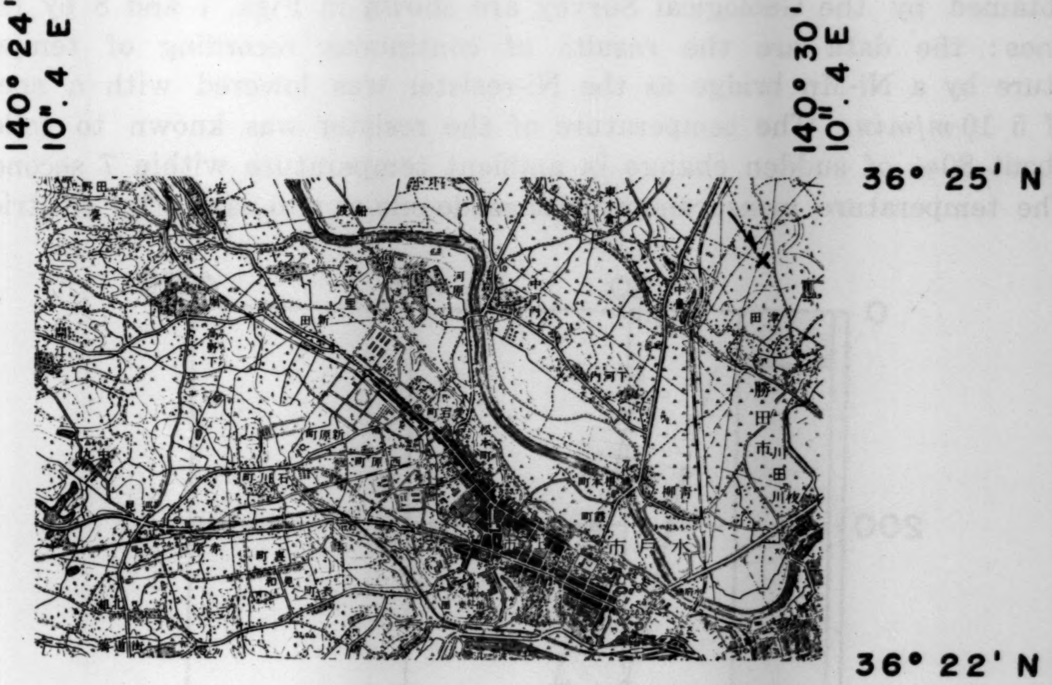
140° 24'
10".4 E
140° 30'
10".4 E
36° 25' N
36° 22' N

Fig. 6, a. Locality map of Katsuta well.

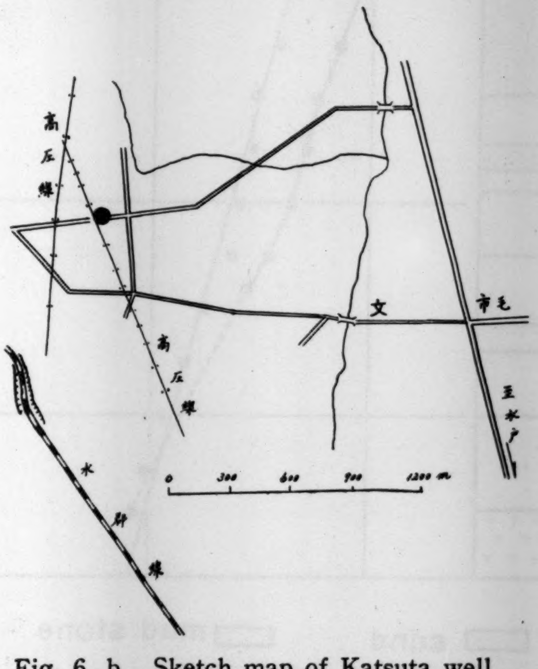
高圧線
高圧線
文
市毛
至水戸
水郡線
0
300
600
900
1200 m

Fig. 6, b. Sketch map of Katsuta well.

strata below 50 *m* are Miocene marine deposits. The conductivity values for water-saturated state are again in Table 2: mean value being 3.02×10^{-3} *cal/cm sec deg*. The temperature-depth relation in these wells obtained by the Geological Survey are shown in Figs. 7 and 8 by thin lines: the data are the results of continuous recording of temperature by a Ni-Mn bridge as the Ni-resistor was lowered with a speed of 5-10 *m/min*. The temperature of the resistor was known to follow about 80% of sudden change in ambient temperature within 7 seconds. The temperature measurement was made one or two days after electrical

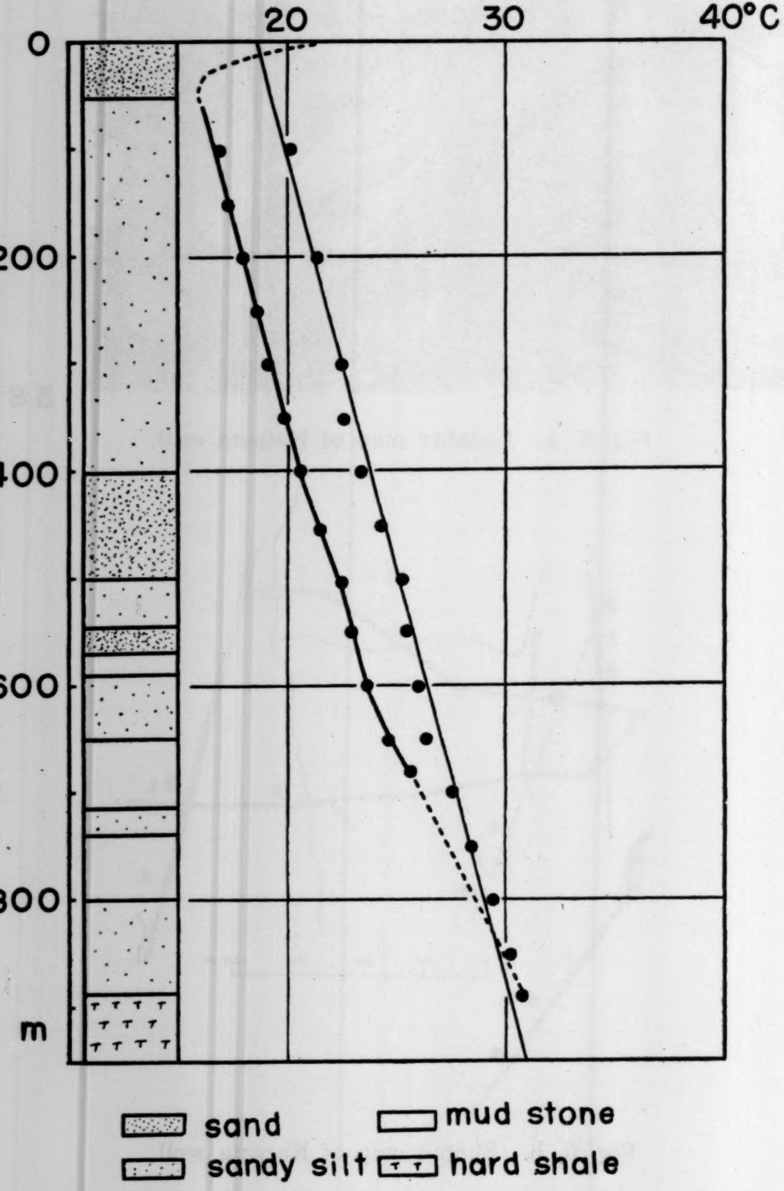

Fig. 7. Temperature-depth curves for Kashima well and the geologic column: thin line.....measurement immediately after drilling, thick line....measurement at 20 months after drilling.

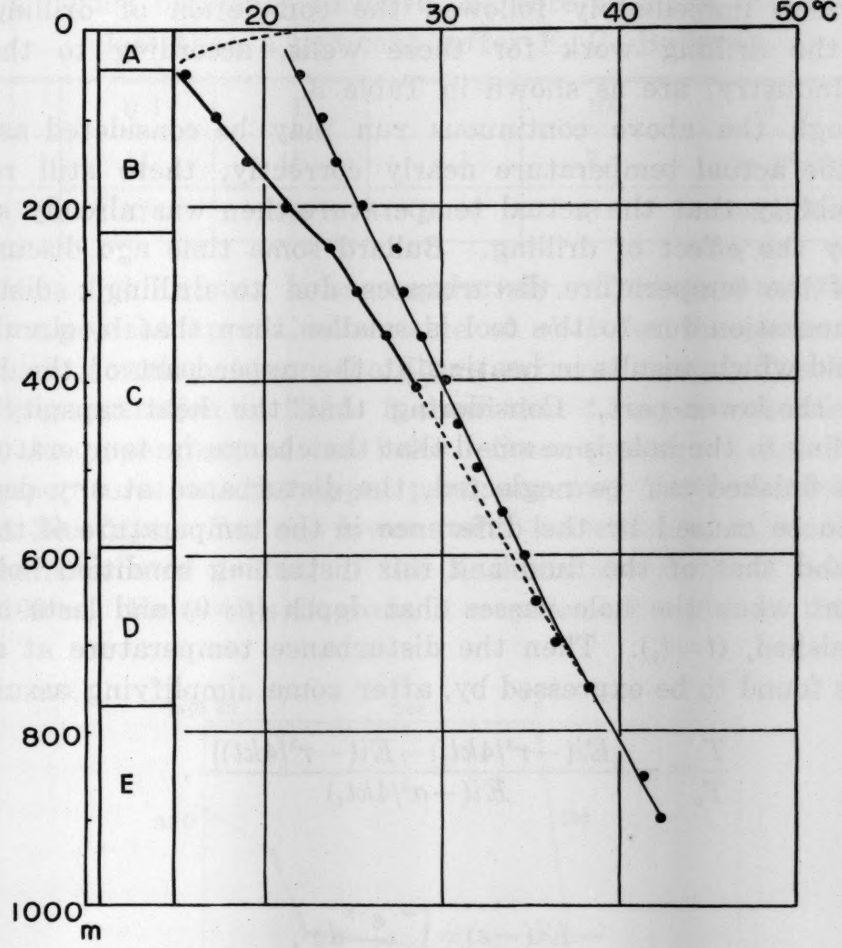

Fig. 8. Temperature-depth curves for Katsuta well, and the geologic column:
A....Kamiichi gravel,
B....Genjigawa bed,
C....Zuiryu bed,
D....Daiman bed,
E....Sionokusa bed,
thin line.....measurement immediately after drilling,
thick line....measurement at 9 months after drilling.

Table 3. Drilling schedule of Kashima and Katsuta wells.

	Kashima (KT-1)	Katsuta (TR-1)
Start	Sept. 1, 1958	Aug. 28, 1959
End	Oct. 10, 1958 at 891 m	Oct. 9, 1959 at 906 m
Electrical Logging	Oct. 13, 1958	Oct. 15, 1959
Temperature Logging	Oct. 15, 1959	Oct. 16, 1959

logging which immediately followed the completion of drilling. The dates of the drilling work for these wells, according to the Nitto Chemical Industry, are as shown in Table 3.

Although the above continuous run may be considered as having recorded the actual temperature nearly correctly, there still remained a fair possibility that the actual temperature then was already seriously affected by the effect of drilling. Bullard some time ago discussed the problem of the temperature disturbances due to drilling[8]: disturbance by heat generation due to the tool is smaller than that by circulation of drilling fluid which results in heating at the upper part of the hole and cooling at the lower part. Considering that the heat capacity of the fluid standing in the hole is so small that the change in temperature after the bore is finished can be neglected, the disturbance at any depth was assumed to be caused by the difference in the temperature of the virgin stratum and that of the fluid and this disturbing condition holds from the moment when the hole passes that depth ($t=0$) and lasts until the bore is finished, ($t=t_1$). Then the disturbance temperature at a time t ($t>t_1$) was found to be expressed by, after some simplifying assumptions,

$$\frac{T}{T_0}=-\frac{\{Ei(-r^2/4kt_2)-Ei(-r^2/4kt)\}}{Ei(-a^2/4kt_1)}\,, \qquad (2)$$

where

$$-Ei(-z)=\int_z^\infty \frac{e^{-z}}{z}dz\,,$$

and

T=disturbance temperature at a point r from the axis of the hole,
T_0=disturbance temperature at the wall of the hole at $t=t_1$.
k=thermal diffusivity of the stratum,
$t_2=t-t_1$, and a=radius of the hole.

When $r^2/4kt$ is small, (2) can be approximated by,

$$T/T_0=\log(1+t_1/t_2)/(\log 4kt_1/a^2-0.577)\,. \qquad (3)$$

From these Bullard calculated, as a function of t_1, the value of t_2/t_1, needed to reduce the disturbance to 1 per cent of its initial value, for extreme values of $a^2/4k$ likely to be encountered in practice. His results are as shown in Table 4.

In the present cases, the diameters are 7.7 inches and $6\frac{3}{4}$ inches for

---

[8] E. C. BULLARD, *Mon. Not. Roy. Astr. Soc., Geophys. Suppl.*, **5** (1947) 127.

Table 4. Time necessary to leave the bore to make the disturbance less than a per cent (after E. C. Bullard).

t_1	0.1	1	10	100	in days
t_2/t_1	14	11	8.3	7.4	for $a^2/4k=58$
t_2/t_1	51	28	18	13	for $a^2/4k=38{,}000$

the Kashima and Katsuta holes respectively. Taking 10 *cm* for a, 0.005 for k, we get the approximate value of $a^2/4k$ for the present cases as 5000, which is well between the above extreme cases. The records of the drilling operation in Table 3 show that t_1 in our cases is about 30 days for the upper part of the holes. Consequently, in order of obtain true temperatures at the upper part, one may have to leave the hole for some 300 days. For the lower part, however, t_1 is small. Fig. 9 shows the records of drilling of the Kashima and Katsuta holes for the last ca 100 *m*. From this diagram, it may be observed that the last few

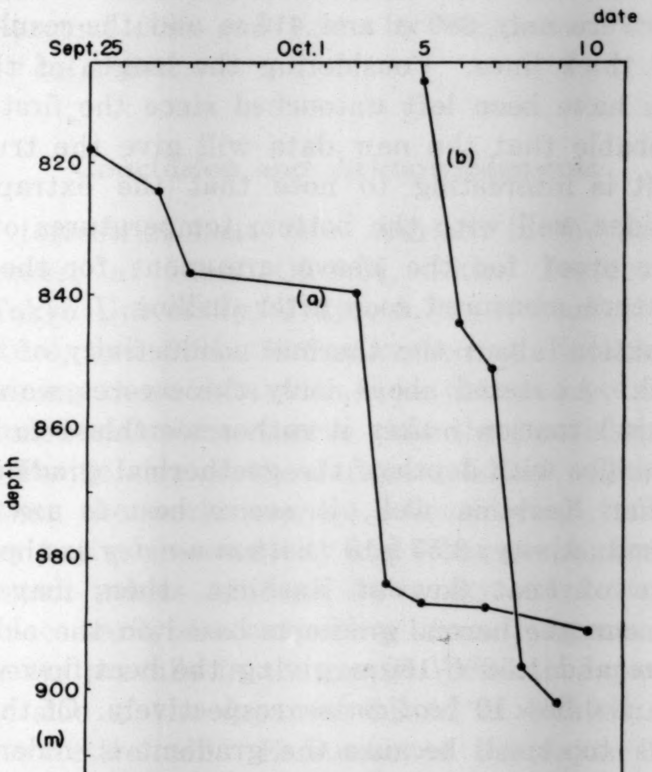

Fig. 9. Diagram showing the depth of the bores at final stage of drilling:
(a)....Kashima well, (b)....Katsuta well.

meters were drilled in a time which is a fraction of a day, and therefore the measurement at one or two days after the bore was finished would give very nearly the true temperature for the bottom. Such a fact has recently been reported by Cooper and Jones[9]. Moreover, in the actual drilling of these wells, water supply being insufficient and the drilling fluid being expensive, circulations of the fluid was made in such a way that fluid coming up from the bottom was recovered and filtered to be used as many times as possible. This, in fact, resulted in a rise of the temperature of the circulating fluid, both by heating at the bottom part and by heating on the sunlit surface, nearly to the bottom temperature. Therefore, as for the thermal disturbance, the cooling at the bottom must have been much smaller than the heating near the top.

Recently, the Nitto Chemical Industry has kindly allowed the authors to re-measure the temperatures in these wells. The measurements were made on June 24 and 25, 1960 for Kashima and Katsuta wells respectively. Unfortunately, owing to various difficulties, the depths covered were only 680 *m* and 410 *m* and the results are shown in Fig. 7 and 8 by thick lines. Considering the length of the time during which the wells have been left untouched since the first measurement, it is highly probable that the new data will give the true temperature in the wells. It is interesting to note that the extrapolation of the new data coincides well with the bottom temperatures of the old data. This may be a proof for the above argument for the correctness of bottom temperature measured soon after drilling.

The information about the thermal conductivity of the strata concerned is limited. As stated above, only three cores were measured for each holes. This situation makes it rather worthless to try to correlate the observed changes with depth of the geothermal gradient and thermal conductivity. For Kashima well, it seems best to use the average of the measured conductivity, 3.57×10^{-3} *cal/cm sec deg* as the representative one. The value of heat flow at Kashima, then, may be obtained as follows; The mean geothermal gradients based on the old and new data are $1.28°C/100\ m$ and $1.50°C/100\ m$ giving the heat flow values of $0.46 \times 10^{-6}\ cal/cm^2sec$ and $0.56 \times 10^{-6}\ cal/cm^2sec$ respectively. Of these two values, the first one is too small because the gradient is underestimated, and the second one may be closer to the true value. Below 600 *m*, (Fig. 8), the temperature data lie well on the line which passes through the bottom temperature of the old data. On account of the possible correctness of the bottom temperature, the gradient below 600 *m* seems to be 2.6°*C*/100 *m* giving the heat flow value of 0.96×10^{-6} *cal*/*cm*^{2}*sec*. This is the highest value from the data available at present. Considering the above stated situation, the terrestrial heat flow at Kashima may be safely estimated to be about $0.56 \sim 0.96 \times 10^{-6}$ *cal*/*cm*^{2}*sec*, the mean value being 0.76×10^{-6} *cal*/*cm*^{2}*sec*. For Katsuta well, the average conductivity being 3.02×10^{-3}*cal*/*cm sec deg*, the old data of temperature give geothermal gradient and the heat flow as 2.40°*C*/100 *m* and 0.73×10^{-6} *cal*/*cm*^{2}*sec*. The new data clearly show (Fig. 9) a kink in temperature-depth curve at about 250 *m*. As no conductivity data are available above 250 *m*, we take, from the new data, the gradient between 400 *m* and 250 *m* which is 3.12°*C*/100 *m*. This gives the heat flow value as 0.94×10^{-6} *cal*/*cm*^{2}*sec*. In this case, the extrapolation to the old bottom temperature gives the gradient of 2.90°*C*/100 *m* and the heat flow of 0.88×10^{-6} *cal*/*cm*^{2}*sec*. From these three values, the first being definitely underestimatimad we may be able to state that the terrestrial heat flow at Katsuta is around 0.88 and 0.94×10^{-6} *cal*/*cm*^{2}*sec*, their mean value being 0.91×10^{-6} *cal*/*cm*^{2}*sec*.

---

[9] L. R. COOPER and C. JONES, *Geophys. Journ. Roy. Astr. Soc.*, **2** (1959), 116.

Conclusion and Acknowledgments

Values of terrestrial heat flow obtained in the present work are, 1.49×10^{-6} *cal*/*cm*^{2}*sec* at Innai Oil-field, Akita Prefecture, 0.74×10^{-6} *cal*/*cm*^{2}*sec* at Tokyo University, Tokyo, 0.76×10^{-6} *cal*/*cm*^{2}*sec* at Kashima, Ibaraki Prefecture, and 0.91×10^{-6} *cal*/*cm*^{2}*sec* at Katsuta, Ibaraki Prefecture. Combining these data with those obtained previously (Table 1), it may be concluded with some reserve that the heat flow is consistently smaller on the Pacific side of the Japanese Island. These small values are even less than the world average. Considering that the Japanese Islands are very active in seismicity and other geophysical and geological events, these small values of heat flow may seem strange. It may, however, not necessarily be surprising if one assumes that some convective movements prevails in the mantle beneath Japan in such a way that the Pacific side of the Japanese Island is located on the sinking part of the convective cell. Existence of the Japan Trench off coast may, if the same pattern of oceanic heat flow should exist as was found in the south-eastern Pacific by Herzen[10)], incorporate this hypothesis.

---

10) R. von HERZEN, *Nature*, **183** (1959), 882.

Many more reliable determinations of terrestrial heat flow all over Japan as well as in the Pacific Ocean are undoubtedly required to establish this premature speculation.

In concluding, the authors wish to express their sincere thanks to Dr. T. Rikitake for his encouragement. They are also grateful to Prof. C. Tsuboi and Prof. T. Nagata for their interest in the present work. Kind offices of the staff of the Teikoku Oil Company, Nitto Chemical Industry, and Japan Geological Survey, especially Messrs. Y. Izumibe, J. Suyama and Y. Ono are cordially acknowledged.

---

26. 地球熱学 (第6報) 秋田県院内油田，および，関東地方三地点における地殻熱流量

地震研究所 上田誠也
東京大学大学院地球物理学専門課程 宝来帰一

第五報に報告したように，堆積岩の熱伝導度は，水による飽和状態において最大値を有する．油田，ガス田等の深井では，地層は，飽和状態にあると考えられるので，そのような場所での地殻熱流量の推定には上記の最大熱伝導度が用いられるべきである．このような考えに従つて，本州内四地点での地殻熱流量をもとめた．結果は，秋田県院内油田において $1.49\times10^{-6}\ cal/cm^2sec$，東京大学において $0.74\times10^{-6}\ cal/cm^2sec$，茨城県鹿島において $0.76\times10^{-6}\ cal/cm^2sec$，および同県勝田において $0.91\times10^{-6}\ cal/cm^2sec$ である．従来得られた結果と照合すると，東北日本に関する限り，太平洋側では，地殻熱流量は，世界的平均より更に低いようである．更に測点を増し，この傾向を確めることが望まれる．また，ボーリングに伴う地中温度の擾乱の程度，およびこの擾乱の恢復について有用な測定が，鹿島，勝田のガス井について行なわれた．

BULLETIN OF THE EARTHQUAKE
RESEARCH INSTITUTE
Vol. 38 (1960), pp. 437-449

27. *Stability and Non-Steady State of Self-Exciting Dynamos. II.*

By Takesi YUKUTAKE,*

Graduate School, University of Tokyo.

(Read June 28, 1960.—Received June 30, 1960.)

Summary

The variation of the magnetic field and the angular velocity with time are studied for two conducting spheres rotating in an infinitely extended conductor. Induction equations are approximated by those expanded up to the second time-derivatives of the magnetic field.

In some special cases, the magnetic field was found to change its polarity with diminishing amplitudes. The periods of the damping oscillation are about 1.3×10^4 *years* when the spheres of 500 *km* in radius are supposed to be rotating about 1100 *km* apart from each other in the earth's core. If the work done by the external torque is assumed to be 10^{-9} *erg/sec.cm*^{3}, the induced mgnetic field and the surface velocity of the sphere become about 1 *gauss* and 0.7 *cm/sec.* respectively.

1. Introduction

In the previous paper[1], the writer studied the time-dependent behaviours of two conducting spheres rotating in an infinitely extended conductor. In some cases, the physically unacceptable result that the magnetic field continues its growth without limit in spite of decaying of the motion of the spheres was obtained. The difficulty was supposed to be caused by the crudeness of approximation for the induction equations. In this paper approximate equations containing the second time-derivatives are integrated numerically.

2. Field equations

Suppose that two spheres (I) and (II) are rotating as in Fig. 1 and the distance between them is large enough so that, for each sphere, the magnetic field produced by the other sphere can be regarded as uniform. The spheres are so oriented that the axis of rotation of each sphere may become nearly parallel to the magnetic field induced by the other sphere. If no less energy than dissipated by Joule heating is constantly given by some driving forces, the magnetic fields of each sphere may possibly be maintained.

---

*) Communicated by T. RIKITAKE.

[1] T. YUKUTAKE, *Bull. Earthq. Res. Inst.*, **38** (1960), 1.

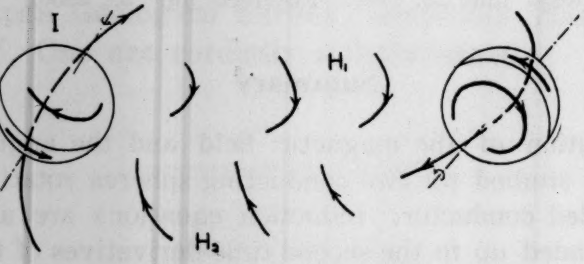

Fig. 1. A system of self-exciting dynamo.

When two spheres of the same radius a are rotating at the distance r from each other, the induced field of this system is obtained as follows,

$$H_1 = -\frac{2}{3}\pi^2\sigma^2a^2\left(\frac{a}{r}\right)^{\frac{1}{2}} J_{\frac{5}{2}}(ka)\, Y_{\frac{5}{2}}(kr)\,\Omega_1 H_2 \frac{dP_2}{d\theta}\ , \tag{1}$$

$$H_2 = -\frac{2}{3}\pi^2\sigma^2a^2\left(\frac{a}{r}\right)^{\frac{1}{2}} J_{\frac{5}{2}}(ka)\, Y_{\frac{5}{2}}(kr)\,\Omega_2 H_1 \frac{dP_2}{d\theta}\ , \tag{2}$$

where $k^2 = 4\pi\sigma p$, Ω_1 and Ω_2 represent the angular velocity of sphere I and II respectively. p is the operational representation of $\partial/\partial t$, and σ denotes the electrical conductivity both inside and outside the spheres. We have the following equations of motion,

$$C_1\frac{d\Omega_1}{dt} = G_1 - \frac{8\pi}{75}\sigma a^5 \Omega_1 H_2^2\ , \tag{3}$$

$$C_2\frac{d\Omega_2}{dt} = G_2 - \frac{8\pi}{75}\sigma a^5 \Omega_2 H_1^2\ , \tag{4}$$

where C_1 and C_2 denote the moments of inertia of the spheres. The second terms of the righthand side are the decelerating torques due to electromagnetic coupling.

3. Slowly changing magnetic field

In the case of relatively slow variation, ka and kr take small values. Accordingly Bessel functions involved in (1) and (2) can be replaced by a few terms of ascending power series expressions of ka and kr. If we assume that the radius of the rotating spheres is 500 *km* and the electrical conductivity is 3×10^{-6} *e.m.u.*, for example, the following may be valid as approximations of equations (1) and (2), so long as changes having a period larger than 5000 *years* are considered.

$$H_1=-\frac{2}{5}\pi\sigma a^2\varepsilon^3\Big[\,\Omega_1H_2+\frac{2}{3}\pi\sigma r^2\Big(1-\frac{3}{7}\varepsilon^2\Big)\frac{d}{dt}(\Omega_1H_2)$$

$$+\frac{2}{3}\pi^2\sigma^2r^4\Big(1-\frac{2}{7}\varepsilon^2+\frac{1}{21}\varepsilon^4\Big)\frac{d^2}{dt^2}(\Omega_1H_2)\Big]\,, \qquad (5)$$

$$H_2=-\frac{2}{5}\pi\sigma a^2\varepsilon^3\Big[\,\Omega_2H_1+\frac{2}{3}\pi\sigma r^2\Big(1-\frac{3}{7}\varepsilon^2\Big)\frac{d}{dt}(\Omega_2H_1)$$

$$+\frac{2}{3}\pi^2\sigma^2r^4\Big(1-\frac{2}{7}\varepsilon^2+\frac{1}{21}\varepsilon^4\Big)\frac{d^2}{dt^2}(\Omega_2H_1)\Big]\,, \qquad (6)$$

where $\varepsilon=a/r$. Solving the above four equations (3), (4), (5) and (6) simultaneously, we can see the approximate time-dependent behaviours of the system. Because of the difficulty of solving these non-linear equations analytically, we shall rely upon numerical calculation. For the sake of facility, all variables involved in the equations are made dimensionless by the following transformations.

$$t=\mathfrak{T}t', \qquad H=\mathfrak{H}H', \qquad G=\mathfrak{G}g'\,,$$

where $\mathfrak{T}=\pi\sigma a^2$, $\mathfrak{H}^2=C/\pi^2\sigma^2a^7$, $\mathfrak{G}=C/\pi^2\sigma^2a^4$. Substituting these into (3), (4), (5) and (6), and dropping primes, we have

$$H_1=-\frac{2}{5}\,\frac{\varepsilon^3}{\tau}\Big[\,\Omega_1H_2+\frac{2}{3}\,\frac{1}{\tau\varepsilon^2}\Big(1-\frac{3}{7}\varepsilon^2\Big)\frac{d}{dt}(\Omega_1H_2)$$

$$+\frac{2}{3}\,\frac{1}{\tau^2\varepsilon^4}\Big(1-\frac{2}{7}\varepsilon^2+\frac{1}{21}\varepsilon^4\Big)\frac{d^2}{dt^2}(\Omega_1H_2)\Big]\,, \qquad (7)$$

$$H_2=-\frac{2}{5}\,\frac{\varepsilon^3}{\tau}\Big[\,\Omega_2H_1+\frac{2}{3}\,\frac{1}{\tau\varepsilon^2}\Big(1-\frac{3}{7}\varepsilon^2\Big)\frac{d}{dt}(\Omega_2H_1)$$

$$+\frac{2}{3}\,\frac{1}{\tau^2\varepsilon^4}\Big(1-\frac{2}{7}\varepsilon^2+\frac{1}{21}\varepsilon^4\Big)\frac{d^2}{dt^2}(\Omega_2H_1)\Big]\,, \qquad (8)$$

$$\frac{d\Omega_1}{dt}=g\tau^2-\frac{8}{75}\tau\Omega_1 H_2^2\,,$$

$$\frac{d\Omega_2}{dt}=g\tau^2-\frac{8}{75}\tau\Omega_2 H_1^2\,. \tag{10}$$

For simplicity, $C_1=C_2$ and $G_1=G_2$ are assumed in the above transformation.

When changes are so gradual that the higher order terms than the second time-derivative can be ignored without serious loss of accuracy, the analytical treatment will be available to some extent. In some special cases, *i.e.* if $H_2=-H_1$ or $H_2=H_1$ in addition to the same angular velocity prescribed to the two spheres, phenomena regarding the spheres are quite the same.

If we take $H_2=-H_1=H$ and $\Omega_1=\Omega_2=\Omega$, neglecting the second order terms, we have,

$$\frac{d\Omega}{dt}=g\tau^2\Big(1-\frac{\Omega H^2}{\Omega_0 H_0^2}\Big)\,,$$

$$\frac{dH}{dt}=\Big[\Big(g\tau^2\frac{H^2}{H_0^2}-\frac{3\tau\varepsilon^2}{2A}\Omega_0\Big)\frac{\Omega}{\Omega_0}-\Big(g\tau^2-\frac{3\tau\varepsilon^2}{2A}\Omega_0\Big)\Big]\frac{H}{\Omega}\,,$$

where $A=1-(3/7)\varepsilon^2$, Ω_0 and H_0 denote the steady state values, *i.e.*

$$\Omega_0=\frac{5\tau}{2\varepsilon^3}\,,\qquad H_0^2=\frac{15}{4}\varepsilon^3 g\,.$$

If $H_2=H_1=H$, $\Omega_1=\Omega_2=\Omega$, we have

$$\frac{d\Omega}{dt}=g\tau^2\Big(1-\frac{\Omega H^2}{\Omega_0 H_0^2}\Big)\,,$$

$$\frac{dH}{dt}=\Big[\Big(g\tau^2\frac{H^2}{H_0^2}-\frac{3\tau\varepsilon^2}{2A}\Omega_0\Big)\frac{\Omega}{\Omega_0}-\Big(g\tau^2+\frac{3\tau\varepsilon^2}{2A}\Omega_0\Big)\Big]\frac{H}{\Omega}\,.$$

In Fig. 2, the states of $dH/dt=0$ and $d\Omega/dt=0$ in these particular cases are shown by full and broken lines respectively. Accordingly the intersecting points of full and broken lines represent the steady states of the system. If $H_1=H_2$, where the magnetic fields are induced in such a way as to weaken the fields already existing, no steady states exist. How the magnetic field and the angular velocity vary in these cases may be shown schematically by arrows in the same figures. From these, we can see, once the magnetic field gets smaller than a certain value, the

Fig. 2. Trajectories of representative points when $\varepsilon=1/10^{\frac{1}{8}}$ and $\tau=10$. Full lines represent $dH/dt=0$ and broken lines $d\Omega/dt=0$. The arrows are drawn only in half plane $H/H_0>0$ owing to the symmetrical configuration of trajectories with respect to the ordinates.

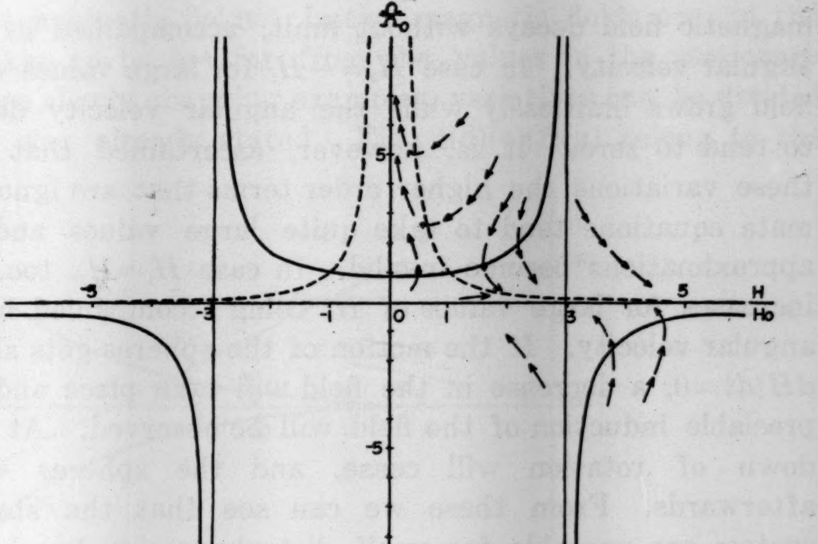

Fig. 2(a). $\Omega_1=\Omega_2$, $H_2=-H_1$, $g=1$

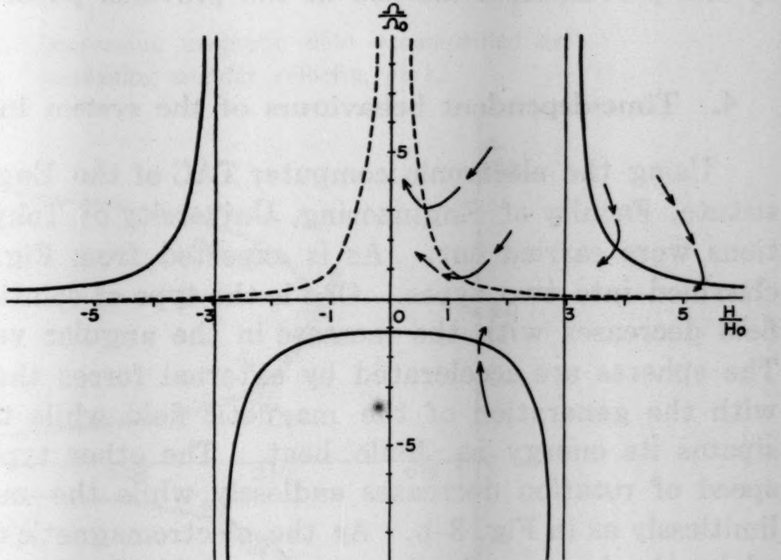

Fig. 2(b). $\Omega_1=\Omega_2$, $H_2=H_1$, $g=1$

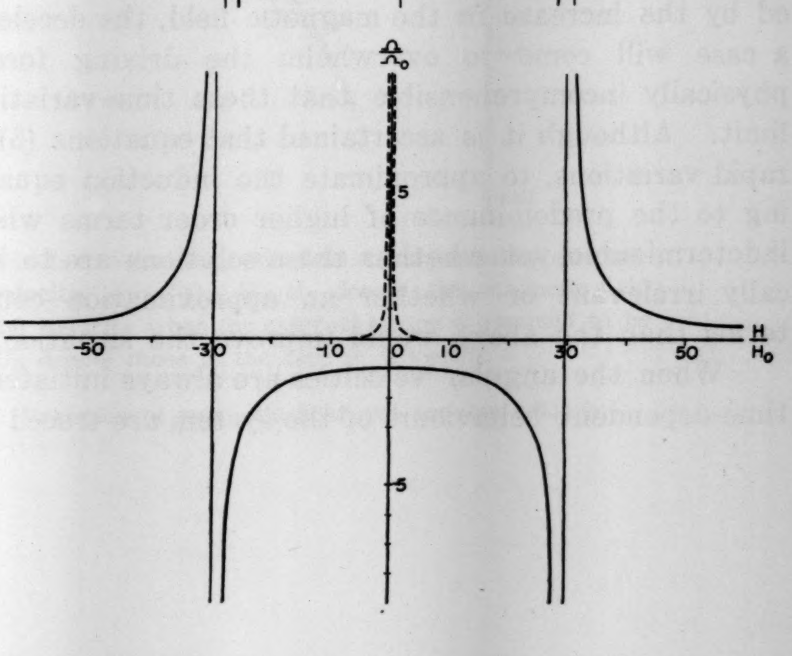

Fig. 2(c). $\Omega_1=\Omega_2$, $H_2=H_1$, $g=1/100$

magnetic field decays without limit, accompanied by an increase in the angular velocity. In case $H_2=-H_1$ for large values of H, the magnetic field grows limitlessly while the angular velocity decreases and seems to tend to zero. It is, however, ascertained that in such a state of these variations the higher order terms that are ignored in the approximate equations tend to take quite large values and that the adopted approximations become invalid. In case $H_1=H_2$, too, the magnetic field increases for large values of H, being accompanied by a decrease in the angular velocity. If the motion of the spheres gets slow across the curve $dH/dt=0$, a decrease in the field will take place and afterwards no appreciable induction of the field will be observed. At length the slowing down of rotation will cease, and the spheres will be accelerated afterwards. From these we can see that the steady states of this system are unstable for small disturbances as has been already proved by the perturbation method in the previous paper[1].

4. Time-dependent behaviours of the system in some special cases

Using the electronic computer TAC of the Engineering Research Institute, Faculty of Engineering, University of Tokyo, numerical integrations were carried out. As is expected from Fig. 2, the solutions are classified into two types. One is the type of solution in which magnetic field decreases with the increase in the angular velocity as in Fig. 3–a. The spheres are accelerated by external forces that have nothing to do with the generation of the magnetic field while the magnetic field dissipates its energy as Joule heat. The other type is one in which the speed of rotation decreases endlessly while the magnetic field increases limitlessly as in Fig. 3–b. As the electromagnetic coupling is strengthened by the increase in the magnetic field, the decelerating torque in such a case will come to overwhelm the driving force. It is, however, physically incomprehensible that these time-variations continue without limit. Although it is ascertained that equations (5) and (6) fail, in such rapid variations, to approximate the induction equations (1) and (2) owing to the predominance of higher order terms which are ignored, it is indeterminable yet whether these solutions are to be given up as physically irrelevant or whether an approximation containing higher order terms than the above would improve the situation.

When the angular velocities are always initiated from a fixed value, time-dependent behaviours of the system are traced in Fig. 4 for various combinations of the magnetic fields. Initial magnetic fields are, in the cases of Fig. 4, taken to be not far from the values in the stationary state. Even in these slowly changing examples, variations can be divided into two types as was already stated. Fig. 4(d)(e)(f)(g) belong to the

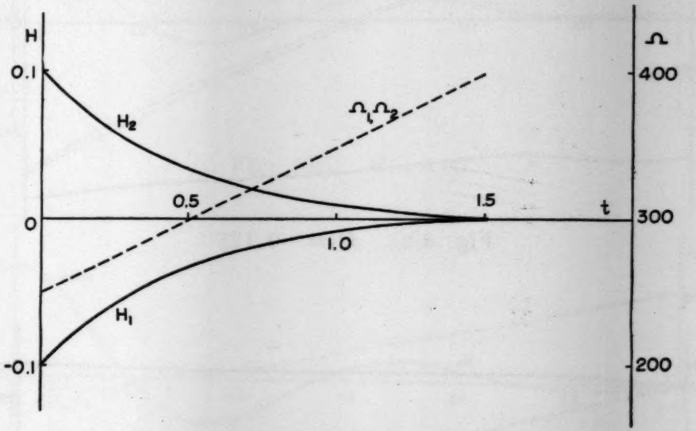

Fig. 3(a). Decreasing magnetic field accompanied by increasing angular velocity, $g=1$.

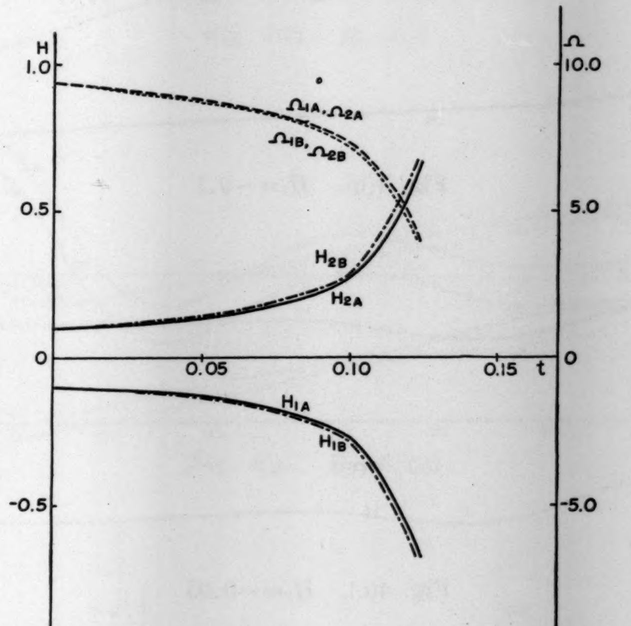

Fig. 3(b). Increasing magnetic field accompanied by decreasing angular velocity, $g=1/100$. H_A, Ω_A denote the magnetic field and the angular velocity when the external torque is assumed to be $G=g\tau^2$; H_B, Ω_B denote those in the case of $G=g\tau^2/\Omega$.

Fig. 3. Variation of magnetic field and angular velocity

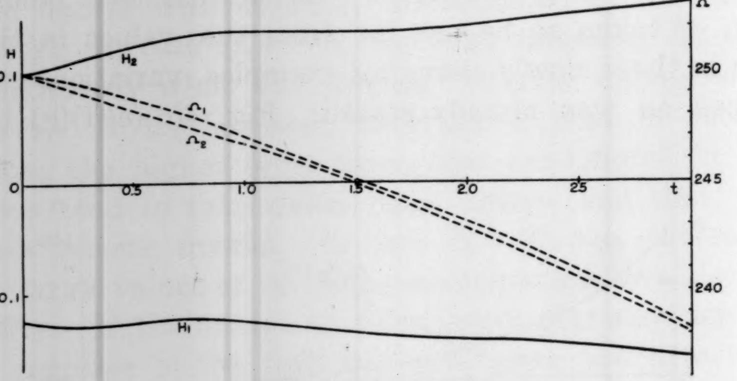

Fig. 4(a). $H_1=-0.125$

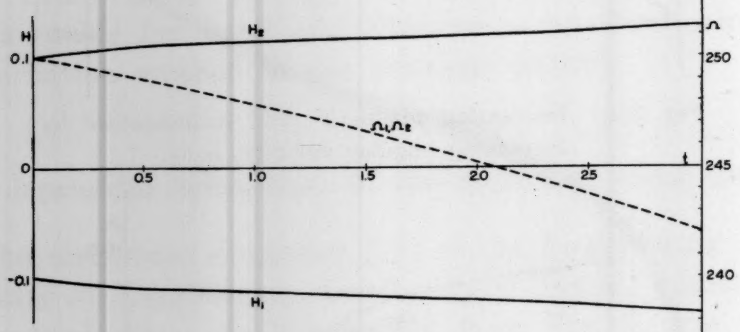

Fig. 4(b). $H_1=-0.1$

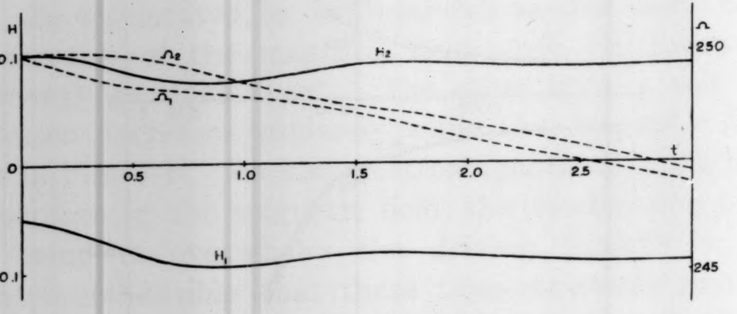

Fig. 4(c). $H_1=-0.05$

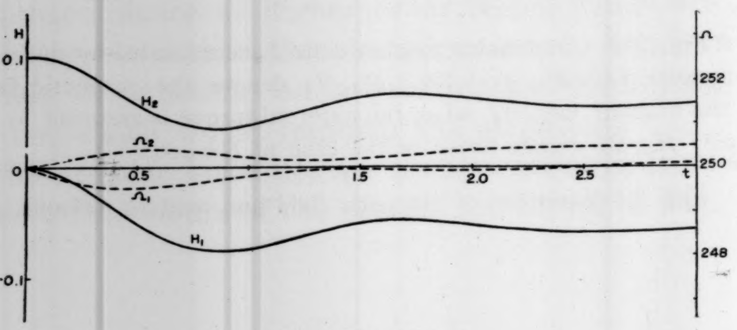

Fig. 4(d). $H_1=0$

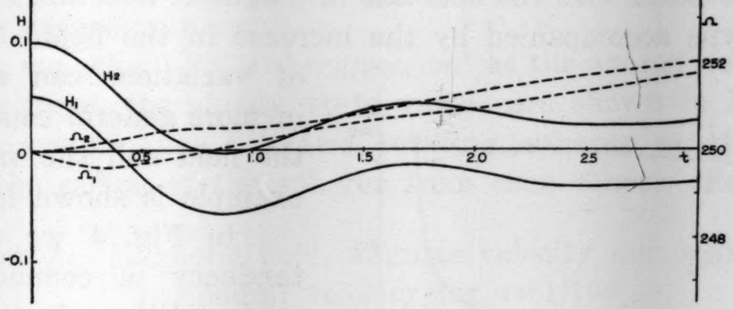

Fig. 4(e). $H_1=0.05$

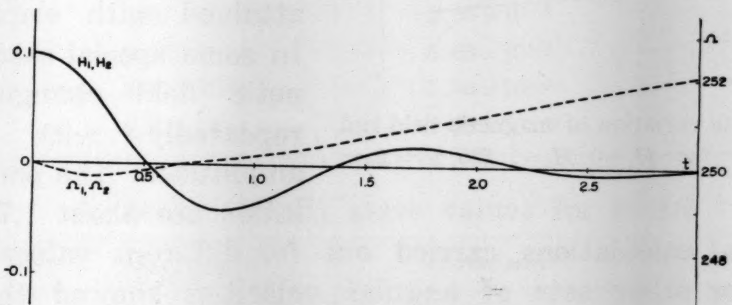

Fig. 4(f). $H_1=0.1$

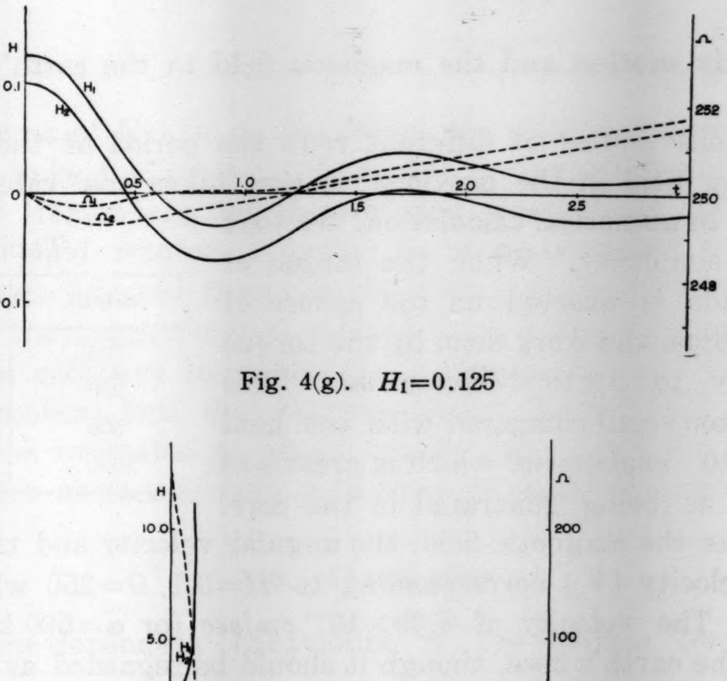

Fig. 4(g). $H_1=0.125$

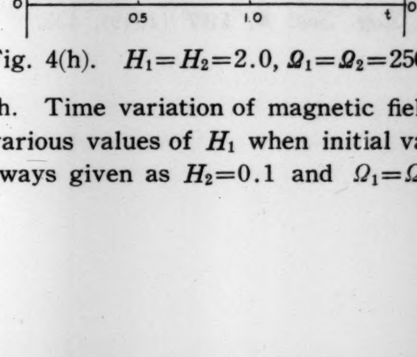

Fig. 4(h). $H_1=H_2=2.0$, $\Omega_1=\Omega_2=250$.

Fig. 4a∼h. Time variation of magnetic field and angular velocity for various values of H_1 when initial values of H_2, Ω_1 and Ω_2 are always given as $H_2=0.1$ and $\Omega_1=\Omega_2=250$, except in (h).

first type accociated with the decrease in magnetic field and Fig. 4(a)(b)(c) the second type accompanied by the increase in the field. These types of variations can also be seen in more general combinations of the field and the motion. One example is shown in Fig. 5.

In Fig. 4 we can see the tendency in common that the equi-partition of energy between the two spheres is likely to be attained with elapse of time. In some special cases, the magnetic field changes its sign repeatedly with diminishing amplitudes. The periods of oscillation are about 1.7.

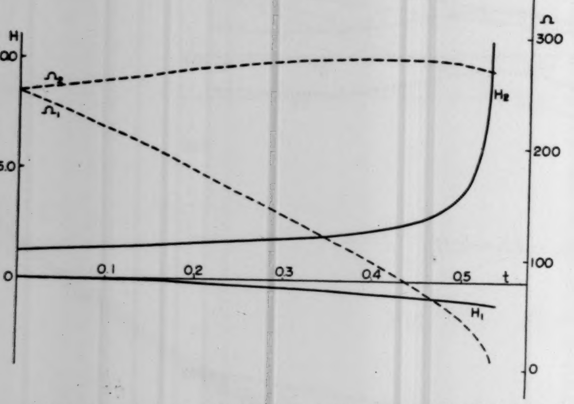

Fig. 5. Time variation of magnetic field and angular velocity for $H_1=0$, $H_2=1.225$, $\Omega_1=\Omega_2=250$, $g=1$.

Numerical calculations carried out for different values of external forces and for other sets of angular velocities showed that the main features of the field and motion stated above were essentially general.

5. Eddy motion and the magnetic field in the earth's core

For various eddies of different radii the period of the alternating but decreasing field in the previous section takes the values as shown in Table 1. In numerical calculation, we took $g=1/100$ for simplicity. When the torque of this magnitude is exerted on the sphere of 500 *km* in radius, the work done by the torque amounts only to 2×10^{-16} *erg/sec.cm*^{3}. This value seems too small compared with the heat energy 1.7×10^{-7} *erg/sec.cm*^{3} which is presumed by Bullard[2)] as being generated in the core. Table 2 shows the magnetic field, the angular velocity and the maximum peripheral velocity (V_φ) corresponding to $H=0.1$, $\Omega=250$ when $g=1/100$ is assumed. The velocity of 5.30×10^{-2} *cm/sec* for $a=500$ *km* seems acceptable in the earth's core, though it should be regarded as the velocity superposed on the general flow such as westward drift whose velocity

Table 1.

$a(km)$	$T(years)$
100	5.08×10^2
200	2.03×10^3
500	1.27×10^4
1000	5.08×10^4

---

2) E. C. BULLARD, *Proc. Roy. Soc.* **A**, **197** (1949), 433.

is inferred to be 3×10^{-2} *cm/sec*[2),3)]. The magnetic fields obtained from Table 2 are exceedingly small.

In case we take 1.7×10^{-9} *erg/sec. cm*^{3} as the energy supplied by the accelerating force, the steady state values are shown in Table 3 in regard to the system that has two rotating spheres at the distance of five times the radius of the spheres from each other. For the system having spheres of 500 *km* in the radius, the maximum peripheral velocity is obtained to be 0.67 *cm/sec*. Though it is compatible with the velocity obtained by Herzenberg and Lowes[4)] and Herzenberg[5)] in the induction problem of rigid rotator, it seems too large compared with the value, 3×10^{-2} *cm/sec*, inferred from the observation of magnetic field. On the other hand the magnetic field induced in the steady state is 1.26 *gauss* which seems sufficient to explain the irregular part of the earth's field, when we recollect that the intensity of the dipole field at the surface of the core is estimated as about 4 *gauss* and that the non-dipole field at the earth's surface is only a fraction of the dipole field.

Table 2. Magnetic field, angular velocity and maximum peripheral velocity for $\varepsilon=1/10^{\frac{1}{3}}$

$a(km)$	$H(gauss)$	$\Omega(rad/sec)$	$V_\varphi(cm/sec)$
100	4.97×10^{-3}	2.65×10^{-8}	2.65×10^{-1}
200	2.28×10^{-3}	6.63×10^{-9}	1.33×10^{-1}
500	9.11×10^{-4}	1.06×10^{-9}	5.30×10^{-2}
1000	4.97×10^{-4}	2.65×10^{-10}	2.65×10^{-2}

Table 3. Steady state values for $\varepsilon=1/5$

$a(km)$	$H(gauss)$	$\Omega(rad/sec)$	$V_\varphi(cm/sec)$
100	2.75×10^{-1}	3.32×10^{-7}	3.32
200	5.04×10^{-1}	8.28×10^{-8}	1.65
500	1.26	1.33×10^{-8}	6.65×10^{-1}
1000	2.75	3.32×10^{-9}	3.32×10^{-1}

6. Conclusion

The time-dependent behaviours of the system for two spheres

---

3) E. C. BULLARD, *Phil. Trans. Roy. Soc. London*, **A**, **243** (1950), 67.

4) A. HERZENBERG and F. J. LOWES, *Phil. Trans. Roy. Soc. London*, **A**, **249** (1957), 507.

5) A. HERZENBERG, *Phil. Trans. Roy. Soc. London*, **A**, **250** (1958), 543.

rotating in an infinitely extended conductor were studied by numerical calculation. So long as the changes are relatively slow, the main features of the magnetic field and the motion of the spheres are classified into the two types. One is that the magnetic field decays with time while the spheres are accelerated infinitely by external forces. The other is that the angular velocity decreases with the increase in the magnetic field. In some special cases, which belong to the former type, the magnetic field changes its polarity alternately with the period of about 1.3×10^4 *years*, when the spheres, 500 *km* in radius, are assumed in the core. If we assume the energy of 1.7×10^{-9} *erg/sec. cm*^{3} being supplied to the spheres, which is only 1% of the heat generated in the core, we obtain 0.67 *cm/sec* and 1.26 *gauss* as the steady state values of the peripheral velocity and the magnetic field respectively, even when the spheres are located 2500 *km* apart from each other.

Although thus obtained velocity of the sphere is unexpectedly large, the induced field seems sufficient to explain the non-dipole part of the earth's field. If the extreme simplification of the model such as the sharp boundary of the eddy is improved, it may not always be hopeless of explaining the irregular field of the earth by the induction model of the eddy.

Acknowledgments

The writer would like to express his sincere gratitude to Dr. T. Rikitake for his kind direction and advice, and to Dr. S. Uyeda for valuable discussion. He is also grateful to Mr. Shimizu and Mr. Matsutani, Institute of Mathematical Engineering, for their advice in carrying out the numerical calculation with the electronic computer TAC, and to Dr. Miyama and others, Engineering Research Institute, who gave the writer facilities in using TAC. The writer is also grateful to Prof. Nagata for his interest in this study.

27. 非定常ダイナモ (2)

東京大学大学院
地球物理学課程 行 武 毅

前報に引き続き，導体中で回転する 2ケの導体球によつて誘導される磁場と角速度との時間的変化を調べた．本報では誘導方程式として，2 次導函数までを含む近似式を採用したが，得られた結果は，前報と同様，大別して 2 種類の解に分類できる．一つは磁場が減衰し，外からの駆動力のために回転が次第にはやまる場合で，他の一つは，磁場が急激に増大し，回転速度が急速に減少する場合である．2ケの球に関する現象の起り方が全く同等で，その時間的変化がゆるやかな場合，例えば電気伝導度として地球核と同程度の 3×10^6 *e.m.u.* を考え，半径 500 *km* の球が回転しているとすると，周期が 5000 年以上の現象に対しては，上の 2 種の場合しか起らないことが解析的にも予想される．2 ケの球が，互いに異る強さの磁場を誘導する時の，種々の場合について電子計算機 TAC を使用して数値計算を行なつた．最初に2ケの球に関して非対称的な，強さの異る磁場が誘導されていても，時間の経過と共に，磁場の強さが等しくなろうとする傾向がある．それ以後は，前にのべた種類の現象のいずれかが起るものと考えられる．

磁場が減衰する種類の解で，特殊な場合には，磁場の向きが交互に逆転する減衰振動がみられる．地球核内で半径 500 *km* の球が 1100 *km* 離れて回転している場合を考えると，減衰振動の周期は，1.3×10^4 年となる．今半径 500 *km* の球が 2500 *km* 離れて存在し，地球核内で発生する熱の 1% が回転力として消費されたとすると，2 ケの球によつて維持される磁場と，表面速度はそれぞれ 1.26 *gauss*, 0.67 *cm/sec* となる．従来から想像されてきた値に比べると，磁場の強さは受容できる値であるが，速度の方は異常に大きい．これは剛体球のモデルによつたためであろう．

BULLETIN OF THE EARTHQUAKE
RESEARCH INSTITUTE
Vol. 38 (1960), pp. 451-466

28. *Pumice-flow Deposits of Komagatake Volcano, Southern Hokkaido.*

By Isamu MURAI,

Earthquake Research Institute.

(Read Feb. 23, 1960.—Received June 30, 1960.)

Introduction

Komagatake Volcano, situated in the eastern part of the Oshima Peninsula in Southern Hokkaido, is one of the noted active volcanoes in Japan. This volcano seems to have been active scince prehistorical ages, and violent eruptions have occurred repeatedly in historic times, that is, great eruptions took place in 1640, 1856 and 1929. During the course of the 1926 eruption, a large quantity of pumice-blocks and ash-materials effused from the crater descended the mountain-slope in a state of pumice-flow, and the deposits consisting of fragmentary materials of all grades occupied a wide area on the lower slope of the volcano. Similar fragmentary deposits consisting of pumice-blocks and ash-materials are distributed widely on the mountain-slope of the volcano, which may be the products of pumice-flows of the former eruptions. Besides these, mud-flow deposits caused by disruption of the apical part of the volcanic cone constructed in the earlier stage occupied the southern and eastern skirts of the volcano, forming the characteristic topography of flowed-mounds.

The writer studied these deposits of pumice-flows and mud-flows on the spot. He collected several specimens and carried out mechanical analyses of them. The results will be presented in this paper. The writer wishes to express his gratitude to Prof. Hiromichi Tsuya of the Earthquake Research Institute, Tokyo University, for constant guidance in the course of the work. He is also indebted to Mr. Yoshichi Hosoya of the Komoro Branch of the Earthquake Research Institute, for his aid in the work as well as for preparation of figures in this paper.

General Structure of the Volcano

Komagatake Volcano is composed of repeated layers of lava flows and fragmentary materials of two-pyroxene-andesite. Some of the fragmentary deposits are the products of pyroclastic flows. A conical volcano had been built up by accumulation of lava flows and fragmentary materials in the earlier period. The apical part of the cone was destroyed by explosions to result in formation of a horseshoe-shaped caldera. The disrupted materials, descending down the mountain-side, occupied the southern and eastern skirts of the volcano, forming flowed-mounds (Horseshoe-shaped crater mud-flow). Subsequently, a large quantity of fragmentary materials was effused and descended down the northern, eastern and southern moutain-slope (Horseshoe-shaped crater pumice-flow). The horseshoe-shaped caldera is surrounded on its north, west and south sides with a ring-wall, while on its east side there is a great gap in the ring-wall. A small central cone is built up in the caldera, only the eastern side of which is developed, and the other sides are absent. The ring-wall of the somma and the crest of the central cone embrace an oval crater, the major and minor diameters of which are 1 *km* from *NNE* to *SSW* and 0.7 *km* from *WNW* to *ESE* respectively. Several active pit-craters are opened in the oval crater. The configuration of the inside of this oval crater has changed from time to time. On the flanks of the somma, there are several knobs, one on the northwestern flank may be a parastic cone consisting of fragmentary materials of quartz-bearing hypersthene-andesite effused in the earlier period, while the other on the southeastern flank are the mounds composed of pumice-flow deposits of two-pyroxene-andesite descended repeatedly from the oval crater in the later period. The northwestern part of the ring-wall was blown away by a side-explosion to result in formation of Oshidashizawa explosion-crater, and the disrupted materials caused a mud-flow, simultaneously a cloud of scoria, pumice and ash descended down to the northwestern skirt in a state of pyroclastic flow (Oshidashizawa mud-flow and scoria-flow). During the eruptions in the latest period, perhaps in historic times, lava-flow and pumice-flow discharged from the oval crater descended the eastern side through the eastern gap of the ring-wall (Kurumizaka lava-flow and pumice-flow). In the 1929 eruption, new pumice-flows discharged from the crater, spreading down to the skirts in all directions.

The Eruption of 1929

Komagatake Volcano seems to have been active from ancient ages, although noting about its activity has been recorded but the eruptions since 1640. In historic times the eruptive activity has been repeated frequently in the oval crater. Eruptions took place in the years: 1640, 1765, 1784, 1856, 1888, 1905, 1919, 1929, 1937 and 1942. Among them, the eruptions of 1640, 1856 and 1929 were the most violent.

On June 17, 1929, a great eruption took place. The volcano had continued its solfataric activity before the eruption, and steam and solfataric gas had been issued from several vents in the oval crater. Many reports were written of the eruption, founded on accounts by eyewitnesses.[1] According to them, the course of eruption was as follows:

The eruption began with an earthquake and rumbling noises. At about 0 *h.* 30 *m. a.m.*, June 17, a slight earthquake occurred and rumbling noises from the volcano were heard at Ônuma. Volcanic ashes began to fall in Shikabe district at about 3 *h. a.m.* The activity had gradually become violent, the amount of volcanic ashes discharged from the crater had increased and rumblings had grown worse before about 10 *h. a.m.*, when a great explosion came accompanied by an earthquake. Volcanic ashes and lapillis began to fall heavily in Shikabe district. After that, emission of dark ash-laden cloud and ejection of pumice-blocks continued almost uninterruptedly, increasing in violence. At about 0 *h.* 20 *m. p.m.*, a mass of pumice-laden cloud ran over the southern saddle in the ring-wall, descending down the mountain-slope. This was the first pumice-flow. The ash-cloud attained an enormous height, at 2 *h. p.m.* measuring about 13,200 *m.* Ejected materials were borne southeastward by the upper atmospheric current, falling on the wide area southeast of the volcano. At 2 *h.* to 3 *h. p.m.*, the second pumice-flow ran over the northwestern saddle in the ring-wall, pouring into the Oshidashizawa gully. After that, great masses of pumice-flow successively descended the mountain-slope in all directions. Thus, discharging of pumice-flows continued till at about 10 *h. p.m.* of the same day. Ejection of incandescent pumice, lapilli and ash continued almost steadily till about 11 *h.* 30 *m. p.m.*, when the eruption subsided. At about 1 *h.* 30 *m. a.m.* in the next morning, showers of the ejected materials in Shikabe district ceased entirely. Emission of ash-laden cloud continued for the next several days.

---

[1] Hiromichi TSUYA *etc.* 7, "*The Eruption of Komagatake, Hokkaido, in* 1929" *Bull. Earthq. Res. Inst.*, **8** (1930), 237–319.

Shukusuke KOZU, "*The great activity of Komagatake in* 1929" *Min. Petr. Mitt.*, **45** (1934), 133–174.

Pumice-flows were discharged during the paroxysmal phase of the activity, running over the ring-wall and descended the mountain-slope with surprising speed, still retaining hot gas. The deposits, occupying most of the lower slope of the volcano, maintained a high temperature for a fairly long time after deposit. Temperatures as high as 300° to 560°*C* were measured with thermometer and electric pyrometer in the interior of the deposits, several days after the eruption. Constituents of the deposits were oxidized by circulating air for their high temperature. Secondary solfataras developed on the surface of the deposits. Trees

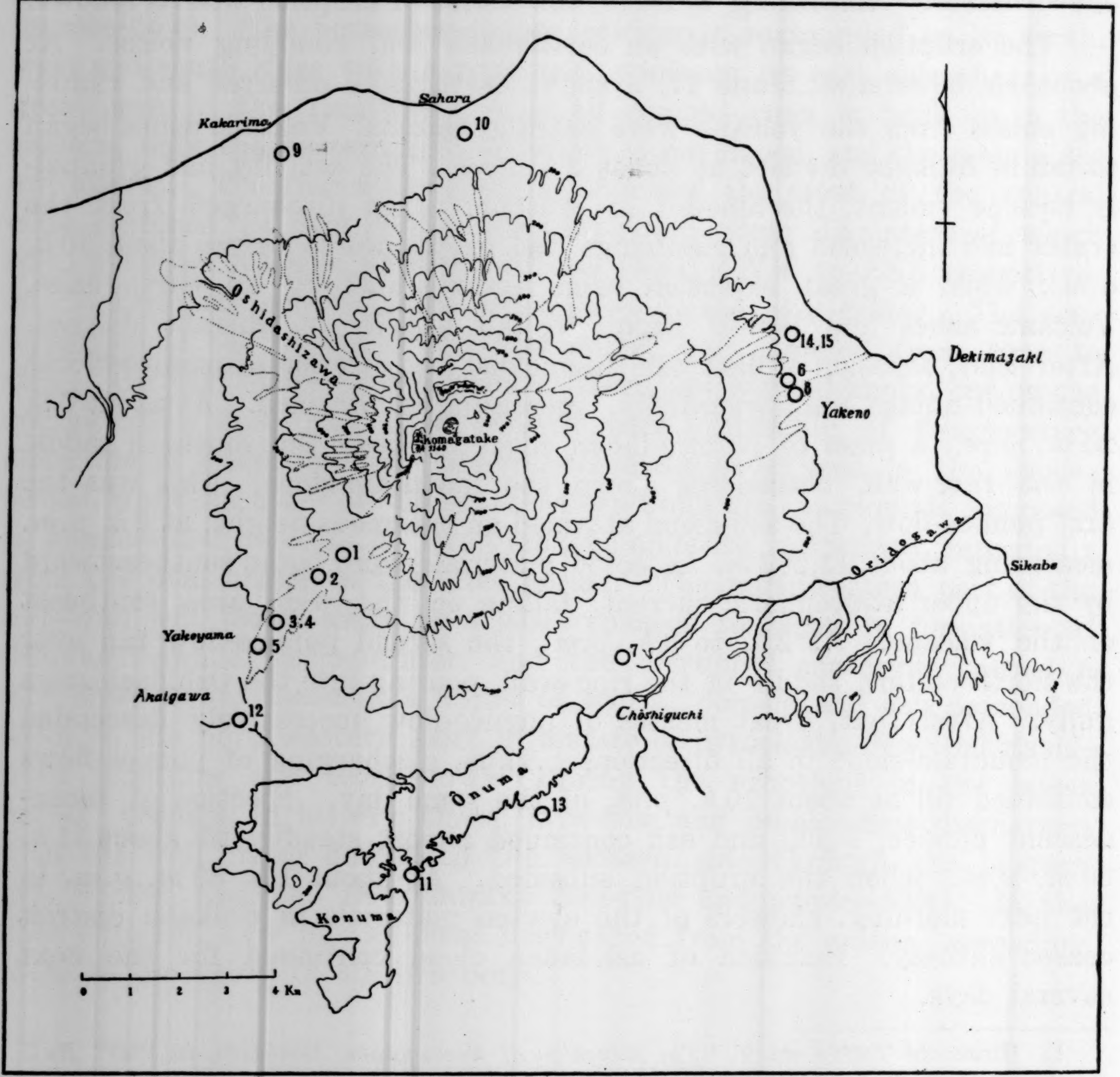
Kakarima
Sahara
10
9
Oshideshizawa
14,15
6
8
Dekimazaki
Yakeno
Komagatake
1140
1
2
3,4
5
Yakeyama
Akaigawa
12
7
Choshiguchi
Oridogawa
Sikabe
Onuma
13
11
Konuma
0 1 2 3 4 Km

Fig. 1. Map of Komagatake Volcano, showing the distribution of the pumice-flow deposits discharged by the 1929 eruption and localities of specimens collected for mechanical analyses.

buried in the deposits were turned into natural charcoal.

A large quantity of fragmentary materials was projected and covered not only the ground around the crater but also the wide area of south-eastern skirts of the volcano. The whole area covered with the projected materials was estimated at about 400 to 500 km^2, and the volume of the projected materials was estimated at about 0.4 km^3. The area covered with pumice-flow deposits was estimated at about 27 to 30 km^2. Assuming that the thickness of the deposits is 5 m on the average, the volume of the deposits is calculated at about 0.15 km^3.

Mechanical Characteristics of the Pumice-flow Deposits discharged by the 1929 Eruption

A large number of pumice-flows were discharged, spreading down to the skirts of the volcano, in the 1929 eruption. The pumice-flow deposits occupy a vast area on the mountain-slope. Their distribution is shown in Fig. 1. The farthest front of the flows reaches about 6 *km* from the crater.

The writer collected 5 specimens from the Akaigawa pumice-flow deposits, extending southwestward from the crater, and collected one specimen from the front of the Yakeno pumice-flow deposits, extending eastward from the crater. Localities where the specimens were collected are shown in Fig. 1. Specimens of about 1 *kg* weight were collected for mechanical analyses. Mechanical analyses were carried out by means of the decantation, sieving and pipette methods in sequence. Then, all the results obtained through such steps of laboratory work were corrected for the coarser fractions by referring to the photographs of the outcrops from which the specimens were picked up. Detailed description of such steps of the mechanical analyses will be omitted here. The final results of the mechanical analyses are shown in Table 1, where figure listed in the column represents the weight per cent of each fraction sized out by the mechanical analyses. Fig. 2 and Fig. 3 show the particle size distribution of the specimens by cumulative curves and histograms respectively. The diameters of particles in millimeters ξ are replaced here by ϕ as expressed $\phi = -\log_2 \xi$ for convenience. The phi values of the percentiles ϕ_5, ϕ_{16}, ϕ_{25}, ϕ_{50}, ϕ_{75}, ϕ_{84} and ϕ_{95} were read on the cumulative curves, and the approximate values of every sort of parameter of the particle size distribution were calculated from the following relations. The values of these parameters are listed in Table 2.

$$Md_\phi = \phi_{50}\ , \qquad M_\phi = (\phi_{16} + \phi_{84})/2\ ,$$

$$Q' = |\ \phi_{75} - \phi_{25}\ |/2\ , \qquad Q'' = (\phi_{75} + \phi_{25} - 2\phi_{50})/Q'\ ,$$

$$\sigma_\phi = |\ \phi_{84} - \phi_{16}\ |/2\ , \qquad \alpha_\phi = (M_\phi - \phi_{50})/\sigma_\phi\ ,$$

$$\alpha_{2\phi} = \frac{(\phi_5 + \phi_{95})/2 - \phi_{50}}{\sigma_\phi}\ , \qquad \beta_\phi = \frac{(\phi_{95} - \phi_5)/2 - \sigma_\phi}{\sigma_\phi}$$

Md_ϕ, Q' and Q'' are median, deviation and skewness respectively, obtained by the quartile method, while M_ϕ, σ_ϕ, α_ϕ and $\alpha_{2\phi}$, and β_ϕ are mean, deviation, skewness and kurtosis of the INMAN's phi measure system.

The results of the mechanical analyses of 6 specimens of the pumice-flow deposits discharged by the 1929 eraption are summarized as follows:

1) The median diameters Md_ϕ of specimens Nos. 1, 2, 3, 4 and 5

Table 1. The results of the mechanical analyses. The result of the mechanical analysis of a given specimen is noted in the column beneath its specimen number with weight per cent of each fraction.

a: pumice-flow deposits and mud-flow deposits,

ϕ \ sp. no	1	2	3	4	5	6	7	8	9	10	11	12	13
−10 ∼ −9											1.2		
−9 ∼ −8	2.0	1.2				1.5					1.4	2.0	2.7
−8 ∼ −7	2.8	1.8		1.6	1.6	6.8		1.4	1.4		2.6	3.6	4.4
−7 ∼ −6	3.1	3.0	0.4	3.2	4.1	8.1	1.8	2.4	3.5	3.2	4.0	3.8	5.3
−6 ∼ −5	3.5	3.6	2.9	6.7	8.1	7.9	3.9	3.9	4.6	4.8	4.8	5.3	6.7
−5 ∼ −4	4.4	4.7	7.5	12.8	9.2	8.6	5.6	7.6	5.7	6.8	5.3	5.8	10.1
−4 ∼ −3	7.2	6.7	6.8	7.4	6.2	6.8	6.5	8.2	5.2	6.4	6.3	6.3	10.1
−3 ∼ −2	6.1	5.8	5.6	3.5	4.5	3.9	5.5	6.1	4.6	4.0	7.5	6.4	8.0
−2 ∼ −1	3.1	3.5	3.8	3.8	3.3	2.7	4.7	4.0	5.0	3.1	9.1	6.4	6.4
−1 ∼ 0	12.3	11.5	9.8	9.5	8.7	8.3	12.2	11.8	15.6	9.0	13.5	8.5	7.6
0 ∼ 1	26.0	26.7	27.8	22.3	22.3	19.0	27.6	22.2	23.8	25.0	17.6	13.6	9.0
1 ∼ 2	13.2	13.8	15.7	12.3	13.9	10.9	16.3	14.5	12.9	14.0	10.9	11.6	7.8
2 ∼ 3	5.0	5.5	6.1	4.8	5.3	4.2	5.9	5.7	6.8	6.3	6.7	9.0	5.1
3 ∼ 4	2.1	2.7	2.8	1.8	2.4	2.4	1.3	2.5	3.3	2.7	3.4	6.2	3.9
4 ∼ 5	1.7	1.9	1.9	1.5	1.7	1.3	1.4	1.9	3.1	1.8	2.4	4.5	4.1
5 ∼ 6	2.3	1.9	1.7	2.3	2.8	1.3	1.2	2.0	2.2	4.1	1.1	2.3	3.3
6 ∼ 7	2.5	2.8	3.5	3.5	2.8	3.0	2.2	2.8	1.5	4.6	1.0	1.9	2.9
7 ∼ 8	2.2	2.0	2.4	1.7	1.9	2.6	2.2	1.7	0.5	2.2	0.5	1.4	1.3
8 ∼ 9	0.3	0.7	1.1	1.0	0.8	0.6	0.5	1.0	0.1	1.1	0.3	1.0	0.3
9 ∼	0.2	0.2	0.2	0.3	0.4	0.1	1.2	0.3	0.2	0.9	0.4	0.4	1.0

b: pumice-fall deposits.

ϕ \ sp. no	14	15
−6 ～ −5.5	15.0	
−5.5～ −5	22.4	24.5
−5 ～ −4.5	24.8	19.7
−4.5～ −4	21.6	15.0
−4 ～ −3	10.1	18.0
−3 ～ −2	1.8	8.4
−2 ～ −1	1.0	5.7
−1 ～ 0	1.0	4.3
0 ～ 1	1.0	2.7
1 ～ 2	0.5	1.1
2 ～ 3	0.3	0.2
3 ～ 4	0.2	0.2
4 ～	0.2	0.2

(Akaigawa pumice-flow deposits) stay exclusively in a narrow range of 0.06 to 0.47, and systematic variation of Md_ϕ values with distauce from the crater as in the case of pumice-fall deposits can not be found. The value of Md_ϕ of specimen No. 6 (Yakeno pumice-flow deposits) is the same order, −0.30.

2) The particle size distribution of all specimens is quite similar to each other. There are two distinct modes as shown in the histograms (Fig. 3). The main-mode always lies in the fraction of 0 to 1 in ϕ scale, and the sub-mode is found in the tailing-out part of the coarser fractions, whose position varies in each specimen. In the tailing-out part of the finer fractions, there is another weak sub-mode·

3) In spite of the fact that the size distribution has a surpassing main mode, the sorting is fairly bad, as the values of Q' are in a range of 1.6 to 3.0, and the values of σ_ϕ are 2.9 to 4.0. This is due to the appearance of a distinct sub-mode in the coarser fractions. The values of α_ϕ, which represent the degree of skewness of particle size distribution, stay in a negative range of −0.4 to −0.3. The values of β_ϕ, the parameter of kurtosis, are in a range of 0.5 to 1.2.

Such features of the particle size characteristics as mentioned above are typical ones of the pumice-flow deposits, being in striking contrast to the normal projected pumice-fall deposits. The writer collected 2 specimens of pumice-fall deposits, one from the deposits of the 1929 eruption and the other of a former eruption, and carried out mechanical analyses of them. The results are shown in Table 1b. Table 2, Fig. 2 and Fig. 4. The size characteristics of the pumice-fall deposits show better sorting, lack of tailing-out of the coarser fractions, regular variation of coarseness with distance from the crater, values of α_ϕ tend to fall in a positive range and the other features.[2]

The pumice-flow deposits of the 1929 eruption are two-pyroxene-andesite petrologically and identical with the projected materials. The deposits consist of several different constituents. The coarser fractions

---

[2] Hisashi KUNO, "Characteristics of Deposits formed by Pumice Flows and Those by Ejected Pumice" *Bull. Earthq. Res. Inst.*, **19** (1941), 144–149.

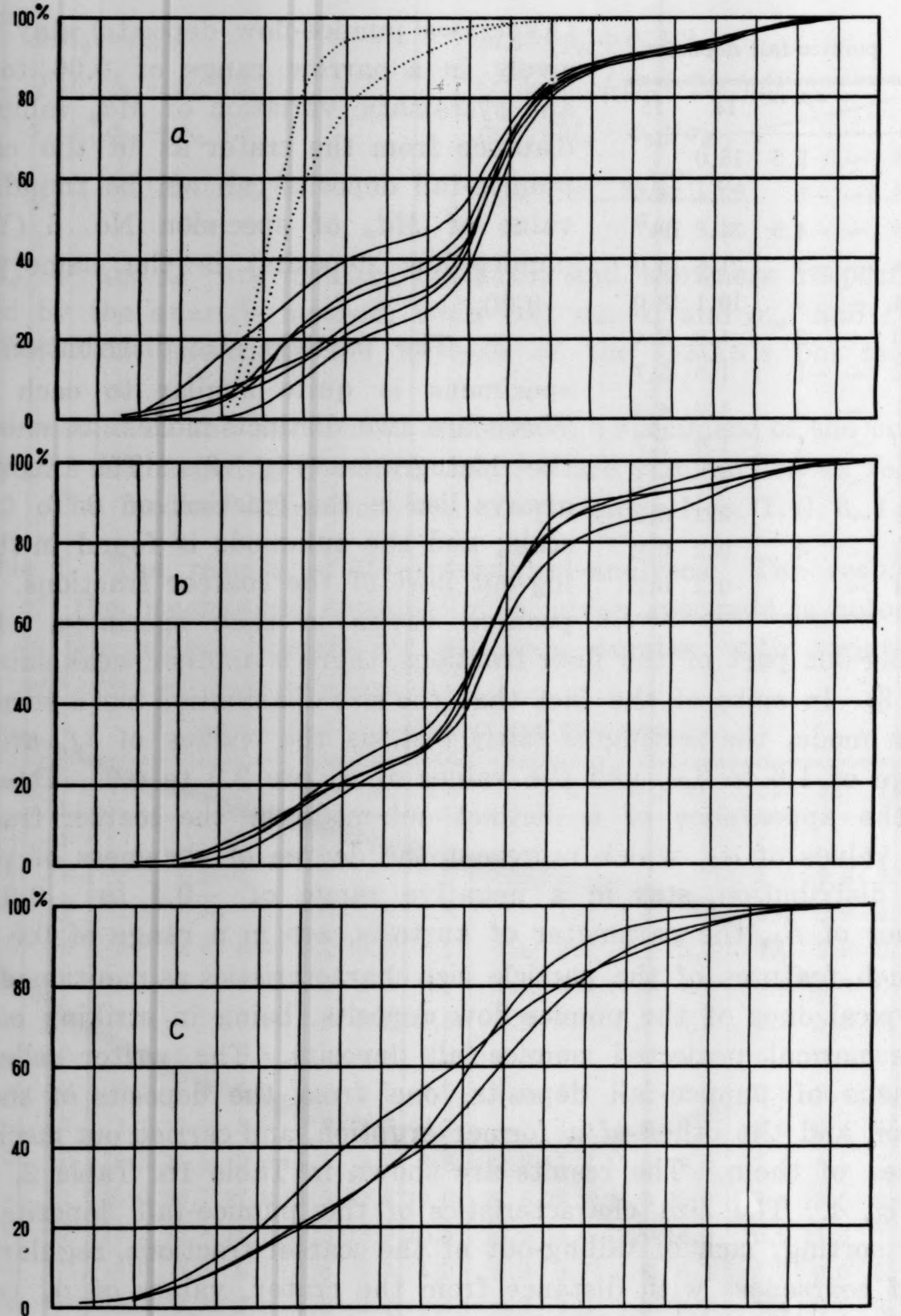

Fig. 2. Cumulative curves of particle size distribution.
a: dotted lines; pumice-fall deposits (Sp. Nos. 14 and 15), solid lines; pumice-flow deposits of the 1929 eruption (Sp. Nos. 1, 2, 3, 4, 5 and 6),
b: pumice-flow deposits of the former eruption (Sp. Nos. 7, 8, 9 and 10),
c: mud-flow deposits (Sp. Nos. 11, 12 and 13).

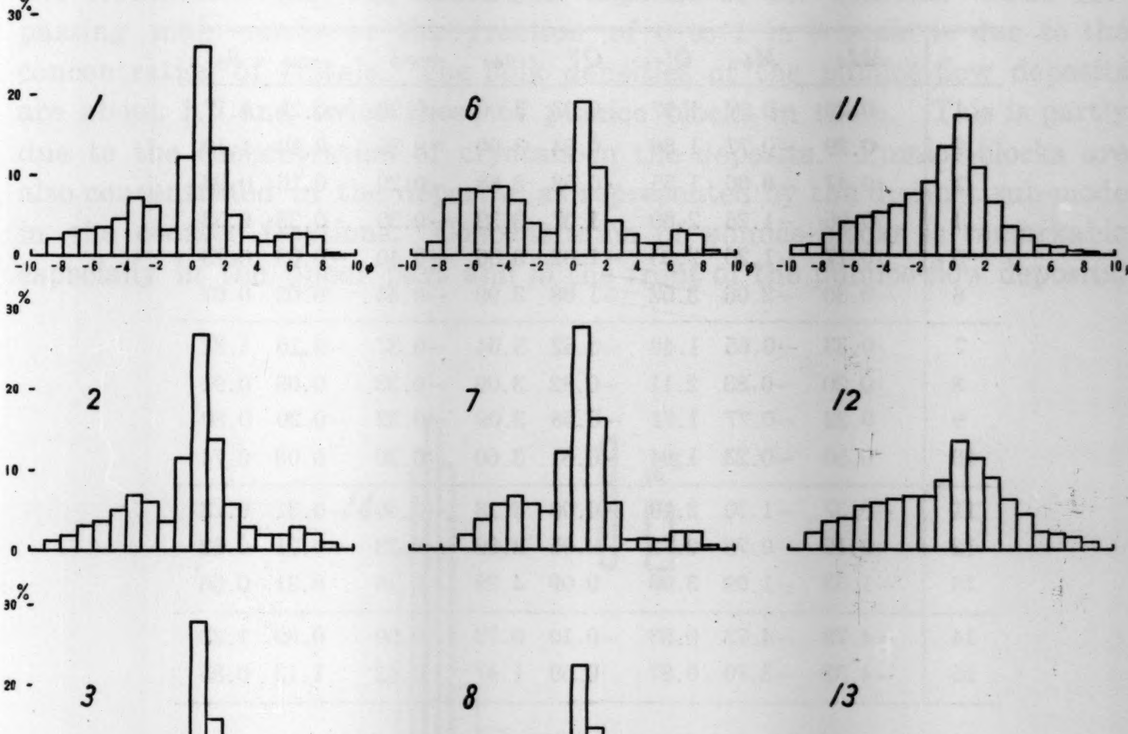

Fig. 3. Histograms of particle size distribution. The number of specimen is noted on the left of each histogram.

Table 2. Data on parameters of particle size distribution.

	Md_ϕ	M_ϕ	Q'	Q''	σ_ϕ	$\alpha\phi$	$\alpha_{2\phi}$	β_ϕ
1	0.20	−0.97	1.97	−0.93	3.00	−0.39	−0.21	1.17
2	0.29	−0.77	1.86	−0.84	3.00	−0.35	−0.10	1.10
3	0.47	−0.36	1.55	−0.58	2.88	−0.29	0.16	0.98
4	0.06	−1.26	2.60	−1.07	3.39	−0.39	0.33	0.53
5	0.17	−1.26	2.55	−1.02	3.56	−0.40	−0.03	0.73
6	−0.30	−2.06	3.02	−1.08	3.99	−0.44	0.05	0.67
7	0.33	−0.65	1.48	−0.62	3.64	−0.37	−0.16	1.21
8	0.20	−0.83	2.11	−0.82	3.09	−0.33	0.05	0.91
9	0.22	−0.77	1.72	−0.58	3.09	−0.32	−0.20	0.80
10	0.50	−0.23	1.94	−0.61	3.60	−0.20	0.03	0.74
11	−0.37	−1.30	2.10	−0.06	3.28	−0.30	−0.31	0.73
12	0.15	−0.76	2.72	−0.05	3.99	−0.23	−0.21	0.62
13	−1.53	−1.09	3.96	0.09	4.29	0.10	0.21	0.58
14	−4.73	−4.73	0.53	−0.10	0.73	0.00	0.89	1.23
15	−4.32	−3.70	0.87	0.59	1.47	0.42	1.12	0.85

consist of pumice-blocks and rock fragments, both accessory and accidental, which come out in distinct sub-mode of particle size distribution. The medium fractions consist dominantly of crystal grains and less amount of pumice fragments and rock fragments, which represent the surpassing main mode of the fraction of 0 to 1 in ϕ scale. The finer fractions consist of vesicular glass flakes and crystal fragments.

Pumice-blocks in the pumice-flow deposits are composed of phenocrysts of plagioclase, hypersthene and augite, and vitreous groundmass. The bulk densities of them are in a range of 0.7 to 1.4, and 0.9 on the average. These are the same values as in the cases of the pumice-flow deposits of Asama Volcano (0.7 to 1.0, 0.85 on the average), Nantai Volcano (0.8 to 1.1, 0.9 on the averange), and of Tokachidake Volcano (0.5 to 1.2, 0.9 on the average), but somewhat heavier than the values (0.5 on the average) of the pumice-flow deposits of Towada Caldera, Kutcharo Caldera, Shikotsu Caldera, Akan Caldera, and of the Shirasu deposits.

Pumice-blocks consist of 45 per cent phenocrysts and 55 per cent vesicular glass in weight percentage, while, in the pumice-flow deposits, crystals form a greater percentage than vesicular glass flakes. Crystals were concentrated especially in the medium fraction as in the case of the crystal-ricn glowing avalanche deposits of St. Vincent.[3] The surpassing main mode in the fraction of 0 to 1 in ϕ scale is due to the concentration of crstals. The bulk densities of the pumice-flow deposits are about 1.5 and twice those of pumice blocks in them. This is partly due to the concentration of crystals in the deposits. Pumice-blocks are also concentrated in the deposits, as represented by the distinct sub-mode in the coarser fractions. Concentration of pumice-blocks is remarkable especially in the upper part and in the front of the pumice-flow deposits.

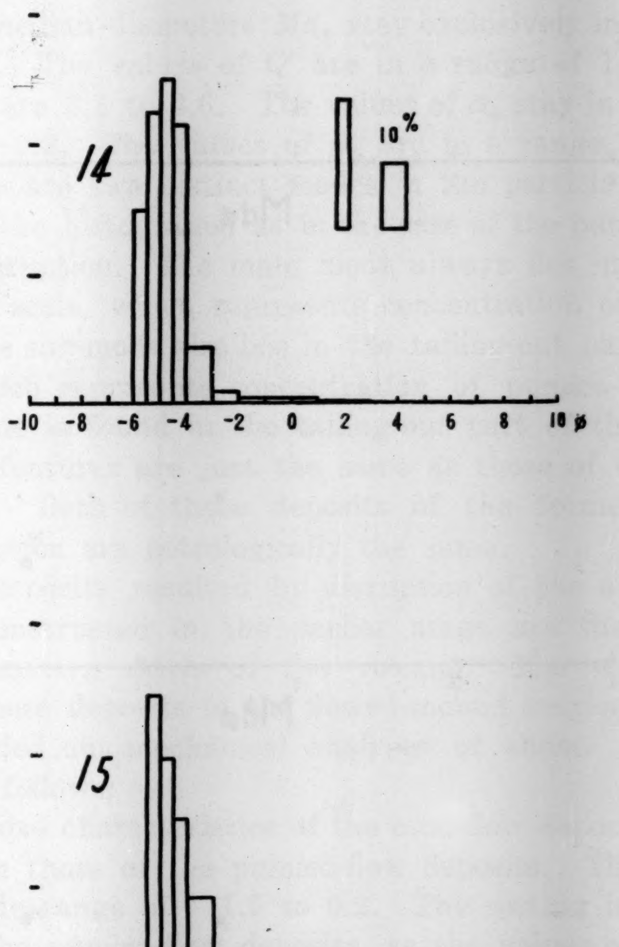

Fig. 4. Histograms of pumice-fall deposits.

---

[3] RICHARD L. HAY, "Formation of the Crystal-rich Glowing Avalanche Deposits of St. Vincent, B. W. I." *Journ. Geol.*, **67** (1959), 540–562.

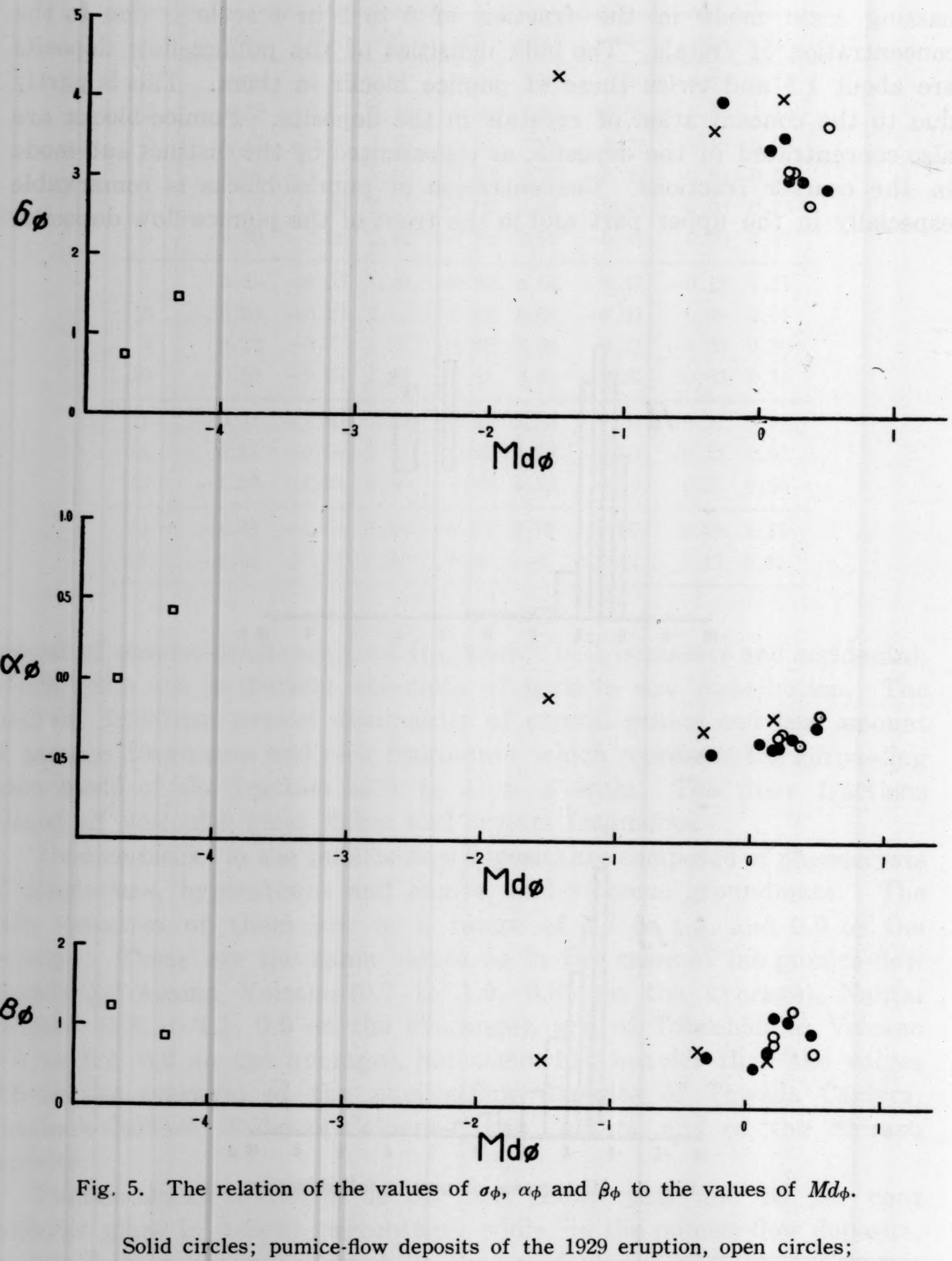

Fig. 5. The relation of the values of σ_ϕ, α_ϕ and β_ϕ to the values of Md_ϕ.

Solid circles; pumice-flow deposits of the 1929 eruption, open circles; pumice-flow deposits of the former eruption, crosses; mud-flow deposits, opon squres; pumice-fall deposits.

Mechanical Characteristics of the Pumice-flow Deposits and the Mud-flow Deposits of the former Eruptions

Pumice-flows were discharged repeatedly by the former eruptions. They are distributed widely on the mountain-slope of the volcano. The writer collected 4 specimens of the pumice-flow deposits, and carried out the mechanical analyses of them. The results are summarized as follows:

1) All specimens have quite similar size characteristics to those of the pumice-flow deposits of the 1929 eruption. The values of all sorts of parameters of the particle size distribution in both are the same. The median diameters Md_ϕ stay exclusively in a narrow range of 0.2 to 0.5. The values of Q' are in a range of 1.5 to 2.1, and the values of σ_ϕ are 3.1 to 3.6. The values of α_ϕ stay in a negative range of -0.4 to -0.2. The values of β_ϕ are in a range of 0.7 to 1.2.

2) There are two distinct modes in the particle size distribution as shown in the histograms, as in the case of the pumice-flow deposits of the 1929 eruption. The main mode always lies in the fraction of 0 to 1 in ϕ scale, which represents concentration of crystals in this fraction. The sub-mode also lies in the tailing-out part of the coarser fractions, which represents concentration of pumice-blocks. Another weak sub-mode is found in the tailing-out part of the finer fractions. All of these features are just the same as those of the 1929 pumice-flow deposits. Both of these deposits of the former eruptions and the 1929 eruption are petrologically the same.

Mud-flow deposits resulted by disruption of the apical part of the volcanic cone constructed in the earlier stage are distributed on the southern and eastern skirts of the volcano. The writer collected 3 specimens of these deposits in the flowed-mound reagion on the southern skirts, and carried out mechanical analyses of them. The results are summarized as follows:

1) The size characteristics of the mud-flow deposits are somewhat different from those of the pumice-flow deposits. The values of Md_ϕ vary in a wide range of -1.5 to 0.2. The sorting is worse than in the case of the pumice-flow deposits, as the values of Q' is in a range of 2.1 to 4.0 and the values of σ_ϕ are 3.3 to 4.4. The values of α_ϕ in a range of -0.3 to 0.1, and the values of β_ϕ are 0.5 to 0.7.

2) The shape of the particle size distribution is very flat as shown in the histograms. Tailing-out of both in the coarser and the finer fractions are found. A main mode lies in the fraction of 0 to 1 in ϕ scale as in the case of the pumice-flow deposits. A sub-mode in

the coarser fractions disappears on one occasion, and surpasses on another occasion. Size characteristics of 3 specimens are unstable and show disparity with each other.

Origin of the Pumice-flows of the 1929 Eruption

Pumice-flows were discharged during the paroxysmal phase of the 1929 eruption. Violent emission of ash-laden cloud succeeded the first explosion, and an ash column rose vertically to an enoumous height. Pumice-laden cloud descended laterally from the lower, and perhaps the outer, part of the ash column, judging from the photographs of the eruption, as they may have became denser than the surrounding atmosphere, although the process cannot be analysed properly here. Initial verocities of gas in the ascending magma at the crater-rim, which may have been no longer an effervescing melt but have had already been disintegrated into frothing clots of pumice and droplets of liquid disrupted into crystals and finely comminuted flakes of vesicular glass, may have been lower than in the case of a major explosion such as that of Asama Volcano. However, the gas content of the magma must have been high, for violent emission of ash-laden cloud continued over a half-day. It may be possible to infer that most of crystals and coarse pumice-blocks may have concentrated in the slowly rising outer part of a column of ash cloud, settling in turbulent currents of gas rising from the crater, lighter particles of vesicular glass have been born vertically in suspension.

When the dense pumice-laden cloud began to descend the mountain-slope, crystals and coarse pumice-blocks separated from the vitric ash and concentraed in the lower layers of the descending cloud. Thus the pumice-flow deposits rich in crystals and coarse pumice-blocks were settled on the lower slope of the volcano. The size characteristics of these deposits were described in the preceding chapter. Concentration of crystals is found distinctly in the lower part of the deposits, while concentration of coarse pumice-blocks is seen in the upper part and especially in the front of the deposits as already mentioned. Fine-grained pumice-flow deposits rich in vesicular glass were settled from the upper layers of the descending cloud, lighter and relatively rich in gas and vitric ash, along the front of the coarse-grained deposits of pumice-flows.

Summary

Pumice-flows discharged from Komagatake Volcano, on June 17, 1929, descended from the lower, and perhaps slowly rising outer part of a vertically rising column of ash-laden cloud, during the paroxysmal phase of the eruption. The outer part of an ash column became denser than the surrounding atmosphere, and pumice-laden dense cloud discharged laterally. Crystals and coarse pumice-blocks were concentrated in the lower layers of descending dense cloud, and crystal-rich pumice-flow deposits were deposited on the mountain-slope of the volcano. Similar pumice-flows were discharged by former eruptions, and their deposits are quite similar to those of the 1929 eruption.

---

28. 北海道，駒ヶ岳火山の軽石流堆積物

地震研究所　村　井　　勇

北海道南端の渡島半島東部に位置する駒ヶ岳火山は，活火山として知られ，古くから烈しい噴火を繰返えしてきた．寛永17年(1640年)，安政3年(1856年)，昭和4年(1929年)の噴火は特に烈しかつた．昭和4年の噴火の際には，軽石流の噴出が起つた．噴火は6月17日午前0時30分頃より始まり，午前10時頃に烈しい爆発が起つた．噴煙は空中高く噴き上げられ，軽石や火山礫火山灰が間断なく抛出された．正午を少しすぎた頃，最初の軽石流が噴出した．噴煙はますます烈しさを増し，その高さは午後2時頃には13,200 m と測定された．午後2時より3時にかけて，軽石流はあいついで噴出し，北西，南西，南東斜面を流下した．その後も軽石流の噴出は続き，午後10時頃最後の軽石流が南西斜面に流下した．噴火は午後11時30分頃まで続き，そのご衰えて，18日午前1時30分には降灰もおさまつた．軽石流は，北，西，東方の山腹斜面上に拡がり，その面積は27～30 km^2 におよんだ．堆積物の厚さを平均 5 m と仮定すれば，総体積は約 0.15 km^3 となる．筆者はこの軽石流堆積物の試料を数ヶ所から採集して機械分析を行つた．その結果は一般の軽石流堆積物と共通の特徴を示した．すなわち，分級が相当悪く，粗粒部および細粒部に長く尾を引き，主モードの位置は ϕ スケールで 0～1 の間に常に現れ，粗粒部に副モードを持ち，採集地点の相異にかかわらず共通の粒度分布を示し，中位粒径の値はほとんど変化がない，等の特徴を示した．駒ヶ岳火山の軽石流堆積物の粒度組成の特徴として特に注目すべき点は，結晶粒の集中が著しいことである．すなわち，軽石塊では，斑晶が45% に対してガラス質が55% を占めているが，軽石流堆積物では，軽石塊および石質破片を除くと，結晶粒がガラス破片よりもかなり多くの比率を占めている．ヒストグラムで見られるような中粒部の顕著な主モードがこれを表わしている．結晶粒の集中は堆積物の下部において著しく，これに対し，堆物の上部および末端部では粗粒の軽石塊の集中が認められる．軽石流堆積物のこのような特徴は，軽石流の噴出の機構を示唆するもののように考えられる．すなわち，垂直に上昇する噴火雲の中の比較的ゆるやかに上昇する外側部で，比重の大きな結晶粒と粗粒の軽石塊とが分級されて集中し，その部分が周囲の大気よりも比重が大きくなつて，側方に流下して軽石流を生じたと解釈することも可能であろう．いつたん軽石流の流下が始まれば，その流下雲の中で更に結晶粒の分級が続き，堆積物の下部に集中すると考えられる．さらに粗粒の

軽石流は堆積物の上部および末端に集中する．細粒のガラス破片は上層にまい上り，粗粒な堆積物の前面にそつて堆積して，細粒のガラス質の軽石流堆積物となる．

駒ケ岳火山では，古くから火山砕屑流を繰返して噴出した．筆者はこれらの火砕流の堆積物から4個の試料を採集して，機械分析を行つた．その結果は昭和4年の軽石流堆積物と全く同一であつた．駒ケ岳火山では，同じような噴火が古くから繰返えして行われたものと見られる．駒ケ岳火山は，かつて烈しい爆発により，その頂部が破壊され，泥流が発生して南方および東方山麓に流下し，特徴的な流れ山地形を作つた．この泥流堆積物から個の試料を採集して機械分析を行つた．泥流堆積物では，分級が一層悪く，粒度分布の形は不安定で，中位粒径の値も大きく変化する，等の特徴が認められた．

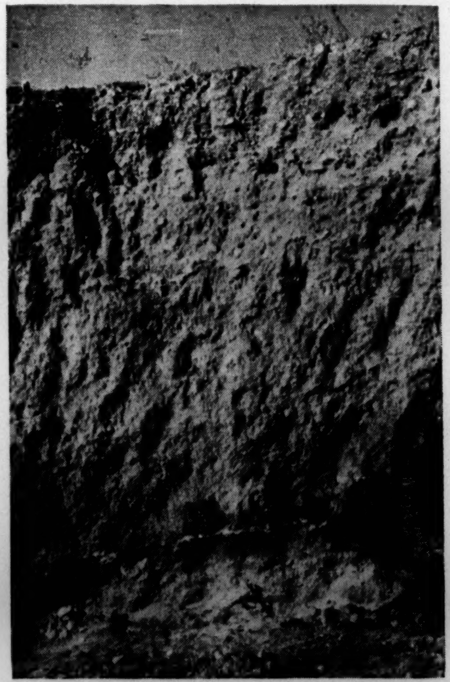

Fig. 6. The outcrop of the Akaigawa pumice-flow deposits, from which Sp. Nos. 3 (middle part) and 4 (upper part) were collected.

Fig. 7. The outcrop of the Yakeno pumice-flow deposits, from which Sp. No. 6 was collected.

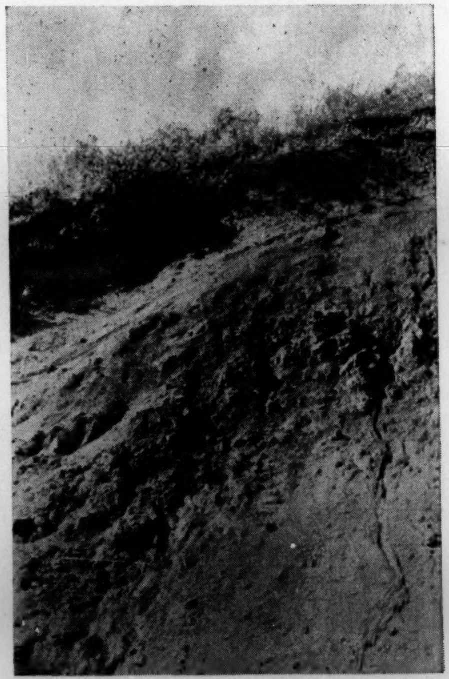

Fig. 8. The outcrop of the pumice-fall deposits, from which Sp. Nos. 14 (upper layer) and 15 (lower layer) were collected.

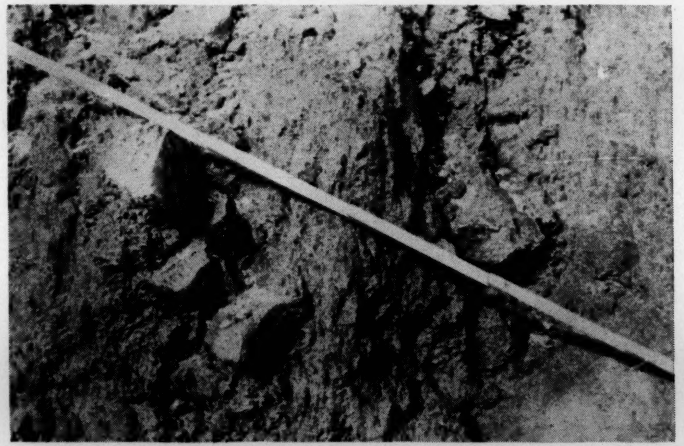

Fig. 9. The outcrop of the Horseshoe-shaped crater mud-flow deposits, from which Sp. No. 13 was collected.

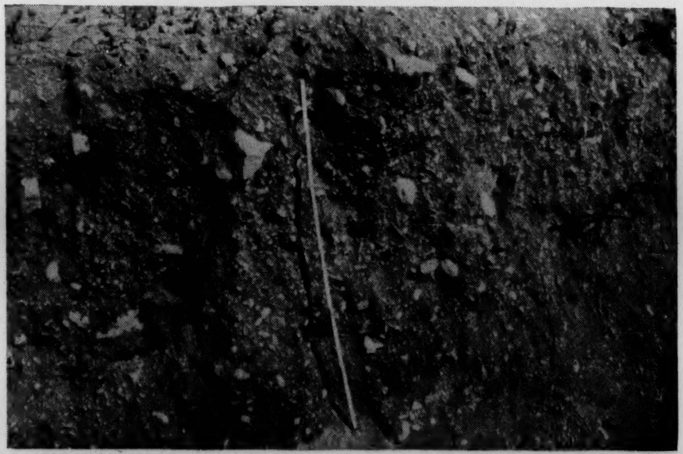

Fig. 10. The outcrop of the Akaigawa pumice-flow deposits, from which Sp. No. 4 was collected.

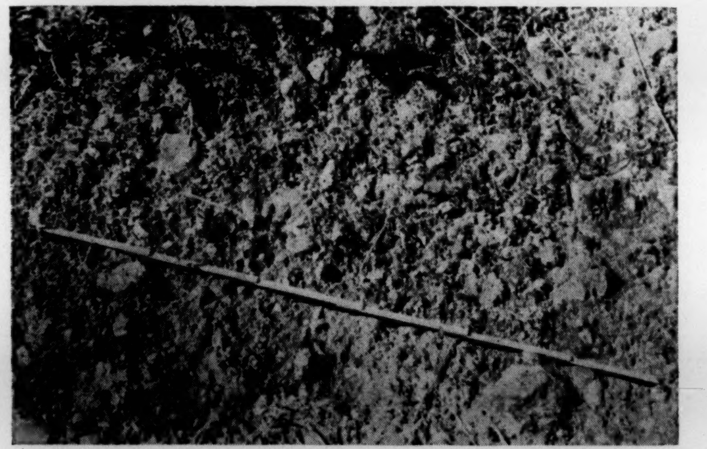

Fig. 11. The outcrop of the Kurumizawa pumice-flow deposits, from which Sp. No. 8 was collected.

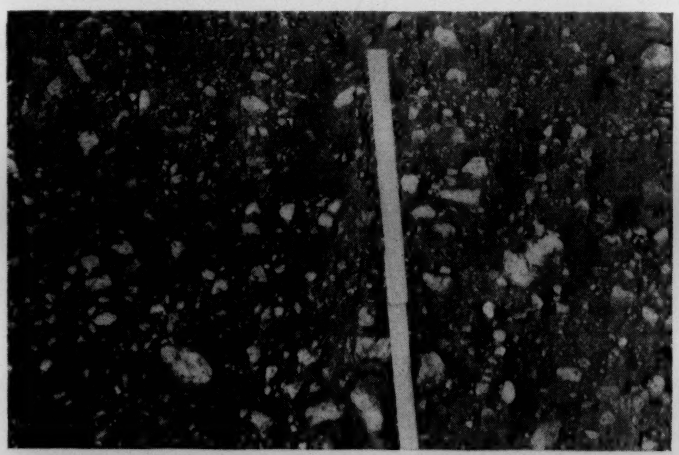

Fig. 12. The outcrop of the Horseshoe-shaped crater pumice-flow deposits, from which Sp. No. 7 was collected.

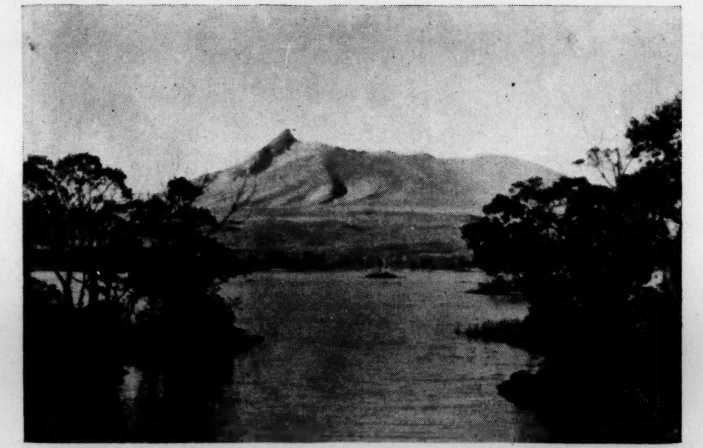

Fig. 13. Komagatake Volcano and the flowed-mounds in Ônuma.

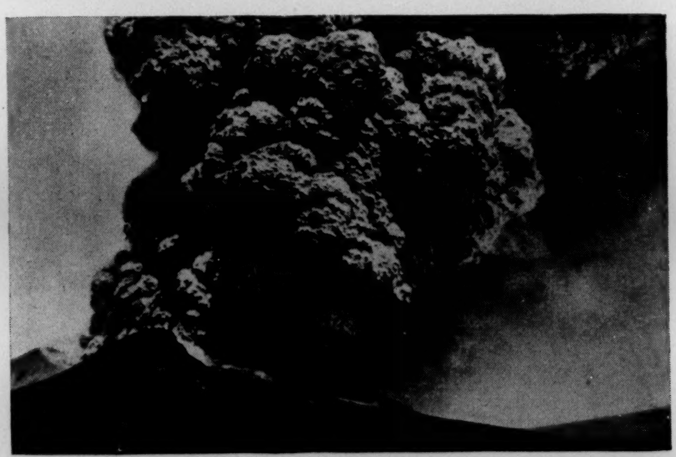

Fig. 14. Komagatake Volcano at a paroxysmal phase of eruption, as seen from Ônuma, June 17, 1929.

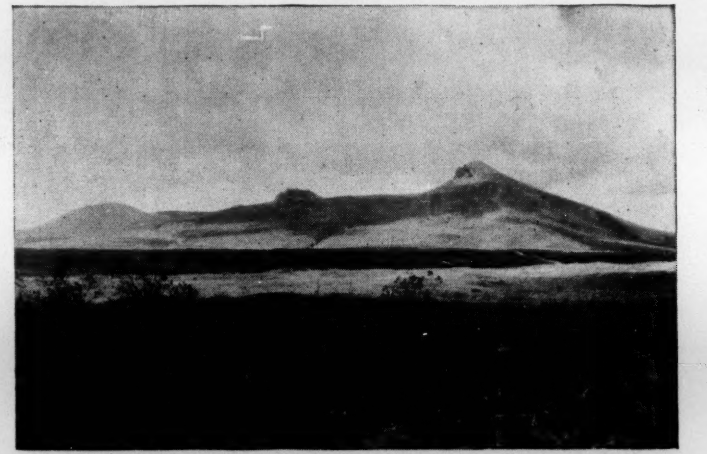

Fig. 15. General view of the eastern side of Komagatake, looking from Yakeno.

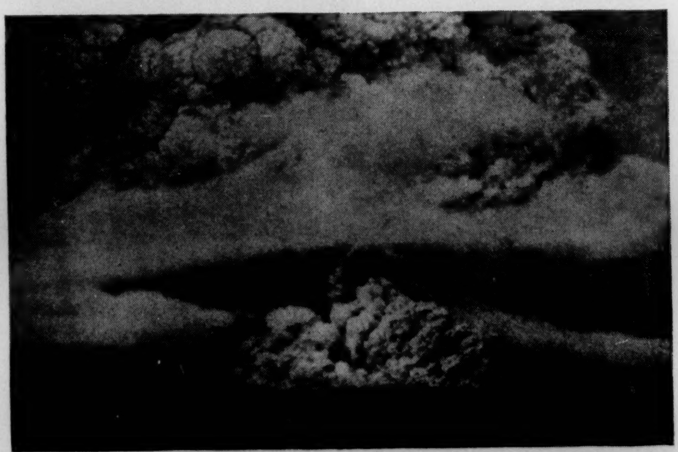

Fig. 16. A flow of pumice-laden cloud descending the southwestern slope of the volcano. About 5h. 30m.p.m., June 17, 1929.

（震研彙報 第三十八号 図版 井村）

昭和35年10月1日印刷
昭和35年10月5日発行

東京都文京区本富士町一番地
東京大学構内
編纂兼発行者　東京大学地震研究所

東京都新宿区山吹町一八四番地
印刷者　笠井康頼

東京都新宿区山吹町一八四番地
印刷所　株式会社国際文献印刷社

売捌所
東京都中央区日本橋通二丁目六番地
丸善株式会社

Sold by Maruzen Co., Ltd., Nihonbashi-dôri, Chûô-ku, Tôkyô.
Price of this copy: 298 Yen. (Postage exclusive.)